LA-SUB--98-17

Institute for Solid State Physics RAS

FINAL REPORT
on Contract No. 075 AK 0005-35

Fabrication and Testing of Long Length High-T_c Composite Conductors

Principal Investigator

L. M. Fisher

1997

Contents

DISCLAIMER

DISCLAIMER

Portions of this document may be illegible electronic image products. Images are produced from the best available original document.

1 Introduction

Presently some methods of HTS-conductors processing are under study in our laboratory. "Powder-in-tube" (PIT), "Jelly-roll", electrophorethis are among them. PIT process has developed predominantly both in a view of the achieved J_c values Bi-2223 phase was used as a core material for these tapes. Since the main purpose of the task order was to enhance the development of long length high temperature superconductor tapes, we have considered reasonable to lay the perfection idea of the PIT process "step by step" or "tape by tape".

To realize it we have assumed, keeping stable the basic scheme of PIT process, to vary some technological parameters which are as follows:

- type of initial powder;
- sheath material;
- tape construction (filaments number, cross section e.a.);
- processing regimes

2 Fabrication process of long length HT_c superconductors

This scheme was developed for tape fabrication by methods of cold drawing followed by cold rolling, which combination provides the adequate geometry of tape conductors.

2.1 Preparation of starting tubes

Silver (99,95 grade) or silver-nickel-yttrium alloy ingots were used for tube processing. Half-finished tube then was cut for requirement size and wire-edges were removed. To fabricate monofilamentary Ag-sheathed conductors, silver (99.99%) tubes with OD=15.0 mm, ID=11.4 mm and 1 m in length were used. After sealing of one of the ends the vibrofilling was performed in dry cleaned Ar. Silver tubes with OD=8.0 mm, ID=6.4 mm and 2 m in length were used for 19-filamentary Bi-2223/Ag conductor.

Hardened alloys based on silver were prepared by powder metallurgy technique and by vacuum melting and casting. Ag-Ni-Y powder alloy was prepared on following route:

- mixing silver, nickel and Y_2O_3
- powders in ball mill in C_2H_5OH;
- cold working of powder mixture to prepare the compact billet;
- double vacuum heat treatment with intermediate cold working;
- hot extrusion to fabrication the tube with OD=10 mm, ID=6 mm and 1 m in length.

The tube prepared by this method was used for making monofilamentary Bi-2223/Ag-Ni-Y conductor. The 19-filamentary Bi-2223/Ag-Ni-Y conductor was made with using double vacuum melted Ag-Ni-Y alloy. The tubes from this alloy were produced by hot extrusion and had OD=13 mm, ID=10 mm, length 1 m. The deviation of wall thickness was ± 0.1 mm. Then, the as prepared tubes were degreased by acetone. The silver plugs were placed in one of the ends, then vacuum cleaning procedure was undertaken and control weight was determined.

2.2 Powder preparation

Non completed powders or precursors were used as a core materials for Bi-2223 conductors. "Freeze-drying" or "spray-drying" techniques, developed in our laboratory, were conventional for this purpose.

To prepare $Bi_{1,8}Pb_{0,4}Sr_{2,0}Ca_{2,2}Cu_{3,0}O_x$ powder precursors the "freeze-drying", as well as the "spray-drying" methods were used with the same nitrate solutions in both methods. Some characteristics of this solutions were following:

- solution density — 1,455 g/ml
- pH — - 0,52
- cation ratios:

- Bi — 1,79
- Pd — 0,39
- Sr — 2,01
- Ca — 2,17
- Cu — 3,05

Cryoprecursor was prepared by vacuum drying in temperature interval from −190°C to +65°C with followed pyrolisis of nitrates at 660°C, 1 hour in air. To form the required phase composition, cryopowder was heat treated at 750–780°C during 4 hours in cleaned O_2. Some characteristics of cryoprecursor are presented in Table I.

"Spray-dried" precursor was prepared by pulverization of a nitrate solution into temperature zone 700–800°C at dynamic vacuum. To form the required phase composition, the heat treatment at 800°C during 24 hours in air was performed. Characteristics of "spray-dried" precursor were the same with ones presented in Table I.

Morphological features of "freeze-dried" as well as "spray-dried" precursors are shown in Fig. 1. Before filling into the tube the following test was put for powders:

- determination of powder density in accordance with Russian standards (GOST 19440-74);
- determination of density after shaking down (GOST 25279-82);
- particle size (granulometry) by sieve analysis (GOST 18318-73);
- densification under pressing.

The precursors before its use in composite conductors were kept in dry and cleaned atmosphere to preserve from adsorption of water vapor. By preliminary investigations performed it was established that the composite conductors with silver-doped core (up to 20%wt. Ag) have sufficiently high values of tolerant bend deformation without signs of critical properties decreasing compared with non-doped composites. So, we have used our experience to production of the L3-conductor with silver-doped core.

2.3 Filling procedure

The filling procedure was fulfilled by feeding a powder with it periodical densification by vibrofilling in control dry cleaned Ar-atmosphere at the proper equipment, specially designed. After supplying and hermetic sealing the assembly weight was determined and the control weight of powder in tube was estimated.

2.4 Cold working

As prepared assembly was then processed by drawing on the drawing machine through the conic dies made of alloy hard "W-C" alloy or diamond. The profile of dies was under control to avoid cracks, cavities or traces of stick metal. If the defect was revealed the die was cleaned or rejected. The special oil lubricant was employed during the drawing process.

Single core tapes were produced by drawing of sealed "powder-tube" billets at 10% reduction ratio per pass. Round conductors 2.0–3.06 mm in outer diameter were tape rolled at 10% reduction ration per pass. The round section wire is being fabricated by flat rolling in rolls 40–200 mm in diameter to a final size, the gap between rolls was under control.

To produce multifilamentary tapes, the single core round wires were cut to pieces of a needed length. After assembling pieces in bundle it has been placed in a tube OD = 8 mm, ID = 6,4 mm in the case of 19-filamentary Bi-2223/Ag conductor, and OD = 13 mm, ID = 10 mm in the case of 19-filamentary Bi-2223/Ag-Ni-Y one. Multifilamentary billets were drawn and tape rolled. Characteristics of fabricated composites are presented in Table II.

2.5 Thermomechanical treatment

To form superconducting properties in Bi-2223 conductors, the "sinter-roll-sinter" process was used. Annealing stages of superconductors were performed at the temperature range 830–850°C in air using "Nabertherm" Ceramotherm N100 Kilns having volume equal 100 liters. At the heat treatment of conductors 100–150 m in length they co-wound together with high heat resistant tape in the form of spail. It made it possible to use effectively the volume of furnace, to provide homogeneity of a temperature distribution along superconductor and to except diffusion contacts between turns of

winding. Total time of heat treatment were 100–120 hours in dependence of precursor type, conductor design and sheath material.

Intermediate cold rolling was accomplished in rolling machines with 40–150 mm in roll diameter and 10–30 m/min rolling speed. The number of intermediate roll stages and deformation regime at the rolling were varied in dependence of type of a precursor, conductor design and sheath material.

To elucidate the effectiveness of intermediate rolling process the comparative study was undertaken on control short samples which were processed by intermediate pressing between annealing cycles with the specific force 2 GPa.

2.6 Fabrication of model coils

Insulated HT_c-composites were used for making of prototypes of electrotechnical devices such as pancake coils. ZrO_2-coating stabilized by Y_2O_3 and covered by pyrolysis of metallorganic compound was used as insulation. Specially developed equipment made it possible to electro-insulate the tapes up to 250 m in length. Scheme of insulating processing is shown in Fig. 2. Detailed characterization of such an insulation was reported elsewhere [1].

Pancake coils were made "wind-and-react" as well as "react-and-wind" techniques. To increase the mechanical stability, the coils were impregnated by epoxy resine and placed into stainless steel sheath. To make 5-stacked pancake coil, each of five pancakes were electrically connected together with using silver foil directly by its diffusion welding with conductor sheath during final heat treatment.

3 Characteristics of the produced conductors. Choice of methods

Photos of conductors cross sections are shown in Fig. 3. It should be noted that during thermomechanical treatment of monocore superconductor L2 Bi-2223/Ag based on "spray-dried" precursor the sufficient sheath "bubbling" was observed. Absorbed water as well as CO_2 evaporation might be the reason of such a behavior. So, instead of L2 19-filamentary conductor Bi-2223/Ag-Ni-Y (L6) was fabricated additionally; an alloy Ag-Ni-Y was prepared by vacuum melting and casting. In present study the complete investigation of critical properties as well as structure features of conductors above was

performed.

It is well known that one of the main characteristics of superconducting materials is the critical current density J_c. This parameter defines the maximum value of the nondissipative current density in a sample. On the other hand, owing to temperature and quantum fluctuations, losses exist even in the case $J < J_c$. This means that the concept of the critical current density itself is not strictly defined. Generally, the current capability of a system should be described by means of the voltage-current characteristics (VCC). However, in the majority of cases the next approximation of VCC is valid

$$E(J < J_c) = 0 \tag{1}$$

An universally accepted criterion for the definition of the critical current is the value of the electric field about 1 μV/cm. Additional difficulties exist to define the critical current density in long tapes and wires. They are connected with an inhomogeneity of J_c along the length of the conductor. The critical current is defined by bad portions of a wire in this case, i.e. by the cross sections with the minimum of the critical current. Therefore, one should distinguish between the maximum current and the averaged critical current density which changes along a conductor. At the beginning, let us consider the main equations for the description of the electrodynamics of hard superconductors. Low frequency properties are well described by the critical state model [2]. The main equation of this model has the following form

$$\mathrm{curl}\vec{B} = \frac{4\pi}{c}\vec{J}_c, \tag{2}$$

where $\vec{B}$ is the magnetic induction inside a superconductor. This equation is correct in a low frequency range [3]. Indeed, if the external magnetic field changes so fast that the vortex system has no time to relax to the critical state, the current density will exceed J_c and the system may be characterized by some point on the voltage-current characteristics $E(J > J_c = 0$. Such a state corresponds to the viscous vortex flow. On the other hand, if the field changes very slowly, the critical current density may decrease in comparison with J_c owing to the creep of the magnetic flux [4, 5]. This means that the critical state model is a very rough approximation. However, owing its simplicity, this model is commonly used and it permits to calculate a number of electrodynamics characteristics of hard superconductors and to compare

these results with experiments.

In accordance with a different definition of J_c in Eqs. (1) and (2) there are two alternative methods to measure the critical current density: the usual four probe methods and contactless ones. Various contactless electromagnetic methods are widely used for testing of superconducting materials and wires or tapes [6, 7, 8]. The attractiveness and wide propagation of these methods for investigation and test of hard superconductors are due to the principle possibility to get information about the critical current density J_c. This important parameter of a bulk superconductor determines its response to the external electromagnetic field. The critical current density J_c of a hard superconductor is in the material equation

$$\vec{J} = J_c \frac{\vec{E}}{E}, \tag{3}$$

where $\vec{E}$ is the electric field. This equation together with Maxwell's equations determine the distribution of the ac field and currents inside a superconductor. Special problems arise in description of the electrodynamics of composite wires with a normal metal matrix and fine-filament superconductors. The proximity effects may be very essential in these materials [9]. They become serious when the spacing between the superconducting filaments is comparable with the fundamental characteristics of superconducting media such as the London penetration depth and the coherence length in a normal metal matrix. In the case of the proximity effect the composite is characterized by two scales of shielding currents. Besides the critical currents of superconducting filaments, there are comparatively small proximity current in the matrix [9, 10, 11, 12, 13, 14]. This proximity current between the filaments restricts the scaling of the composite size parameters down. The problem for a superconductor with two current components has been solved for granular superconductors by Dersch and Blatter. They generalized the critical state model for the weak link granular superconductor using the conception of an effective superconducting medium [15]. According to this idea, the magnetization of the superconducting grains may be taken into account in continuum approximation by an introduction of the effective magnetic permeability μ which corresponds to the permeability of the granular medium with the network of weak links broken down. Until the magnetic flux penetration into the grains is negligible, the modified equation of the critical state of the granular

superconductor are valid:

$$\mathrm{curl}\vec{B} = \mu J_c(B)\frac{\vec{E}}{E}. \tag{4}$$

The dependence of J_c on B is essential for ceramic superconductors and must be taken into account in electrodynamics tasks. Summing up this brief introduction we emphasize that one can use the critical state model in its primary or modified form to describe the electrodynamics of practical superconductors at least in restricted conditions.

3.1 Transport Measurements of the Critical Current

The pinning, or interaction, of the flux-line lattice with various crystal imperfections in hard superconductors is responsible for the existence of the critical current density J_c, usually defined as the current density J_c at which a small voltage is observed. The critical current density at an induction B is that which allows the Lorentz force to be balanced by a pinning force F_p. In the mixed state flux-line lattice is pinned by an interaction with pinning centers which are features of the microstructure of the superconductors. Numerous experimental investigations carried out on HTS conductors have clearly confirmed that for these superconductors the critical current density is also highly sample-dependent and is linked with many factors including specific features of microstructure, composition, and texturing [16, 17, 18]. It is for this reason that a detailed investigation of a relation between J_c, magnetic induction B and temperature T (in conjunction with a microstructural analysis) is required. One of the basic methods for determining the critical current I_c is the measurement of voltage-current characteristics (VCC) which represent, in essence, the four-probe method of dc current measurements or pulsed mode measurements [19, 20]. To be able to carry out the VCC measurements in a wide range of magnetic fields one need to have cryostats, appropriate magnets, and high precision thermometry. Design and construction of an apparatus for the transport current measurements of HTS at a range of temperature and magnetic fields as well as experimental conditions which are preferable to ensure high sensitivity and reliable results on $J_c(B,T)$ are considered in [21, 22, 23].

A. Sensitivity

One manages, as a rule, to record the voltage-current characteristic (VCC) in the range of change of the electric field from 2 to 5 orders in magnitude. The sensitivity of the four-probe method are restricted, in particular, by the quality of contacts in the specimen and connections which determine the noise level. The typical value of a sensitivity in measurements of the voltages in the process of the experiments on determination of VCC is $10^{-9} - 10^{-7}$ V. In composite superconductors the VCC measurement at high electric fields is limited by the conductivity of a low-resistance matrix [24]; in the matrix-free specimens the overheating of a specimen may cause the voltage breakaway and a specimen failure. The evaluations of the possible influence of heat generations in the places of contacts on the measured values of I_c have been done in [25]. It was shown that for the samples with of 93 K overheating of 20 K would cause a reduction in I_c of 20 %. The use of pulse currents significantly reduces the overheating. It should be noted that the sensitivity in the measurements of voltages in pulse mode is also significantly lower and equals to $10^{-5} - 10^{-4}$ V. If a temperature gradient exists, then there are various thermoelectric effects which can occur and effect on VCC . The situation is further complicated by the introduction of a magnetic field when thermomagnetic effects are expected [26].

B. Criteria

The criterion for the Ic determination from VCC (e.g., $E = 10^{-6} - 10^{-7}$ V/cm, $R_{eff} = 10^{-11} - 10^{-12}$ Ohm) is given, as a rule, by applied problems, for example, by the admissible power dissipated in the superconductor. Different criteria used for the J_c evaluation yield variety of J_c values especially when the VCC width is broad. Methods for determining I_c have not been standardizes yet, even in practical superconductors like Nb_3Sn. Critical current criteria based on electric field or resistivity may present a number of problems in defining critical current, especially for high T_c superconductors in the vicinity of the critical temperature or upper critical field. To minimize these problems an intrinsic J_c criterion was proposed by Ekin [27] based on the long-standing concept of a flux-flow resistivity. Critical current is defined as the current where the tangent to the $E - J$ curve at a given electric field level extrapolates to zero electric field. This determines an offset J_c that minimizes the above problems. The criterion is particularly useful near the irreversibility field H^* where the $E - J$ characteristic starts to approach

ohmic behavior.

C. Characterization of VCC

Investigation of the $J_c(B,T)$ relationship and parameters characterizing the real shape of VCC is of practical interest for magnet system stability calculations [28]. Another reason for the interest in the shape of VCC is that such studies provide additional opportunities for analyzing processes which occur in superconductors. Voltage-current characteristics of HTS materials have been studied experimentally in [29, 30, 32, 33]. The thermally activated behavior appears in VCCs and the dissipation mechanism should be discussed in terms of the flux creep and the flux flow. Two kinds of VCC were observed experimentally. The first can be well described by a form

$$E(J) = E_0 \exp\left(\frac{-U(J)}{kT}\right). \tag{5}$$

Here $U(J)$ is the flux creep barrier which is a nonlinear function of J [29, 30, 32, 33]. The thermally activated flux flow (TAFF) should lead to a linear behavior of the $\log(I) - \log(V)$-curves [30, 31, 34]. In VCC measurements for sintered bulks having weak links between grains a power law of the form $V \propto I^n$ with an n-value of 4–16 was reported. The n value of 10–25 is typical for short specimens of Bi-2223 tapes [35, 36]. It should be noted that the VCCs of HTS conductors obtained in a wide range of electric fields not always can be approximated by only one function.

The HTSs are to be used successfully in applications such as high-field magnet, power cables, and magnetic energy storages devices. It is necessary to consider various magnetic fields for different applications, such as 0.1 T for cables, 0.2–0.5 T for magnet for industrial usage and 1–6 T for generator magnets. All these applications require minimum critical current densities of 10^4 A/cm^2. At present, the most promising HTS materials are BiPbSrCaCuO/Ag-clad tapes. Bi-based conductors are able to transport high current density without being influenced appreciably by weak links. The critical current density values well above 66 kA/cm^2 (17 μV/cm, 77 K, 0 T) have been reported for short samples [37]. However, long tapes with high J_c will be needed, if the tapes are to be used in magnets, electrical machines or ac power distribution applications. A great deal of progress on Ag-sheathed Bi-based superconducting wire was achieved, such as 1200 m long wire with J_c of 10900 A/cm^2, excellent $J_c \times B$ properties at 4.2–27 K [38]. The transport

measurements of J_c for a long (up to 100 m) pieces of a wire are carried out with intermediate voltage taps to determine its uniformity over the length [39].

The irreversibility line $H^*(T)$, a useful flux-pinning-strength parameter can be determined from $J_c(B,T)$ dependencies measured in a wide range of temperature and magnetic fields. The irreversibility field H^* of a Bi-2223 tapes is found to be an increasing function of thermomechanical treatment [16]. The correlation of $H^*(T)$ and J_c (77 K, 0 T) shows that H^* could be enhanced with an improvement of microstructure of superconductors [34]. To meet this requirement both high J_c and good control over the homogeneity of the transport current path must be achieved over long tapes. Larbalestier et al [40] pointed out that the problems caused by macroscopic defects must be first overcome before full benefits from the optimization of the structure of Bi-2223 ceramic can be expected. The conventional resistive four-probe method is not very convenient method to obtain information about sample inhomogeneities. Hence, additional characterization methods giving more explicit information about the sample homogeneity are required. Such an information may be more easily obtained by some contactless methods (see next section).

D. Critical temperature

The measurements of the resistivity ρ and susceptibility χ as a function of a temperature can be used to determine T_c (onset) and T_c (offset) characterized transition. It is evident that these values depend on the values of the testing current or ac field, sensitivity of the instrument, the presence of the matrix in the conductor and on the matrix resistance. Sintered high-T_c materials [41] and nonhomogeneous on composition and structure low-T_c superconductors [42] may exhibit two or more transitions in a curve $\chi(T)$. In HTSs both intrinsic and coupling critical temperature are field dependent. The measurements of the ac susceptibility in low magnetic fields are very informative testing on the presence of low coupling in HTSs materials. Detailed investigations of the functional relation $\rho(T)$ in the $S-N$ region have been carried out on deformed alloys [43], vanadium films [44], the A15 compounds [45], HTS crystal [46] and BiPb-/Ag sheathed tapes [47]. In homogeneous LTS samples of Nb_3Sn the parameter characterized $\rho(T)$ is uniquely related to the parameter which specified the real shape of VCC [45]. The exponential

dependence $\rho(T)$ which have been obtained for the HTS materials confirmed the presence of thermoactivated mechanism. Parameters which describe the function $\rho(T)$ have been determined out of VCC measurements also [47].

In some cases, the R(T) dependence in the transition region can be represented by the sum of two exponentials, which is attributed to the presence of the characteristic microstructure with interlayers of a low temperature component [48] occurring in the current paths.

Examination of the shape of transition characteristics, in particular, of temperature characteristics, with the available hypothesis describing the transition shape, is important not only for studying the factors influencing the transition width, but also from the metrological point of view, because such examination allows one to compare the results of determination of the critical parameters obtained by various techniques.

3.2 Contactless Methods of J_c Measurements

The problems to study the critical current in superconductors including different experimental techniques have been discussed in a number of beautiful papers. According to experience discussed in these papers, the basic methods of the contactless study and the measurement of the critical current density in superconductors are following:

- (A) measurements of a magnetic moment M;
- (B) inductive (ac) methods;
- (C) measurements of the magnetic flux penetration into the cylinder (or ring) sample or captured by it;
- (D) study of a magnetic field distribution near the sample;
- (E) torque measurements;
- (F) decoration of the vortex structure.

Today this list have to be complemented by the item:

- magneto-optic visualization of the magnetic induction pattern in superconductors in the external magnetic field or carrying an electric current.

A. Magnetic moment measurements

This, the most classic method, is based, as a rule, on the measurements of the hysteresis loop $M(H)$ width ΔM [2].

$$\Delta M = j_c d/30$$

for a long cylinder with a diameter D, and

$$\Delta M = j_c d/20$$

for a thin plate with a thickness d. In both cases the external magnetic field is parallel to the largest dimension of a sample. These simple formulae are valid if the critical current density is unaffected by the magnetic induction gradient inside the sample. The last point is the main lack of the magnetic moment method, since J_c depends on the magnetic field especially in such materials as HTS. The next serious problem is connected with the correct account of the sample shape, or the demagnetization factor. The precise direction of the magnetic field with respect to the sample plane have a great importance for thin superconductors. The last problem becomes more important for the anisotropic superconductors [49]. Finally, the flux creep leads to a remarkable, but not great, error in the evaluation of J_c. Some of problems listed may be overcome, in principle, by using a SQUID magnetometer if its sensor loop envelopes the sample tightly, but in practice it is not the case.

B. Inductive (ac) methods

Applications of ac methods [35, 36, 49, 50, 51, 52] for measurements of the critical current density are based on the critical state model modified for the cases of the ac magnetic fields. Likely the first such an application has been proposed by Bean [53]. It is based on the detection of the third harmonic of the emf induced in the pick-up coil with the superconducting sample by the external ac magnetic field. Campbell [54] developed the "full flux" method by which one studies the penetration of the ac magnetic field

$$h = h_0 \cos(\omega t)$$

into the superconductor put in the dc field $H \gg h_0$ and the variation of J_c with h_0. Authors [55] have suggested some modification of this method based on an analysis of the pick-up signal shape to study the magnetic flux

profiles. The advantages of these two last methods consist in possibility to get information about the critical current distribution inside the sample. Inductive methods are used intensively for studying the HTS materials, e.g. the magnetic flux profiles study [56, 57, 58], "full flux" study [59, 60], the study of various harmonics of a signal [61, 62, 63].

A number of models have been proposed to describe the ac magnetic susceptibility of ceramic (granular) superconductors [64, 65, 66]. A numerous bibliography of the papers devoted various problems of the ac susceptometry are presented in the review [6] that "critically analyzes current practice in the design, calibration, sensitivity determination, and operation of alternating-field susceptometers, and examines applications in magnetic susceptibility measurements of superconductors". In particular, authors [6] pay attention on an importance of the inductive ac measurements for the identification of the critical temperature T_c of high-T_c superconductors. The relationship between the structure of high-T_c superconductor and the shape of the transition in the ac susceptibility and resistivity are discussed. It is demonstrated that the ac susceptibility *vs.* the temperature carries more much information about the sample than the temperature dependence of a resistivity. By such reasons as two transitions, the effect of an ac field on the width of the transition and the role of coupling effects authors [6] consider that it is more convenient to identify the T_c as the onset of transition in the susceptibility.

Authors [67] proposed a comparatively suitable and simple form of experimental determination of the critical current density having a serious advantage enabling to study J_c as a function of the magnetic induction or some other parameters. With ho being less than penetration field hp, the surface impedance Z of a hard superconductor in the critical state is inversely proportional to the local value of $J_c(B)$ [67]:

$$Z = \frac{2}{3\pi}\frac{\mu\omega h}{cJ_c(B)}(1 - \frac{3\pi\imath}{4})$$

In the case of a granular superconductor the coefficient is the effective permeability, for the superconductor characterized by a single function $J_c(H)$ ($\mu = 1$). This formula is derived for a simple geometry - a long cylinder or thin plate in collinear ac and dc magnetic fields parallel to the largest dimension of a superconductor and for a comparatively high dc field $H \gg H_{c1}, h$.

The efficiency of this method has been proved in a study of "Effect of microstructure on the magnetic-field dependence of the local critical current

density in $YBa_2Cu_3O_7$- superconductors" [68]. In this paper the experimental technique and the formulae for $J_c(B)$ calculation in two geometries — cylinder and thin plate — are presented. The simple ways of calibrations of the values measured and of a determination of the effective permeability of a granular superconductor are suggested. This ac method is very suitable in a study of a temperature dependence of J_c [69, 70, 71] and an anisotropy of J_c in a dc magnetic field [72, 73, 74]. To evaluate this anisotropy it is sufficient to measure the ac response of a sample in the rotating dc magnetic field, if some experimental conditions are fulfilled, in particular, if the dc field is much more than the maximum penetration field H_p of a sample and the ac probe field h_0 is comparable with H_p. A high sensitivity of ac measurements enables one to study the critical currents in small samples such as single crystals of HTS [72, 73, 74, 75].

The procedure of the J_c measurements described in [68] is following. The plate-like sample under study is arranged in a central homogeneous field zone of a small solenoid which generate an ac magnetic field $h = h_0 \cos(\omega t)$ with the frequency $\omega/2\pi = 100 - 1000$ Hz. This ac field is parallel to the sample surface. The pick-up coil is wound around the middle part of the sample as close as possible to minimize the ac flux in the gap between the sample and the pick-up coil. The remaining flux in this gap which is not related to the sample is compensated by an additional coil system.

AC methods allow to estimate simply the volume fraction α of weak links in a sample up to a low level of about 10^{-5}. It may be done, for example, by measurements of the ac magnetic susceptibility dependence on the ac field magnitude h_0, when the dc field H is absent. For two stage process of a magnetic field penetration into the granular superconductor the imaginary part of the susceptibility $\chi''(h_0)$ may have two peculiarities. If the global shielding of the sample is due to the weak link currents one have to detect the maximum in the function $\chi''(h_0)$ which height is proportional approximately to α. If the value α is very low, the deviation from the smooth variation of $\chi''(h_0)$ takes place. The ratio $\chi'(h_0)/\chi''(h_0)$ may be more sensitive to weak links than separate components of the susceptibility [76]. However, at $\alpha < 10^{-5}$ this method fails. In such a case it is useful to employ the magneto-optic method (the details see below). Nevertheless, that contactless ac method may be more reliable in the case of little amount of weak links as well if the contactless results will be compared to four-probe ones at fixed H,

T at least (for simplicity, near T_c).

The study of the frequency dependence of the ac magnetic susceptibility, or the surface impedance of ceramics [3, 77, 78] and melt-textured [79] YBCO superconductors reveals that a mistake of the determination of J_c by ac methods is not principal at frequencies below 1 kHz. It is shown how it is possible to use the frequency measurements for the evaluation of the $I-V$ characteristic of a superconductor. To complete this section, one more advantage of inductive methods connected with the demagnetization factor problem have to be noted. It consists in the possibility of a pick-up coil location close to the sample surface and far from its ends perpendicular to the ac probe field.

C. Measurements of the magnetic flux penetration into the cylinder (or ring) sample or captured by it and relaxation process

This method (see, for example, [4, 80, 81]) enables one to reach the voltage threshold in VCC study down to 10^{-5} V/cm. It is used mainly in a study of the critical current of ceramic materials [82, 83, 84], thin films and in some modified form for the study of single crystals [85, 86]. This method accumulates the characteristic problems of a magnetic moment measurements.

D. Study of a magnetic field distribution near the sample

This method is based on the Hall probe measurements of the magnitude of magnetic field near the surface of the superconducting sample induced by the field of constant magnet placed at the other side of the sample. In particular, the method of a homogeneity study of Bi-2223 monofilamentary tapes using Hall sensor magnetometry was proposed by M.Lahtinen *et al.* [87]. The main problem of such measurements is an extremely complicated quantitative treatment.

E. Torque measurements

Torque measurements (see, for example, [88]) are known as a very sensitive method for detecting the magnetic moment of small samples, the HTS single crystal, for example.

F. Decoration and visualization of the vortex flux

In this technique, the critical current may be measured by the profile of the vortices decorated on the sample surface [89, 90, 91]. The method is

good for the study of fundamental problems of the vortex structure in hard superconductors but not for testing the great amount of pilot samples in the process of a technological experiment on the improvement of the material characteristics. The last aim may be attained successfully by the other visualizations method, namely using the advanced magneto-optic technique, which allows to observe the magnetic induction patterns in superconductors [92, 93]. In this method the analysis of the magnetic field distribution at magnetizing the sample in different directions, and at the application of the transport current are available. Its extremely important advantage consists in the possibility to observe the isolated weak-link surface at its intersection with the surface of sample studied [94].

In present study it was considered reasonable to use the following methods of testing short samples and the HTS tapes.

1. The four-probe method to measure the critical temperature and the superconducting transition.

2. The four-probe method to measure the voltage-current characteristics and to define the critical current and the averaged critical current density and their dependencies on the external dc magnetic field H.

3. Contactless methods to define the critical current density and its dependence on H.

4. Contactless methods to measure the anisotropy of the critical current density.

Long length tapes made during present study (Table II) were used:

1. to cut out the short length specimens at the stage prior to the final heat treatment, which were heat treated under the same conditions as long length conductors;

2. to wind spirals of 10 to 40 m in length to study the current distribution over the conductor length;

3. to fabricate pancake coils from wires of various lengths by the "wind-and-react" (W&R) and "react- and-wind" (R&W) methods;

4. to assemble a 5-sectional model coil from resulting pancake coils by the W&R technique.

The connection between five pancake coils is accomplished by diffusion welding of conductor sheaths at the final annealing stage. On the basis of L6 conductor the double pancake coil was produced having racetrack form. The overall length of the tape in this coil was 110 m and turns number was equal to 110. The characteristics of long length articles and their critical currents are given in Table VII of this report.

4 Measurements details and results

The measurement of the superconducting transition temperature profile consists in recording the superconducting transition in a tape conductor positioned between two flat coils. An ac magnetic field generated by one of these coils was perpendicular with a tape. Another one was a pick-up coil. The probe containing coils with the specimen, carbon thermometer, and heater are mounted in an evacuated glass filled with gaseous helium at room temperature. The temperature is determined with an accuracy of 0.5 K at a level of 100 K and 0.05 K at a level of 10 K.

Measurements were conducted at a frequency of 310 Hz; the alternate magnetic field had an amplitude about of 0.1–0.2 Oe. The superconducting transition temperature profiles for some mono- and multifilamentary specimens recorded in the temperature range from 4.2 K to 116 K are shown in Figs. 4 and 5. The transition curves are characterized by the onset, middle and end points of the high-temperature step, as well as by the onset and end points of the low-temperature step for the specimen in which this step was detected.

The temperature transition characteristics for the specimens under study are given in Table III. A significant difference in the transition temperature profile was established in specimens of monofilament conductors which were cut of various parts of 100-m wire. As an example, the temperature transition curves of L1-1 and L1-g53 conductors are plotted in Fig. 6(a). Additional smearing of transition curve for L1-g53 specimen as compared to that for L1-1 may be attributed to the presence of weak links in core material. The lower T_cN value of the 19-filament conductor enclosed in the hardened sheath as compared to the Ag-sheathed specimen can be attributed to diffusion of

Y and Ni impurities into the superconducting core from the sheath. The BiPbSrCaCuO compound is characterized by the structure with thin lamellae of the Bi-2212 and Bi-2223 phases [95, 96]. Low-temperature steps recorded in some specimens may be assigned to small inclusions of the 2212 phase.

4.1 The voltage-current characteristics

The voltage-current characteristics (VCCs) were measured by the conventional dc four-probe method at 77 K and 4.2 K in magnetic fields in the range 0–4 T. Measurements at 77 K were performed in a nitrogen-filled Dewar in magnetic fields 0–0.1 T generated by the coil made of Al wire. The measurements at 77 K in fields up to 4 T were made in a helium cryostat containing a superconducting coil providing magnetic induction up to 7 T. To perform measurements at 77 K in magnetic fields up to 4 T, the probe with a specimen was mounted in a nitrogen glass with double walls made of stainless steel, which was then dropped into a helium cryostat. Space between the walls was preliminary evacuated. In measurements at 77 K, the magnetic field was oriented perpendicular to the specimen current direction and parallel to the specimen plane.

Measurements at 4.2 K in fields up to 4 T were carried out in the helium cryostat at two different field orientations: (i) with the field oriented perpendicular to the specimen current direction and to the specimen rolling plane and (ii) with the field oriented perpendicular to the current direction and parallel to the specimen rolling plane. The critical current was determined from the voltage-current curves using the $E = 1$ V/cm criterion. The VCCs were corrected for the current overflow into the matrix. The specimen voltage was measured with sensitivity of 10^{-9} V/cm. The error of current measurements was not higher than:

- 0.1% — in measuring critical currents with 1 A power supply;
- 1% — in measuring critical currents with 10 A supply;
- 3% — in measuring critical currents with 300 A supply.

Figures 7 and 8 show the VCCs of short length specimens recorded in various magnetic fields at 77 K and 4.2 K. The VCCs of specimen L5 are plotted on the linear and log scale. In all the VCCs we can single out the

voltage range where the power law $V \sim I_n$ holds. The initial parts of VCCs for some specimens show the linear dependence which can be assigned to the current overflow to the matrix. The results of determination of the critical current I_c and critical current density J_c at 77 K and 4.2 K in self-field are summarized in Table IV.

To estimate the reproducibility of the critical current density along the conductors we carried out a series of measurements of I_c and the cross section S on 7–11 specimens cut from the same conductor. The current density dispersion was represented as the average I_c^{av} and the rms derivation (σ_{I_c}) for a set of specimens. The critical current density was determined by dividing the I_c value by the average cross sectional area of the superconducting core of the specimen. The J_c dispersion was represented in the same way as the I_c dispersion. These dispersions are given in Table IV.

The results obtained show that the dispersion in J_c values does not exceed 13% for the L5 conductor specimens, and 20% for the L6 specimens. The dispersion in J_c values of monofilament conductors reaches 50% and is correlated probably with a presence of parts of conductors which contain weak links. The details of that dispersion of J_c will be discussed below. The highest J_c values (that within the superconductor and the construction J_c value) were achieved with a 19-filament Ag-sheathed conductor: $2.3 \cdot 10^4$ A/cm^2 and $1.04 \cdot 10^5$ A/cm^2 at 77 K and 4.2 K, respectively. The magnetic field dependencies of the critical current density for specimens under study (in the field oriented parallel to the tape rolling plane) are shown semilogarithmically in Fig. 9, 10. After the initial drop in the fields to 0.1 T, which is normally attributed to the weak bonds between grains, I_c changes approximately exponentially with increasing magnetic field. Figure 11 shows the I_c anisotropy in differently oriented magnetic fields: The $J_c(B)/J_c(0) = f(B)$ dependencies were taken from specimen L5 at 4.2 K in magnetic fields oriented parallel and perpendicular to the tape plane. The critical current in fields above 1 T is virtually independent of the magnetic field if the latter is perpendicular the specimen plane. Table V summarizes the results of measurements of the magnetic field effect on the critical current in various conductors at 77 K and 4.2 K.

One of the fundamental characteristics of a superconducting wire is the growth rate of the specimen voltage with increasing the current. Shown in Figs. 12 and 13 are the magnetic field dependencies of the parameter n derived from the power-law segment ($V \sim I_n$) of the VCC. The parameter n can serve

as an indicator of nonuniformity of the cross-sectional area over the conductor length [97] or it can characterize specific features of the superconductor microstructure [98]. The $n = f(B)$ curves obtained in the present study behave much like the known curves for Nb_3Sn [99]. The n values determined for short length specimens in self-field fall in the range 15–30 units.

4.2 The effect of bending radius on the VCC

The effect of bending strain on VCCs and I_c was studied at 77 K using a specially designed probe enabling one to vary the bending radius in the range 0–1.7 cm and to perform the entire set of VCC measurements on the same sample without heating it above 77 K. The scheme of the specimen bending is shown in Fig. 14.

The I_c and n dependencies for various conductors (normalized to the $I_c(0)$ and $J_c(0)$ values of unbended specimens) are presented in Figs. 16 and 17. At the bending radius $R = 1.4$ cm, the $I_c/I_0 = f(R)$ ratio for specimen L5 reaches saturation and becomes 0.55. In accordance with the model suggested in [100] for multifilament conductors, the I_c/I_0 value decreases with bending due to the microcrack formation in the extended region of the specimen and tends to 0.5. The current-carrying capacity is then determined by the contraction region localized under the zero-strain axis. The strong $n = f(1/R)$ dependence at low bending radii demonstrates the effect of microcracks formed in the superconducting core not only on the critical current but also on the VCC shape.

4.3 Contactless Study of the Critical Current Density

The results represented above are obtained by direct testing the current capability of the short tape samples. These results are crucially sensitive, of course, to the local defects such as cracks, abruption, weak links etc., but information about the 'internal' current capability is essentially inaccessible. However, during the improvement of the long tape current capability this information may be of principal interest. The most employed and informative methods for such an investigation are different variations of ac technique (see, for example, [6, 49, 70, 72] and references therein) and magneto-optical ones [101, 102, 103, 104]. Below we will outline some details of our ac method for contactless study of the critical current density. The response of a sample to

an external ac magnetic field $h = h_0 \cos \omega t$ may be described by the dynamic magnetic susceptibility. The value of the magnetization in a general case is described by the series

$$M(t) = h_0 \sum_{n=1}^{\infty} \Re(\chi_n e^{in\omega t}) = h_0 \sum_{n=1}^{\infty} [\chi_n' \cos(n\omega t) + \chi_n'' \sin(n\omega t)], \qquad (6)$$

where $\chi_n = \chi_n' + i\chi_n''(n = 1, 2, 3, \ldots)$ are the components of the ac magnetic susceptibility. In the assumptions of Bean's model $dB/dx = (4\pi/c)J_c$ it is easy to obtain the connection of the fundamental components χ_1', χ_1'' (denoted below as χ', χ'' respectively) with the critical current density J_c. For $h_0 < h_p = \frac{4\pi}{c} J_c \frac{d}{2}$:

$$4\pi\chi' = \frac{c}{4\pi} \frac{h_0}{J_c d} - 1, \qquad 4\pi\chi'' = \frac{c}{3\pi^2} \frac{h_0}{J_c d}, \qquad (7)$$

where d is the sample thickness. These relations are valid in the general case and, in particular, when the critical current density is a function of the dc magnetic induction. We prefer the imaginary part of a susceptibility to the real one for the determination of $J_c(H)$ from our experimental data. To calculate the function $J_c(H)$ from the measured dependence $\chi''(H)$ we used the following relations for a thin slab [72]:

$$J_c(H) = \begin{cases} \dfrac{ch_0}{3\pi^2 d} \dfrac{1}{\chi''(H)}, & \text{at } H < H_1, \\ \dfrac{3ch_0}{8\pi d} \left\{ 1 \pm \left[1 - \dfrac{4\pi}{3} \chi''(H) \right]^{1/2} \right\}, & H > H_1, \end{cases} \qquad (8)$$

where H_1 is the dc magnetic field at which the ac probe field penetrates the slab: $h_0 = h_p(H)$. The plus sign in 8 corresponds to $H < H_m$ and minus sing to $H > H_m$, where H_m is the magnetic field value at which the $\chi''(H)$ dependence reaches its maximum.

To study the critical current density in the tapes by the contactless method considered we have used the pieces of the tape with the length of about 1 cm. The sketch of our experimental setup is shown in Fig. 18. The principle of measurements is based on the lock-in detection of the emf in a pick-up coil induced by the ac magnetic flux variation inside a sample in the alternating magnetic field.

To register the sample ac response the pickup coil (usually 20–50 turns) was wound directly around the sample (Fig. 19). Then the sample was positioned near the central homogenous field zone of a long (length/thickness ratio of about 10) flat rectangular solenoid. Two possible geometries of the coils with respect to the superconducting filament direction are shown in the Fig. 19. Figure 19(a) corresponds to the induced ac probe current $\vec{J}$ flowing *across* the filaments, whereas in the geometry Fig. 19(b) $\vec{J}$ flows *along* them, i.e., just like to the transport measurements.

The current flowing through the ac solenoid was supplied by the power amplifier having the current feedback (current stabilizer). An exciting signal for the current stabilizer was taken from the synchronizing circuit of the locking amplifiers via an attenuator to set the ac amplitude required. An ac current frequency was chosen as a trade-off a sensitivity of the method against the effect of the tape silver on the detected signal. The most part of data was obtained at a frequency of 20 Hz. To eliminate the parasitic flux in the gap between pickup coil and the sample as well as one in the silver sheath, the additional couple of coils with the variable mutual inductance was used (Fig. 18).

The pick-up coil signal was measured by two lock-in amplifiers (EG&G PAR-124A) tuned on the reference signal frequency (an internal generator of the lock-in amplifier). One of them was synchronized in phase with the ac magnetic field to measure V' component of the pick-up coil emf and another one was out of phase in $\pi/2$ to measure V'' signal. These voltages are proportional to the fundamental components of an ac magnetic susceptibility:

$$V' = \frac{NS}{c} h_0 \omega \chi'', \qquad V'' = -\frac{NS}{c} h_0 \omega \chi', \tag{9}$$

where N is a turn number of a pick-up coil and S is an effective area of a sample cross section normal to the ac magnetic field. For calibration of the detected signal in the magnetic susceptibility units (see 9) the following procedure was used.

The height of the superconducting transition in the case of an ideal superconductor is known to be equal to $1/(4\pi)$:

$$4\pi\chi'(T < T_c) - 4\pi\chi'(T > T_c) = 1.$$

For a real superconductor thick enough in comparison with the London penetration depth the height of the superconducting transition in $\chi'(T)$ are close

to unity at low ac field amplitude. We made a calibration based on this supposition at amplitudes $h_0 \sim 1$ Oe. Then this 'physical' calibration was compared with 'numerical' one following from 9 that permitted us to confront the observed and constructive filling coefficients (the total area of superconducting filaments cross-section the area of the tape cross-section).

To measure an ac susceptibility of tape with the aim to study the critical current density of the tape a sample with pick-up coil and ac solenoid was attached to the sample holder inserted into the cryostat with liquid nitrogen (or helium) at a pressure 0.1–4 atm. The temperature of a cooling liquid was measured near the sample position by the Cu-constantan thermocouple. The bottom part of the cryostat, where the studied sample was located, was positioned between the magnet poles without mechanical contact with them. The magnet could be rotated around the vertical by the angle 0–360° and around two mutually orthogonal horizontal axes by the ±6°. The field generated by the electromagnet can be varied in the range 0–20 kOe with a rate 0–100 Oe/s.

A rectangular sample cut from the Bi-2223/Ag tape usually about 10 mm in length, as it was said above, was putted inside the small flat coil generating the probe ac magnetic field. This coil was attached to the sample holder usually in such a position that the direction of the main sample axis was close to the longitudinal axis of the holder. The holder axis, in its turn, was close to cryostat axis almost parallel to a vertical and to the main magnet rotation axis 0–360°. The axis of the pick-up coil wound tightly on the sample (tape) was parallel to the ac solenoid axis lying almost in a horizontal plane. The first stage of a sample study consisted in setting the rational angular orientation of the sample plane with respect to the magnet rotation axis. An angle symmetry of an ac response of the sample in a high dc field $H > h_0$ was used as a criterion of such a procedure.

Examples of the imaginary part of the ac magnetic susceptibility versus the dc magnetic field for two samples No. 10 and No. 12 cut from the monofilament tape L1 are shown in Fig. 20(a). We call attention to the maximum value of $\chi''(H)$. It is the maximum that was mentioned just after the formulae in 8. For a homogeneous hard superconductor this maximum corresponds to the condition when the ac probe field reaches the middle of the sample. The height of the χ'' maximum have to be close to 0.24. The observed values of such a maximum for the tapes are lower by a factor of about Ag/HTS ratio (see Table II). We carried out such contactless measurements at ac field

amplitudes of an order of the $h_0 = h_p(H)$ value, when the resolution of the method is advantageous. The results of Fig. 20(a) converted to the $J_c(H)$ dependence are shown in Figs. 20(b) and (c). The curves correspond to the data for the directions of the probe ac current along the tape (dashed line) and across the tape (solid line) consequently. The dark circles denote the results of the four-probe measurements made for the initial pieces of the tapes before cutting the samples for the ac measurements. The dc field directions was the same for all these cases. The results of the ac measurements give the J_c values approximately twice higher than the dc measurements (for the J_c criterion 1μ V/cm). Besides, the J_c value for the in-plane current flowing across the tape length is remarkably higher than for current flowing along it. (It is necessary to note that our measurements did not reveal such an anisotropy in the multifilamentary Bi-2223/Ag IGC tape and practically no discrepancy between the J_c values measured by four-probe and contactless methods was observed.)

Some anisotropy, or difference of the J_c values for different directions in a tape plane, was observed for the multifilamentary tape L6 too (Fig. 20(d)).

In the low field region the anisotropy of in-plane currents is similar to that for the samples prepared from the tape L1. In Fig. 20(e) the difference between the $J_c(H)$ dependencies for the dc field perpendicular to the current in the tape plane (solid line) and perpendicular it (dashed line) is demonstrated.

The results presented in Fig. 20(f) show the variation of J_c with the angle theta in the plane perpendicular to the probe ac current between the tape plane and the direction of the magnetic field $H = 5$ kOe.

The results for $J_c(H, \theta)$ obtained by the described contactless method give, indeed, the value not always the same that by the four-probe method. However, their coincidence testifies a spatial homogeneity of the superconductor being under study. The modification of the contactless measurement technique used gives a spatial resolution of about 1 mm of a tape length. To enlarge the spatial resolution we made some previous magneto-optic visualization of a magnetic flux penetration into a tape. This study made with the resolution of several microns has shown that the superconductor filaments have defects like cracks breaking them into the blocks elongated across the tape. This effect is similar in common sense to that outlined in the paper [105].

Some statistics for short sections of tapes has shown that in the case

of a monofilamentary tape the contactless measurement gives the J_c value approximately in two times higher than the four-probe one. For the 19-filament tape this difference is lower. (In the case of the 39-filament IGC Bi-2223/Ag tape such a difference is absent practically.) Such discrepancy means that there is some microscopic defects confining the transport current but having no or small effect on an ac susceptibility of the tapes. The presence of cracks transverse to the tape length explains these facts. But the presence of cracks can explain hardly the variations of J_c along the tape in 5 times or more. Such great variations are caused rather by a variation of a tape quality having a more complicated character than cracks.

4.4 Critical currents of long length specimens and pancake coils

Using long length pieces of L2 (L = 10 m) and L5 (L = 10 m) conductors wound on ceramic tubes in the form of spirals with separated turns, we recorded the current distribution over the conductor length. The potential contacts were made uniformly over the conductor length by using an In solder; the spacing between the potential terminals being 1 cm.

The Table VI gives the I_c distribution over the length of a 10 m L2 conductor.

The average value, $I_c^{av} = 7.5$ A, is 63% of the current measured over the 10 m length and is 4.7 A. The current value over the 10 m length is 53% of the average current for the short length specimen L2.

The presence of low I_c parts of the conductor is responsible for the lower I_c values for long length conductors as compared to short length conductors.

The VCCs for one-stack and five-stack pancake coils measured at 77 K and 4.2 K in self-field are presented in Figs. 21 and 22. Figure 23 shows VCC of double pancake coil (racetrack) measured at 77 K in self field. The critical current of that pancake determined using $E = 1\mu$V/cm criterion is equal to 7.3 A.

The results of measuring the critical current for long length specimens are summarized in Table VII.

For the one-stack pancake coils (L5-1 and L5-2), as well as for the fivestack coils, we measured the magnetic field on the coil axes by the Hall probe. The measured values for one-stack coils are $H = 0.01$ T as compared to the predicted values 0.015 T and 0.018 T. For the five-stack pancake coil,

the measured value is 0.016 T and the calculated value is 0.023 T. Figure 24 shows the $I_c = f(B)$ curves for the short length specimen at 77 K. This figure also presents currents for the W&R pancake coils L5-1 and L5-2 with different turn numbers and the predicted field values on the coil axis. It follows from Fig. 24 that the current in W&R coils is 55% of the current of the short length specimen. The parameter n inferred from the VCCs of W&R pancake coils is 9.3 and 8.9 for coils L5-1 and L5-2, respectively. The decrease of the critical current value in long-length conductors comparing with short sample critical current is connected with the presence of microcraks, some local parts in conductor having specific features of the structure and composition which can be considered as weak links. It follows from literature that at the present time the current of long-length conductors is 40–70% of the current of short sample [106, 107, 108]. The study of the influence of thermocycling the pancake coil (L5) in the range 77 $\leftrightarrow$ 293 K (immersion in liquid nitrogen $\leftrightarrow$ heating up to room temperature) has shown that the critical current of the pancake coil is virtually the same within the measurement accuracy (Fig .25).

A significant influence of a design, technological parameters and sheath material on critical properties of tested samples noted above might be explain on base of SEM-investigations of conductors core structure. Core structures of monocore tape L1 and 19-filamentary tape L5 are presented in Fig. 26. The presence of large non-superconducting inclusions (up to 10–15 mm in size) is observed into L1-core. Such inclusions as $(Sr, Ca)CuO, Ca_2PbO_4, CaO, CuO$, are distributed non-uniformly across the core. It may be as one of the reasons of significant disorientation of Bi-2223 crystallites mainly in the centre of section and hence more amount of weak links and worse conditions for current flow. On the contrary, in thin filaments of 19-filamentary conductor it is observed uniform distribution of small non-superconducting inclusions, high density of Bi-2223 crystallites stacking as well as connected with those facts the favorable situation for transport current flow. In a number of studies [109, 110, 111] monocore conductor as superconducting object was described enough in details namely transport current distribution across HT_c-core, influence of core thickness on J_c-values, difficulties in achievement of high current carrying capabilities, not favorable behavior of such conductors both at bend deformation and thermocycling. Results obtained by us are well agreed with ones of other authors and give an evidence that at the fabrication of monocore composites it is necessary to solve following dilemma — achievement of high transport currents, critical current density and overall current

density simultaneously. To achieve high transport current values it is needed to have enough thick HT_c-core of conductor. However in this case the degree of influence of "silver-HTSC" interface on the mechanism, kinetics of Bi-2223 formation as well as texture of this phase decreases mainly in the central parts of core. This fact strongly decreases critical current density and makes worse the behavior of conductor in applied magnetic field.

It is obvious that the situation mentioned above is naturally excepted in a multifilamentary conductor, in which thin superconducting filaments are distributed with high area of "silver HTSC" interface over the section. Moreover, in multifilamentary conductor during rolling process more favorable character of core cracking is observed, the conditions are improved for densification and texturing of HTS ceramics and hence effectiveness of intermediate rolling is increased to improve the current carrying capability of the conductor, mainly in the magnetic field. It should be noted that the optimization of the conductor design is one of the reserves to increase the current carrying capability of multifilamentary HT_c composite namely the number, sizes as well as the distribution of filaments over the conductor section.

Some conductors and coils fabricated in present work are shown in Fig. 27.

Results of thermocycling shown in Fig. 25 for pancake coil wound from L5-conductor evidences about principal possibility of repeated cooling such a coil.

In the present work we successfully made the double pancake coil having "racetrack" form guaranteed the safe insulation between the halves of coil.

It should be noted that the critical current of 5-stacked pancake coil (L1-conductor) appears to be defined by inner non-superconducting contacts between single pancakes (Fig. 22).

An analysis of the results presented in this report make it possible to suppose the directions of further investigations and elaborations forward to creation of HTS composites with high current carrying and exploitational properties. It is consider reasonable to attribute to such directions following ones:

- optimization of design as well as processing regimes of multifilamentary conductors;

- further development of design, wind methods, joining techniques, increasing of mechanical strength for wares based on HTS composites;

- optimization of chemical and phase composition, fabrication methods and heat treatment regimes for HTS powder precursors.

As the some example of the studies supposed above, we present in this report VCC of 61-filamentary Bi-2223/Ag tape produced out of the project framework. The VCC data taken at the temperatures 77 K and 4.2 K are plotted in Figs. 7(g) and 8(g) respectively. This tape is shown to be characterized by the higher critical current even as compared with the best from L1–L6 tapes. The value reached in that tape is probably not the upper limit for the critical current, so, the further joint researches in this field are of great interest.

5 Conclusions

1. During 1996 according to LANL Task Order, five conductors based on high temperature superconducting compound Bi-2223 have been fabricated and investigated its critical properties in the temperature range of 115–4.2 K in applied magnetic fields 0–4 T.

2. Some prototypes of electrotechnical devices have been made from HTS-composites of different designs with length of conductor up to 110 meters.

3. (a) The temperature T_N of the onset of superconducting transition is 105–109.5 K in Bi-2223/Ag conductors and 98 K in Bi-2223/(Ag-Ni-Y_2O_3) conductors.

   (b) The maximum J_c were obtained for the 19-filament Bi-2223/Ag conductor:
   J_c (77 K, s.f.) $= 2.3 \cdot 10^4$ A/cm^2, J_c (4.2 K, s.f.) $= 1.0 \cdot 10^5$ A/cm^2,
   J_c (77 K, 1 T)$= 6.9 \cdot 10^3$ A/cm^2, J_c (4.2 K, 1 T)$= 5.5 \cdot 10^4$ A/cm^2,
   J_c (77 K, 4 T)$= 4.6 \cdot 10^2$ A/cm^2, J_c (4.2 K, 4 T)$= 4.0 \cdot 10^4$ A/cm^2.

   (c) The current dispersion for short samples reaches 50% for the monofilament conductor, does not exceed 13% for 19-filament Bi-2223/Ag conductor and 20% for Bi-2223/(Ag-Ni-Y_2O_3) conductor.

   (d) The magnetic field dependencies of the critical current I_c and the parameter n specifying the $V \sim I^n$ curves were obtained. A

19-filament Bi-2223/Ag tape shown the best results in magnetic field. The reduced critical current values $I_c(B)/I_c(0)$ are as follows: $I_c(1\ T)/I_c(0) = 0.94$ and $I_c(4\ T)/I_c(0) = 0.69$ at T=4.2 K, and $I_c(1\ T)/I_c(0) = 0.3$ and $I_c(4\ T)/I_c(0) = 0.02$ at $T = 77$ K.

(e) The resulting n values (15–30) in the zero external magnetic field are close to the values characteristic of Nb_3Sn conductors used for designing magnetic systems. The following n ratios are obtained for the 19-filament Bi-2223/Ag conductor:
$n(4.2\ K, 1\ T)/n(4.2\ K,$ s.f.$) = 0.23$;
$n(4.2\ K, 4\ T)/n(4.2K,$ s.f.$) = 0.076$.

4. The effect of the bending radius on the critical current and parameter n is studied for mono- and multifilament conductors.

5. The measurements on 10-meter wires wound as spirals showed that the I_c of long wires is 53% of the I_c of short samples.

6. The I_c of W&R pancake coils is 10 A at 77 K and 70–100 A at 4.2 K. The magnetic field of a single pancake coil calculated from measured I_c values and coil sizes is 0.015 T. Comparison of pancake coil currents with the $I_c = f(B)$ dependencies taken from the short samples showed that the coil current is 55% of the short samples current. We point out that in accordance with the literature at the present time the current of long length Bi-2223 conductors and coils is 40–80% of short sample.

7. It is revealed the effects of design, methods and regimes of composites processing on current carrying capability. The directions of further studies have been considered.

References

[1] A.D.Nikulin, A.K.Shikov, E.V.Antipova, N.E.Khlebova, I.A.Erokhina, I.I.Akimov. Ultrathin Ceramic Insulation for Ag-Sheathed High Tc-Superconductors. Proc. of 1994 Applied Superconductivity Conference October 16-21,1994. Boston, IEEE, Vol.5 No.2 June 1995 pp. 1842–1844.

[2] C.P. Bean, Phys. Rev. Lett. 8 (1962) 250.

[3] L.M. Fisher, N.V. Il'in, I.F. Voloshin, N.M. Makarov, V.A.Yampol'skii, F. Perez Rodriguez, and R.L. Snyder, Physica C 206 (1993) 195.

[4] P.W. Anderson, Phys. Rev. Lett 9 (1962) 309.

[5] M.R. Beasley, R. Labusch, and W.W. Webb, Phys. Rev. 181 (1969) 682.

[6] R.B. Goldfarb, M. Lelental, C.A. Thompson, published in "Magnetic Susceptibility of Superconductors and Other Spin Systems", Plenum Press, New York (1992).

[7] A.A. Zhukov, V.V. Moshchalkov, SFHT 4 (1991) 850.

[8] M.C. Frischherz, F.M. Sauerzopf, H.W. Weber, M. Murakami, G.A. Emel'chenko, Supercond. Sci. Technol. 8 (1995) 485.

[9] J.R. Cave, A. Fevrier, Hoang Gia Ky, and Y. Laumond, IEEE Trans. Magn. 23 (1987) 1732.

[10] C.M. Bastuscheck, R.A. Buhrman, and J.C. Scott, Phys. Rev. B 24 (1981) 6707.

[11] C. Ebner and D. Stroud, Phys. Rev. B 31 (1985) 165.

[12] P. England, F. Goldie, and A.D. Caplin, J. Phys. F: Met. Phys. 17 (1987) 447.

[13] D.K. Finnemore, R.N. Shelton, J.R. Clem et al., Phys.Rev. B 35 (1987) 5319.

[14] J.W. Ekin, A.I. Braginski, A.J. Panson et al., J. Appl.Phys. 62 (1987) 4821.

[15] H.Dersch, G.Blatter, Phys. Rev. B 38 (1988) 11391.

[16] Sato K., Hikata T., Ueyama M., Mukai H., Shibuta N., Kato T., Masuda T., Cryogenics 31 (1991) 687

[17] Nomura S., Fuke H., Yoshio H., Ando K., Supercond. Sci. Technol. 6 (1993) 858.

[18] Grasso G., Hensel B., Jeremie A., Flukiger R., ASC, Boston, 1994.

[19] Ekin J.W., Adv. Ceram. Mater., 2 (1987) 586.

[20] Dmitriev V.M., Prikhod'ko O.R., Christenko E.V., FNT 15 (1989) 1089.

[21] Hampshire D.P., Jones H., J. Phys. E. Sci. Instrum. 20 (1987) 516.

[22] Frost A.J., Jones H., Beleni I., Cryogenics 32 (1992) 1014.

[23] Friend C.M., Hampshire D.P., Meas. Sci. Technol 6 (1195) 98.

[24] Matthews D.N., Muller K.H., Andrikids K.H., Liu H.K., Dou S.X., Physica C 229 (1994) 402.

[25] Collings E.W., Cryogenics 28 (1988) 724.

[26] Jones H., Cowey L., Dew-Huges, Cryogenics 29 (1989) 795.

[27] Ekin J.W., Appl. Phys. Lett. 55 (1989) 905.

[28] Klimenko E.Yu., Martovetsky N, N., Cryogenics 20 (1982) 367.

[29] Polak M., Hanic F., Hlasnik I., Physica C 156 (1988) 79.

[30] Bungre S.S., Cassidy S.M., Caplin A.D., McAlford N., Button T.W., Supercon. Sci. Technol. 4 (1991) S250.

[31] Ando Y., Motonira N., Kitazawa K., Takeya J., Akita S., Jpn. J. Appl. Phys. 30 (1991) L1635.

[32] Gurevich A., Pashitski A.E., Edelman H.S., Larbalestier D.C., Appl. Phys. Lett. 62 (1993) 1688.

[33] Yu D., Tang J., Zhang D., IEEE Trans. Magn. 25 (1989) 2279.

[34] Larbalestier D.C., Babcock S.E., Cai X.Y., Dorris S.E, Edelman N.S., Gurevich A., Internat. Workshop on SC, 1995, 17, USA.

[35] Mazaki H., Takano M., Kanno R., Takeda Y., Jpn. J. Appl. Phys. 26 (1987) L780.

[36] Khoder A.F., Couach M., Cryogenics 31 (1991) 763.

[37] Yamada W., Satov M., Muraci S., Titamura T., Kamisado W., Adv. in Supercond. 5 (1993) 172.

[38] Sato K., Ohkura K., Hayashi K., Hikata T., Kanako T., Kato T., Ueyama M., Fujikami J., Muranaka K., Kobayashi S., Saga N., Intern. Workshop on SC 1995, 234, USA.

[39] Otto A., Masur L.J., Craven C., Daly D., Podtburg E.R., Shreiber J., Appl. Supercond. Conf., Oct. 16-20, 1994, Boston.

[40] Larbalestier D.C., Cai X.Y., Feng Y., Edelmqan H., Umezawa A., Riley G.N., Jr. and W.L.Carter, Physica C 221 (1994) 299.

[41] Goldfarb R.B., Clark A.F., Braginski A.I., Panson A.I., Cryogenics 27 (1987) 475.

[42] Kozlenkova N.I., Konovalov Yu.V., Skvortsov A.i., Shikov A.K., SFHT 5 (1992) 1309.

[43] Prekul A.F., Rossohin B.A., Volkenshtein H.B., Jurn. Teor. Eksper. Fiz. 67 (1974) 2286.

[44] Fogel N.J., Sidorenko A.s., Ribalkin L.F., J. Teor. Eksper. Fiz. 77 (1979) 236.

[45] Klimenko E, Yu., Bobkov Yu.V., Zastroznov S.I., Kozlenkova N.I., Fiz. Met. Metalov. 59 (1985) 756.

[46] Oda Y., Nakada I., Kohara T., Fujita H., Kaneko T., Toyoda H., Sakagami E., Asayama K., Jpn. J. Appl. Phys. 26 (1987) L481.

[47] Babic E., Kusevic I., Dou S.X., Liiiu H.K., Hu Q.Y., Phys. Rev. B 49 (1994) 15312.

[48] Miller D.J., Steel D, G., Yuan F., Hettinger J.D., Gay K.E., Internat. Workshop on SC., 1995, 234, USA.

[49] Ishida T., Goldfarb R.B., Phys. Rev. B 41 (1990) 8939.

[50] Rollins R.W., Kupfer H., Gey W., J. Appl. Phys. 45 (1974) 5392.

[51] Goldfarb R.B., Minervini J.V, Rev. Sci. Instrum. 55 (1984) 761.

[52] Nara K., Jpn. J. Appl. Phys. 22 (1983) 1815.

[53] Maxwell E., Strongin M., Phys. Rev. Lett. 10 (1963) 212.

[54] Hein R.A., Phys. Rev. B 33 (1986) 7739.

[55] Chu C.W., Huang S., Solid State Comm. 18 (1976) 977.

[56] R.W. McCallum, W.A. Karlsbach, T.S. Padhakrishnan, F.Pobell, R.N. Shelton, Sol. State Commun. 42 (1982) 819.

[57] C.P. Bean, Rev. Mod. Phys. 36 (1964) 31.

[58] A.M.Campbell, J. Phys. C 2 (1969) 1492.

[59] R.W. Rollins, H. Kupfer, W. Gey, J. Appl. Phys. 45 (1974) 5392.

[60] H. Kupfer, I. Apfelstedt, W. Schauer et al., Z. Phys. B 69 (1987) 159.

[61] H. Kupfer, I. Apfelstedt, R. Flukiger et al., Cryogenics 28 (1988) 650; Physica C 153 (1988) 367.

[62] J.R. Cave, M. Mautref, C. Agnoux et al., Cryogenics 29 (1989) 341.

[63] B. Ni, T. Munakata, T. Matsushita, Jpn. J. Appl. Phys 27 (1988) 1658.

[64] T. Matsushita, B. Ni, Jpn. J. Appl. Phys 28 (1989) L419.

[65] F. Gomory, P. Lobotka, Sol. St. Commun. 66 (1988) 645.

[66] S.D. Murpny, K. Renoward, R. Crittenden, S.M. Bhagat, Sol. St. Commun. 69 (1989) 367.

[67] V. Vayes, G.P. Senator, SFHT 3 (1990) 169.

[68] K.H. Muller, Physica C 159 (1989) 717.

[69] V. Calzona, M.R. Cimberle, C. Ferdegnini et al., Physica C 157 (1989) 426.

[70] L. Ji, R.H. Sohn, G.C. Spalding et al., Phys. Rev. B 40 (1989) 10936.

[71] I.F. Voloshin, N.M. Makarov, L.M. Fisher, and V.A. Yampol'skii, JETP Lett. 51 (1990) 225.

[72] L.M. Fisher et al., Phys. Rev. B 46 (1992) 10986.

[73] L.M.Fisher, I.F. Voloshin, V.S. Gorbachev, S.E. Savel'ev, A.V. Kalinov, in "Proc. of the 7th Int. Workshop on Critical Current in Superconductors", Alpbach (1994) p. 439.

[74] L.M. Fisher, A.V. Kalinov, J. Mirkovic, V.M. Soukhov, I.F. Voloshin, presented at Applied Superconductivity, Edinburgh, 3-6 July 1995, p. 263.

[75] L.M. Fisher, A.V. Kalinov, J. Mirkovic, I.F. Voloshin, presented at Fourth Euro-Ceramics, Riccione, 2-6 October 1995, v. 7, p. 99.

[76] L.M. Fisher et al., Appl. Supercond. 2 (1994) 639.

[77] L.M. Fisher, A.V. Kalinov, J. Mirkovic, I.F. Voloshin, A.V. Bondarenko, M.A. Obolenskii, R.L.Snyder, presented at Applied Superconductivity, Edinburgh, 3-6 July 1995, p. 319.

[78] L.M. Fisher, A.V. Kalinov, J. Mirkovic, I.F. Voloshin, A.V. Bondarenko, M.A. Obolenskii, R.L.Snyder, presented at Fourth Euro-Ceramics, Riccione, 2-6 October 1995, v. 7, p. 71.

[79] R.B. Flippen, T.R. Askew, and Ruixing Liang, Physica C 231, 352 (1994).

[80] L.M. Fisher, I.F. Voloshin, S.A. Churin, E.V. Sil'yanov, presented at Applied Superconductivity, Gottingen, 4-9 October, 1993, p. 819.

[81] C.P. Bean, Technical Report Grant 88F034-NYSYS (1991).

[82] L.M. Fisher, I.F. Voloshin, N.M. Makarov, V.A. Yampol'skii, F. Perez Rodrogues, E. Lopez Cruz, presented at Applied Superconductivity, Gottingen, 4-9 October, 1993, p. 815.

[83] L.M. Fisher et al., Appl. Supercond. 2 (1994) 685.

[84] W.W. Webb, J. Appl. Phys. 42 (1971) 107.

[85] C.W. Hagen, R.P. Grissen, E. Salomons, Physica C 157 (1989) 199.

[86] M.R. Cimberle, C.F. Ferdeghini, G.L. Nichiotti et al., Supercond. Sci. Techn. 1 (1988) 30.

[87] G.J. Russel, D.N. Matthews, K.N.R. Taylor, B. Perczuk, Mod. Phys. Lett. B 3 (1989) 437.

[88] F.J. Eberhardt, A.D. Hibbs, A.M. Campbel, IEEE Trans. Magn. 25 (1989) 2146.

[89] A.A.Zhukov, V.V.Moshchalkov, A.A. Bush, Physica C 162 (1989) 1631.

[90] A.A.Zhukov, A.A.Bush, I.V.Gladyshev, Z. Phys. B 78 (1990) 195.

[91] M.Lahtinen, J. Paasi, J. Sarkaniemi, Z. Han, T. Freltoft, Physica C 244 (1995) 115.

[92] N.B. Brandt, L.M. Kovba, V.V. Moshchalkov, JETP 95 (1989) 2021.

[93] L.Ya. Vinnikov, L.A. Gurevich, G.A. Emel'yanenko, Yu.A. Osipian, JETP Lett. 47 (1988) 109.

[94] G.J. Dolan, G.W. Chandrashekhar, T.R. Dinger et al., Phys. Rev. Lett. 62 (1989) 827.

[95] Y. Yamada, M. Sato, S Murase, T. Kitamura, and Y. Kamisada, in Proc. 5th Int. Symp. on Supercond. (ISS92), 717 (1993).

[96] Q.Li, S.Fleshler, P.J.Walsh, M.W.Rupich, W.L.Carter,E.R. Podtburg, and G.N. Riley, in Proc. of ICMC - 1995.

[97] C.Y.Yang, J.G.Wen, Y.F.Yan, and K.K.Fung, Physica C, 160, 161 (1989).

[98] N.I.Kozlenkova, A.D.Nikulin, A.K.Shikov, and V.N.Shishov, Supercond. Sci. Technol. 6, 141 (1993).

[99] H.S. Edelman and D.C. Larbalestier, Adv. Cryogen. Eng., vol.40, Plenum Press, N.Y., 1994.

[100] N. Adamopulos and J.E. Evetts, IEEE Trans. Appl. Supercond. 3, 3533 (1987).

[101] L. A. Dorosinskii *et al.*, *Physica C* **203**, 149 (1992).

[102] V. K. Vlasko-Vlasov, *Phys. Rev. Lett.* **72**, 3246 (1994).

[103] M. Turchinskaya *et al.*, *Physica C* **216**, 205 (1993).

[104] L. A. Dorosinskii, V. I. Nikitenko, A. A. Polyanskii, and V. K. Vlasko-Vlasov, *Physica C* **219**, 81 (1994).

[105] J. A. Parrell, A. A. Polyanskii, A. E. Pashitski, and D. C. Larbalestier, Supercond. Sci. Technol. 9, 393 (1996).

[106] T. Hikata, N. Saga, S. Kobayashi, K. Muranaka, J. Fujikami, M. Ueyama, T. Kato, T. Kaneko, H. Mukai, K. Ohkuura, N. Shibuta, K. Hayashi, and K. Sato in *Proc. 1994 Internat. Cryogenic Material Conf.*, Okt., 1994, Hawaii.

[107] P .Halder, J. G. Hoehn, L. R. Motowidlo, U. Balachandran, Y. Iwasa in *Intern. Cryogenic Mater. Conference*, July 12–16, 1993, Albuquerque, New Mexico.

[108] M. J. Minot, W. L. Carter, J. J. Gannon Jr., R. S. Hamilton *et al.* in *Intern. Cryogenic Mater. Conference*, July 12–16, 1993, Albuquerque, New Mexico.

[109] G.Grasso, B.Hensel, A.Jeremie and R.Flukiger, Transport Properties of Long Monofilamentary Bi(2223) Tapes, Applied Superconductivity Conference, Boston, USA, 1994.

[110] Z. Yi, L. Law, C.Beduz, Y.Yang, R.G.Scuriock, R.Riddle, Transverse inhomogeneities of Pb/BSCCO 2223 tapes from the core-sheath interface to the centre of the core, EUCAS-95, Edinburgh, 3-6 July 1995.

[111] Q. Li, S. Fleshler, P.J.Walch, M.W.Rupich, W.L. Carter, E.R. Potburg, and G.N. Riley, Jr., Jc Performance of Ag sheathed Bi-2223 HTS composite conductors, ICMC, 1995.

Table I. Characteristics of Bi-2223 cryoprecursor.

Average particle size, μm	Content of main phase, % wt.	Content of impurities, x 10^4 % wt.									
		Fe	Al	Si	Ni	Na	Zn	Co	Cr	Mn	C
2,39	30-50, Bi-2212	18	<10	<30	<10	<10	<10	<10	<10	<1	200 ppm

Table II. - Characteristics of composite tapes based on Bi-2223.

Conductor mark	Type of precursor	Cross section, mm^2	Ag: correlation	Number filaments	Lenght, m	Sheath material
L1	$Bi_{1,8}Pb_{0,4}Sr_{2,0}Ca_{2,2}Cu_{3,0}O_x$ "freeze-dried"	0.15x5.0	4:1	1	130	silver
L2	$Bi_{1,8}Pb_{0,4}Sr_{2,0}Ca_{2,2}Cu_{3,0}O_x$ "spray-dried"	0.15x5.0	4:1	1	130	silver
L3*	$Bi_{1,8}Pb_{0,4}Sr_{2,0}Ca_{2,2}Cu_{3,0}O_x$ + 15 % wt.Ag "freeze-dried"	0.15x5.0	3,5:1	1	130	silver
L4	$Bi_{1,8}Pb_{0,4}Sr_{2,0}Ca_{2,2}Cu_{3,0}O_x$ "freeze-dried"	0.17x3.2	4:1	1	90	silver-yttrium-nickel
L5	$Bi_{1,8}Pb_{0,4}Sr_{2,0}Ca_{2,2}Cu_{3,0}O_x$ "freeze-dried"	0.20x4.9	4:1	19	120	silver
L6	$Bi_{1,8}Pb_{0,4}Sr_{2,0}Ca_{2,2}Cu_{3,0}O_x$ "freeze-dried"	0.17x4.9	4:1	19	150	silver-yttrium-nickel

* - silver is introduced to precursor by preparation of $AgNO_3$ solution with following spraying, freeze and pyrolisis of nitrate solutions mixture.

Table III

Characteristics of temperature transitions of different conductors

Wire number	Filaments number	T_{N1}, K	Tmid, K	T_{S1}, K	T_{N2}, K	T_{S2}, K	E_2/E_1
L1	1	105.3	103.7	102.0	43.3	15.1	0.15
L1-g53	1	109.6	104.5	87.6	35.5	4.2	0.2
L2	1	105.8	101.8	92.7	—	—	—
L3	1	102.5	99.9	92.9	45.3	23.4	0.13
L5	19	109.5	100.2	76.7	32.2	18.2	0.04
L6	19	98.1	95.3	92.4	—	—	—

Table IV

The Ic, Jc values at T=77K and T=4.2K (self field) of different conductors

Wire number	Filaments number	Ic, A		Jc, 10^4A/cm^2		Ic, A	Jc,10^4 A/cm^2 core (eng.)
		pressing	rolling	pressing	rolling		
L1	1	30.0±8.0	11.5±2	2.0±0.7	0.8±0.3	50	2.7 (0.7)
L2	1	10.3±0.6	8.0±2	1.5±0.1	0.8±0.4	38	2.0 (0.5)
L3	1	18.8±1.1	12.0±2	1.2±0.1	0.8±0.3	50	2.6 (0.5)
L5	19	34.5±1.5	25.3±7.3	2.9±0.1	2.3±0.3	132	10.3 (1.3)
L6	19	21.9±2.2	16.7±1.2	1.2±0.1	1.0±0.2	127	9.8 (1.5)
T=77 K						T=4.2 K	

Table V

The comparison of conductors on Ic(B)/Ic(0) — parameter

Wire number	B ∥ tape plate				B ⊥ tape plate	
	T=77K		T=4.2K		T=4.2K	
	Ic(1T) /Ic(0)	Ic(4T) /Ic(0)	Ic(1T) /Ic(0)	Ic(4T) /Ic(0)	Ic(1T) /Ic(0)	Ic(4T) /Ic(0)
L1	0.09		0.54	0.39		
L2	0.06	0.009	0.29	0.19		
L3	0.08		0.39	0.30		
L5	0.3	0.02	0.55	0.40	0.32	0.29
L6	0.08	0.002	0.53	0.39		

Table VI

The Ic distribution over the length of a 10-m L2 conductor

Number	1	2	3	4	5	6	7	8
Ic, A	5.6	4.3	9.3	2.5	9.6	4.5	11.9	12.5

Table VII

Transport Ic results (77K, and 4.2K, self field) of long lengths conductors

Wire number	Sample number	Article	Length, m	Turn number	Diameter,mm inner	outer	Ic(77K),A	Ic(4.2K),A
L1	1	Pancake coil (3 piece of tape)	3 piece on 5m in parallel Lsu=15m	70	15	55	9.8	
	2	5-stacked pancake coil	50	60	25	45	4.7	60
L2	1	Spiral	10				8.5	
L3	1	Spiral	40				4.5	
L5	1	Pancake coil W&R	8	60	15	40	8.4	
	2	Pancake coil W&R	5.5	50	35	55	10	
	3	Pancake coil W&R	6	50	35	55	10	
	5-1	Pancake coil W&R	10	70	15	45	8	70
	5-2	Pancake coil W&R	10	70	15	45	7.3	
	5-3	Pancake coil W&R	10	70	15	45	6.0	70
	5-4	Pancake coil W&R	10	70	15	45	7.0	84
	5-5	Pancake coil W&R	10	70	15	45	8.3	87
	5-6	Pancake coil W&R	10	70	15	45	7.8	77
	5-7	Pancake coil W&R	10	70	15	45	7.8	85
	5-8	Pancake coil W&R	10	70	15	45	10	100
	4	Pancake coil R&W	10	102	19	60	3.0	
L6	1	Double pancake coil ("racetrack")	110	110			7.3	

"freeze-dried" precursor

"spray-dried" precursor

Figure 1. Precursors of diffirent types

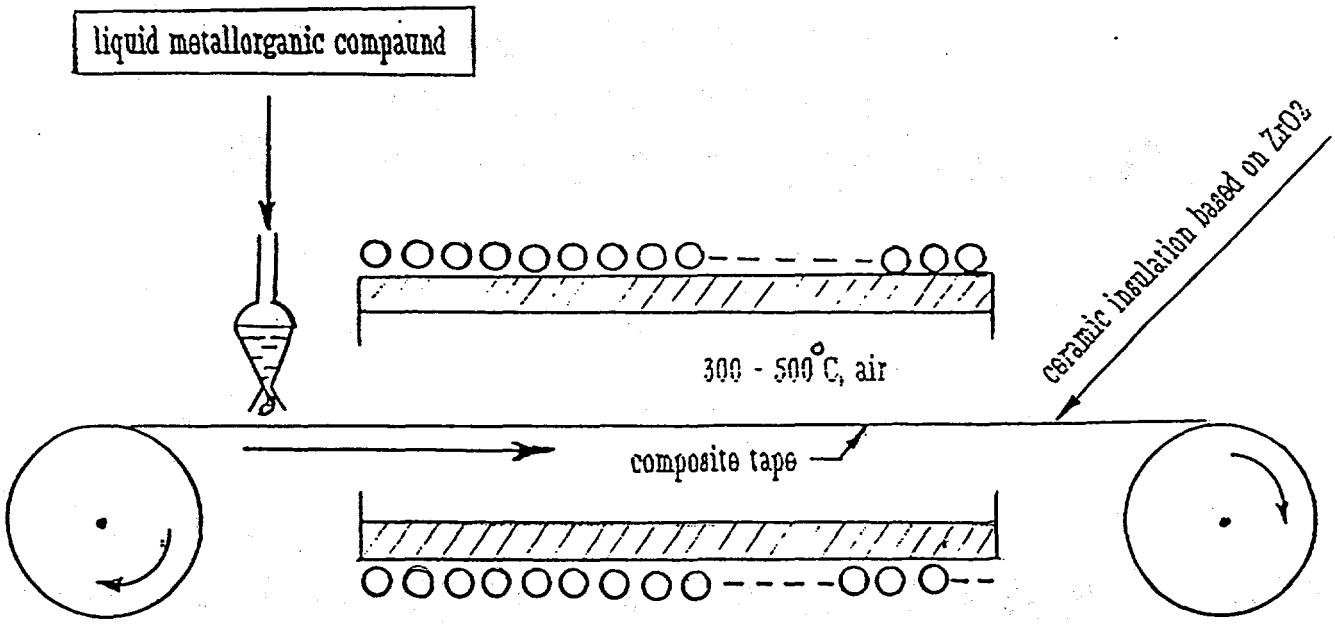

Figure 2. Insulating process.

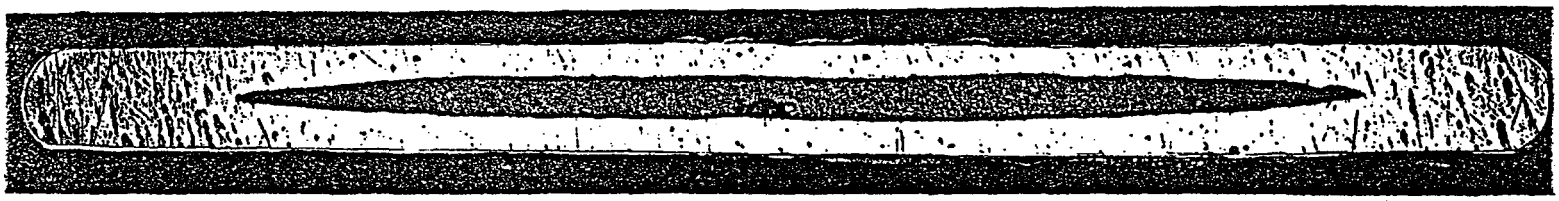

monofilamentary Bi-2223/Ag tape
x 50

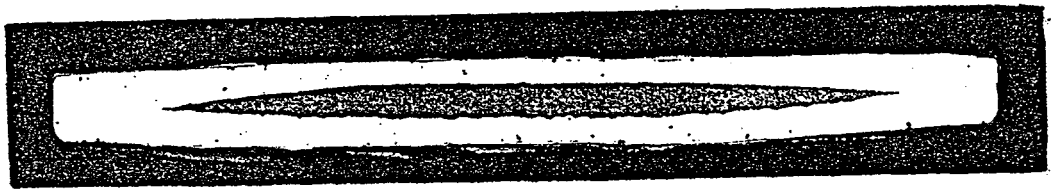

monofilamentary Bi-2223/Ag-Ni-Y
x 50

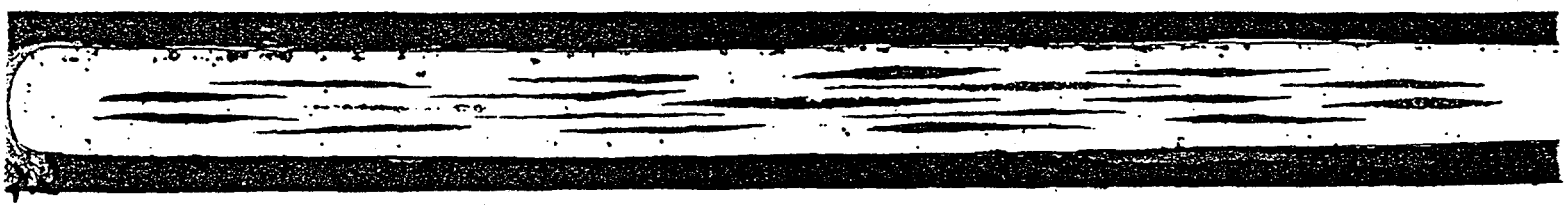

19-filamentary Bi-2223/Ag
x 50

Figure 3. Cross sections of Bi-2223 tapes

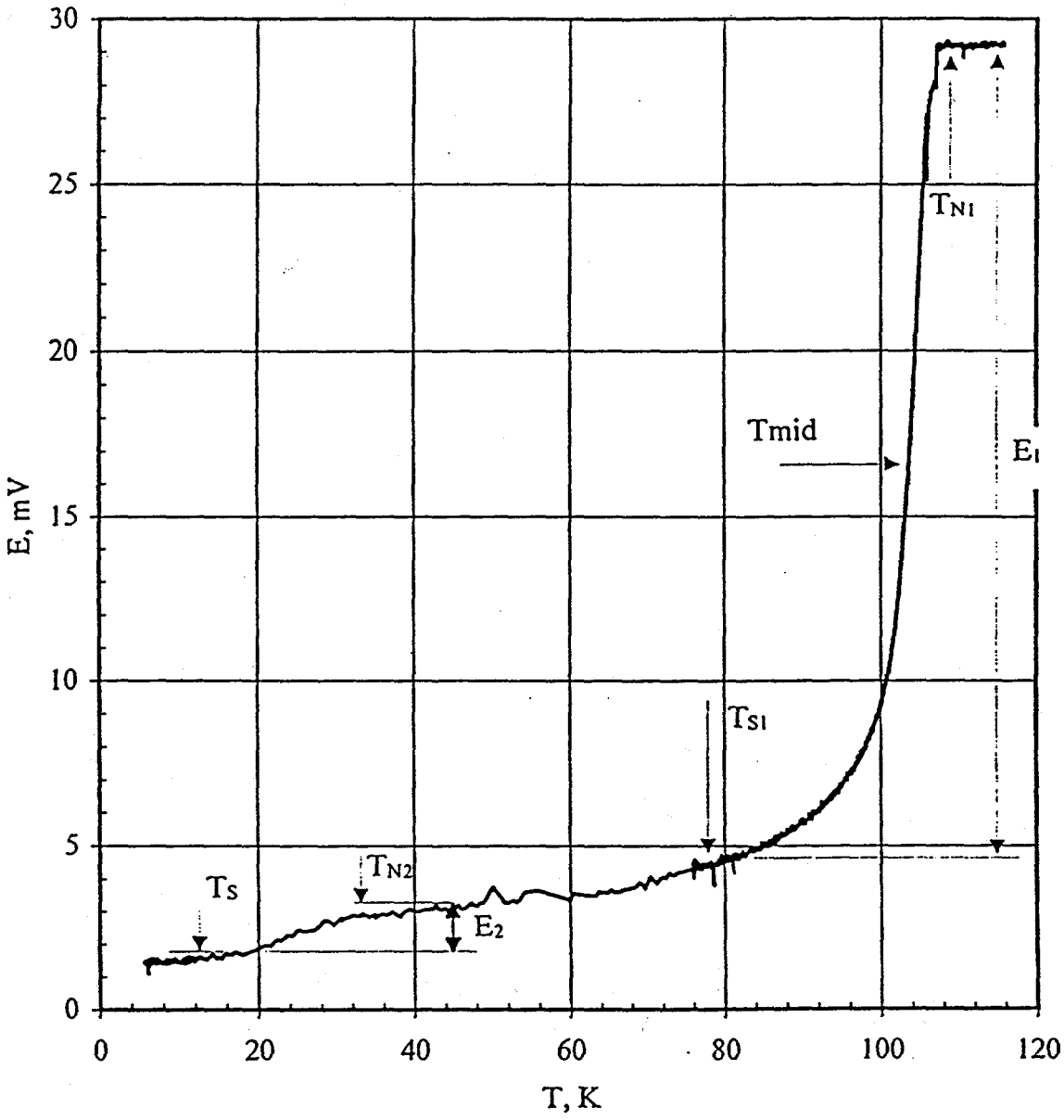

Fig. 4. The transition temperature profile of sample Bi-2223/Ag

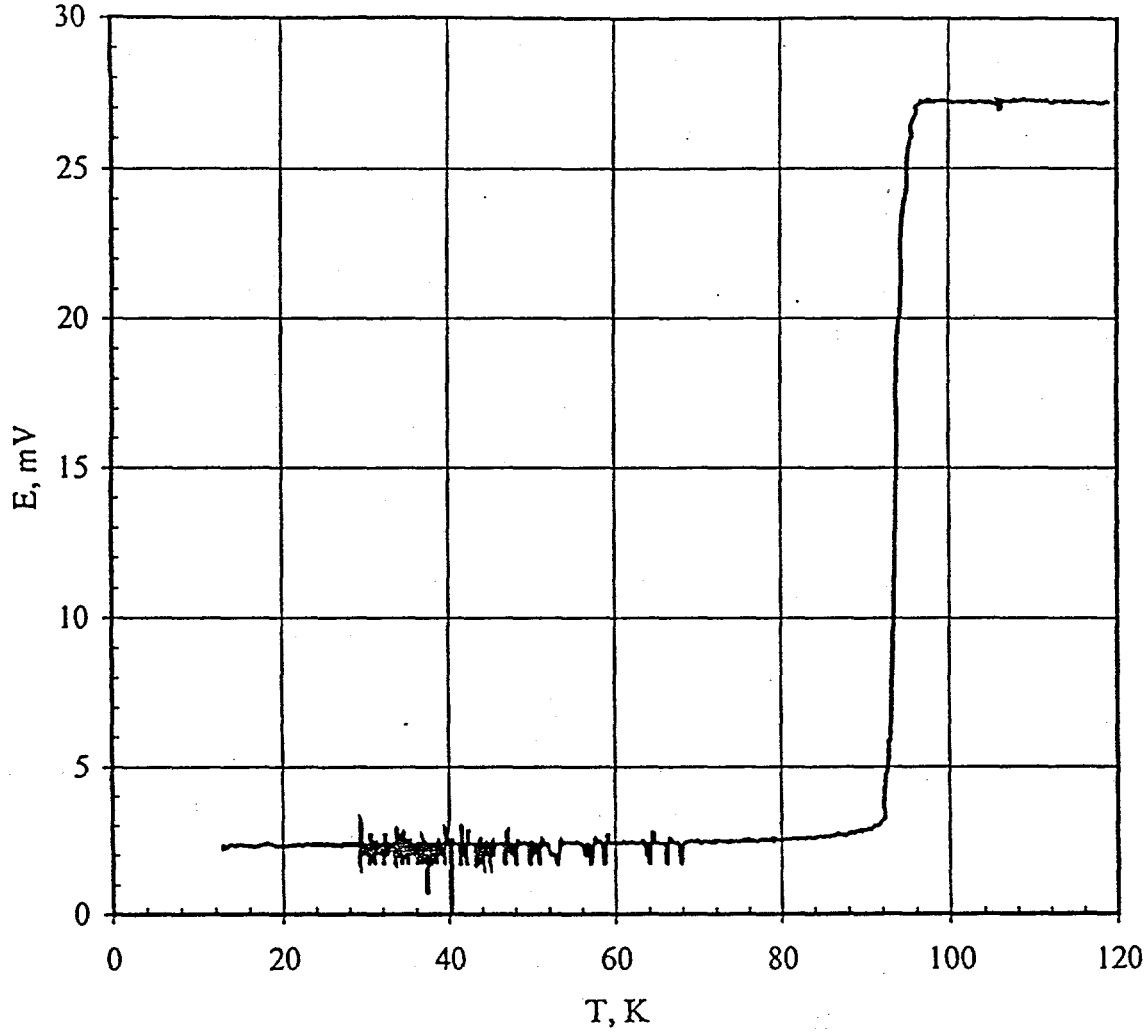

Fig. 5. The transition temperature profile of sample Bi-2223/(Ag + Ni,Y_2O_3)

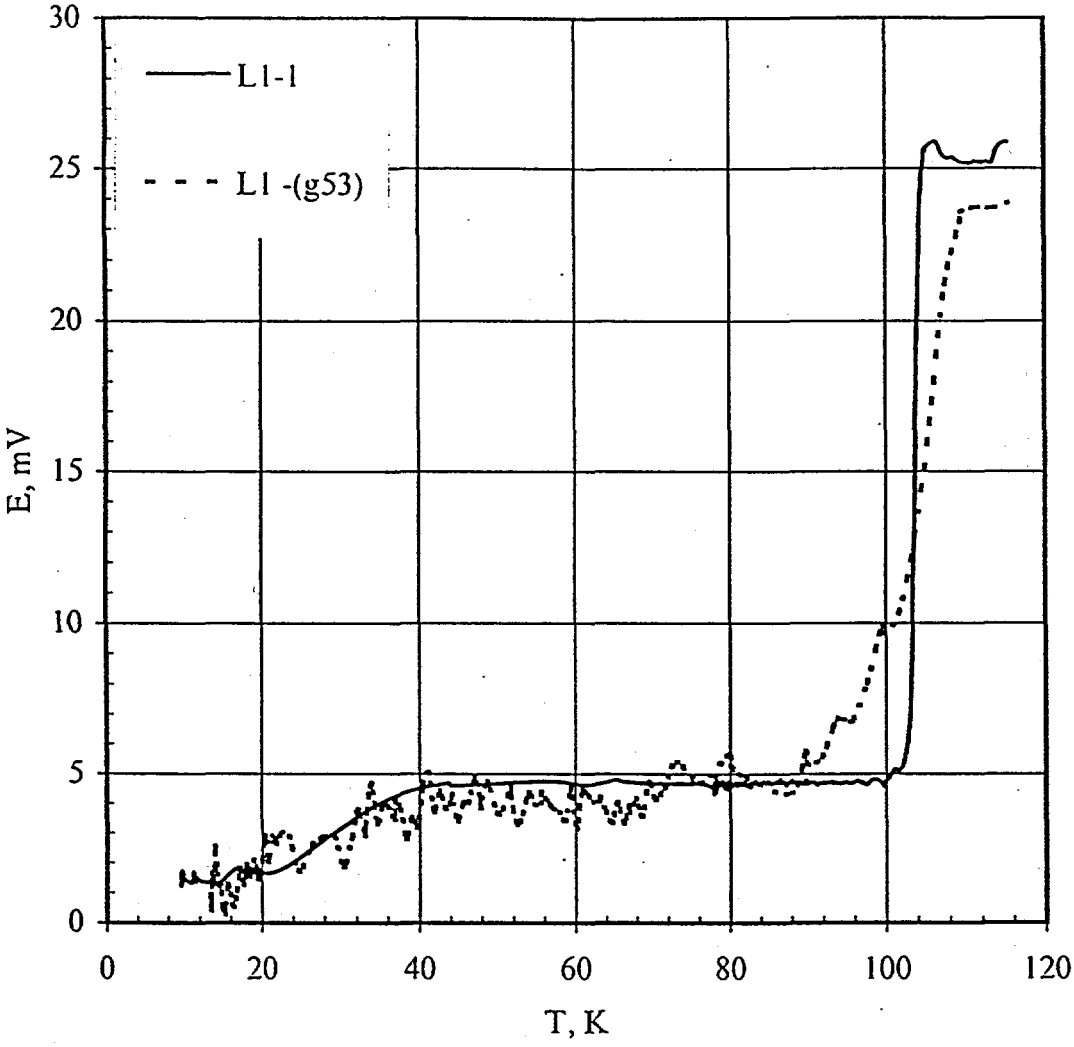

Fig. 6a. The transition temperature profile of samples L1-1, L1-g53.

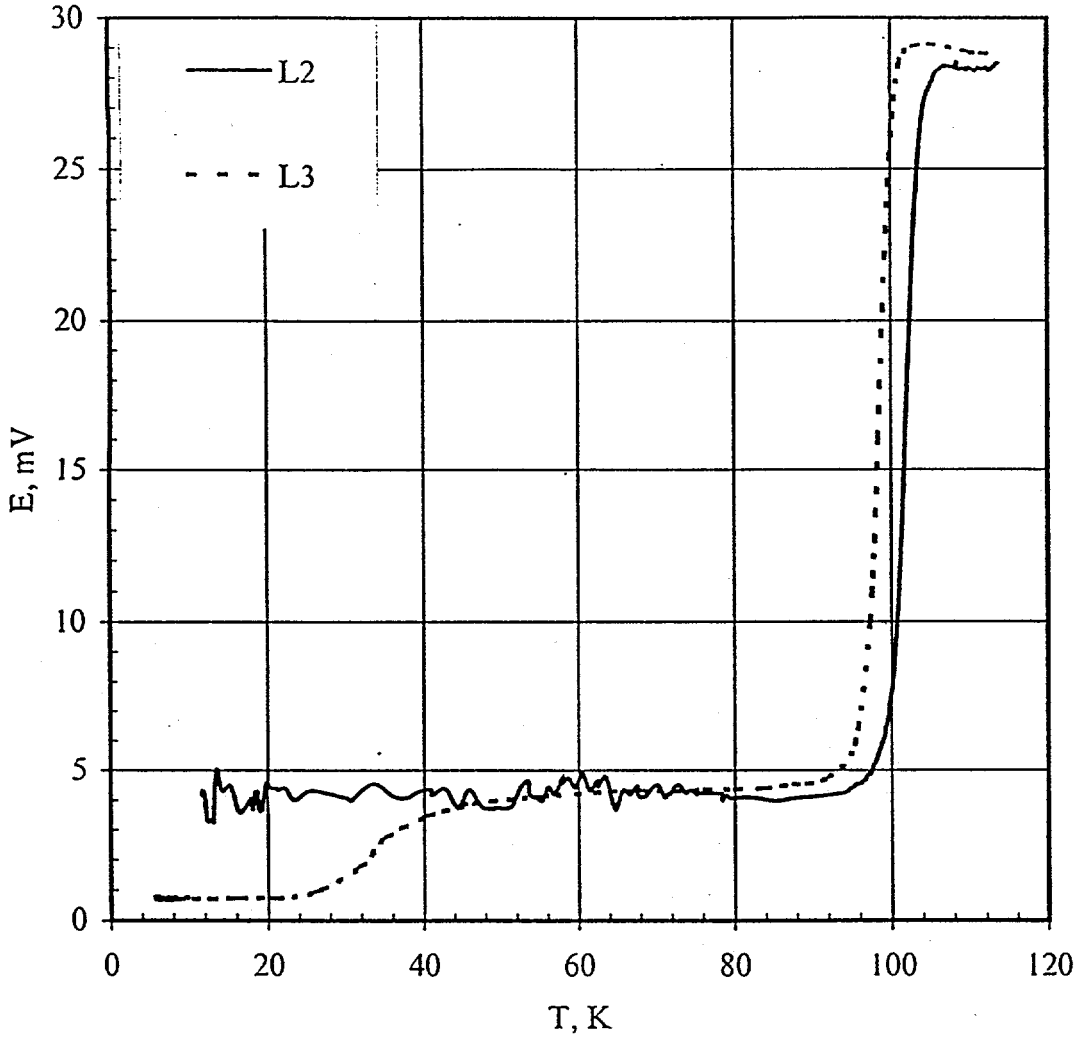

Fig. 6b. The transition temperature profile of samples L2, L3.

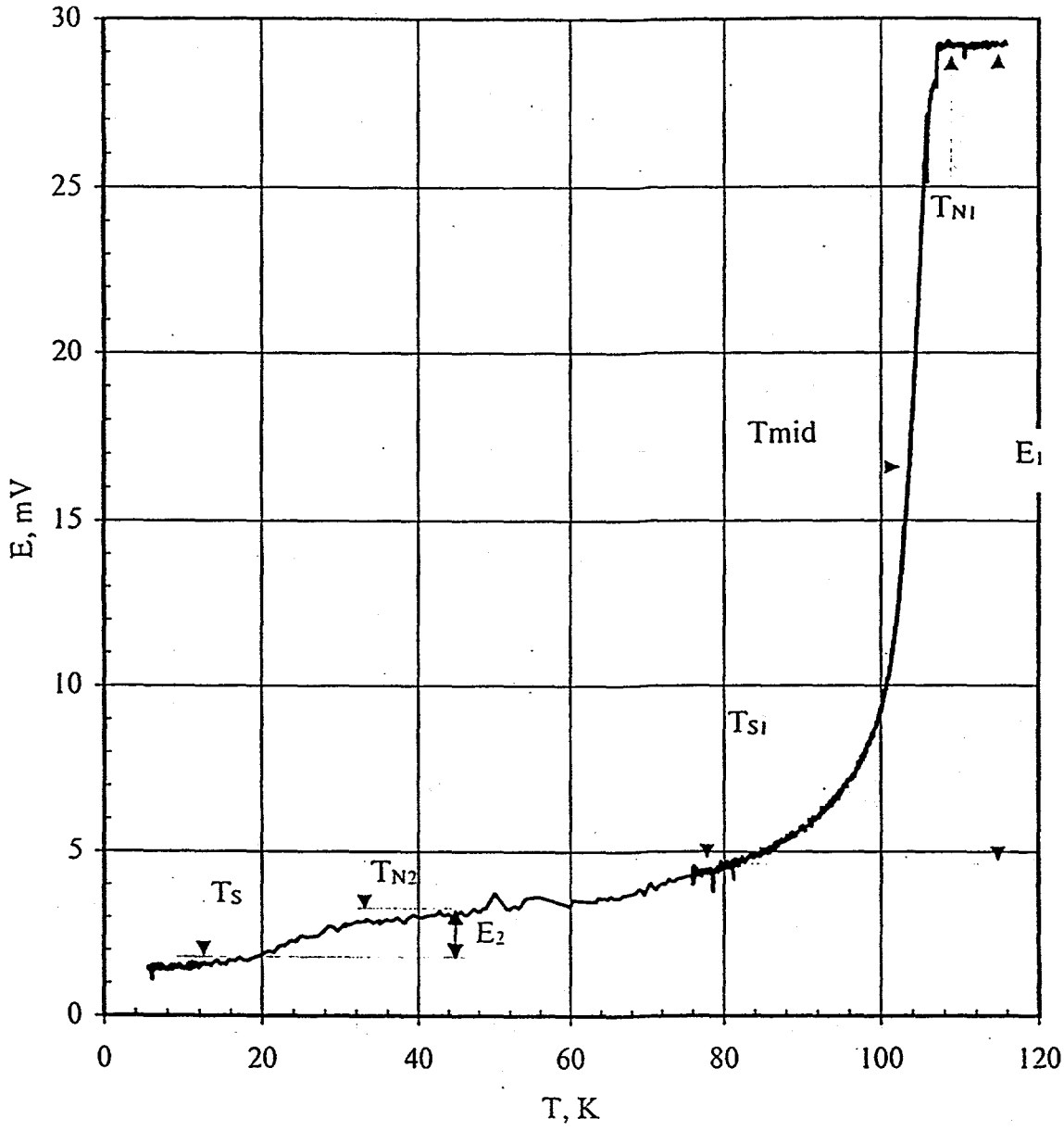

Fig. 6c. The transition temperature profile of sample Bi-2223/Ag (L5)

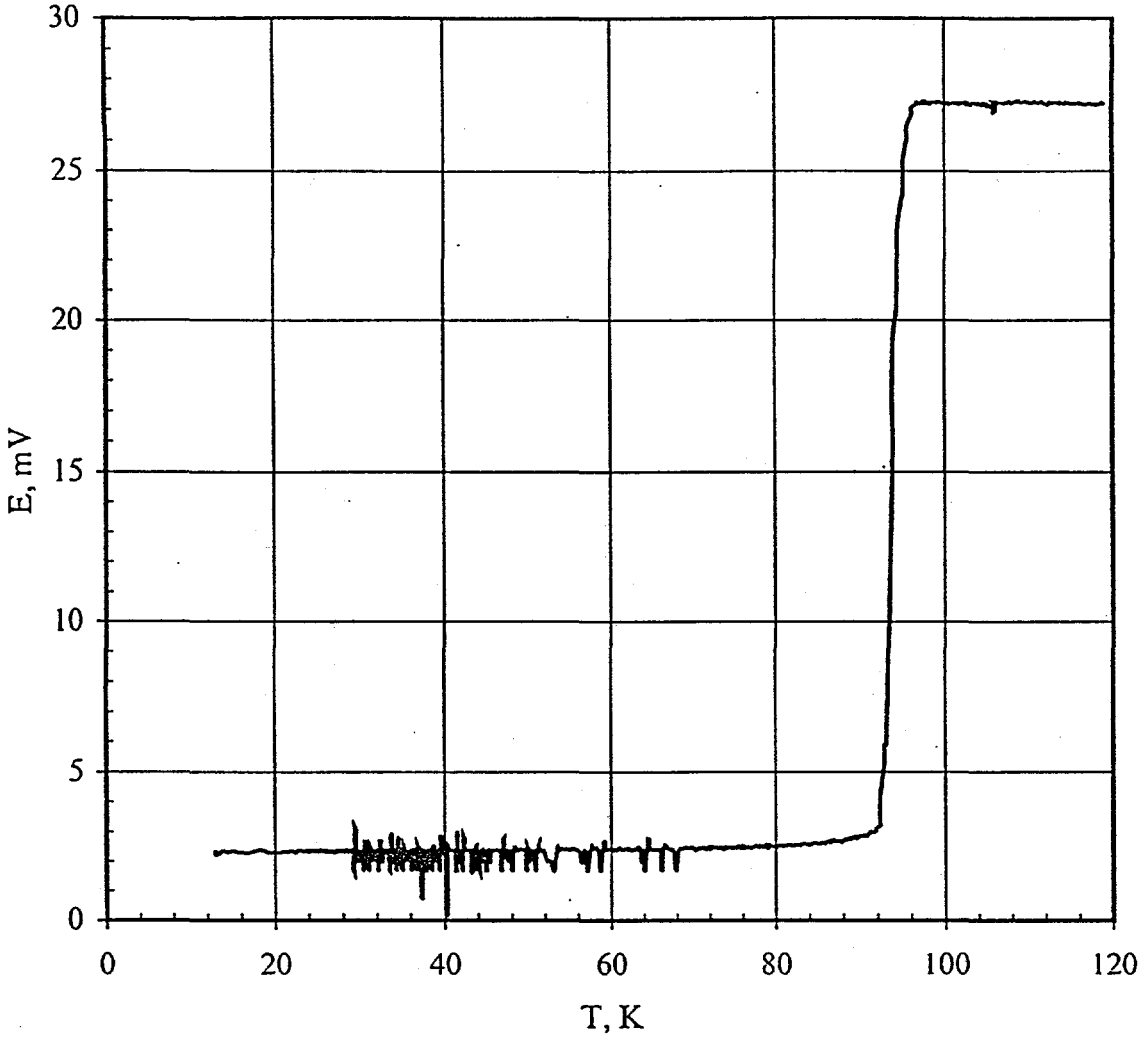

Fig. 6d. The transition temperature profile of sample Bi-2223/(Ag + Ni, Y_2O_3) (L6)

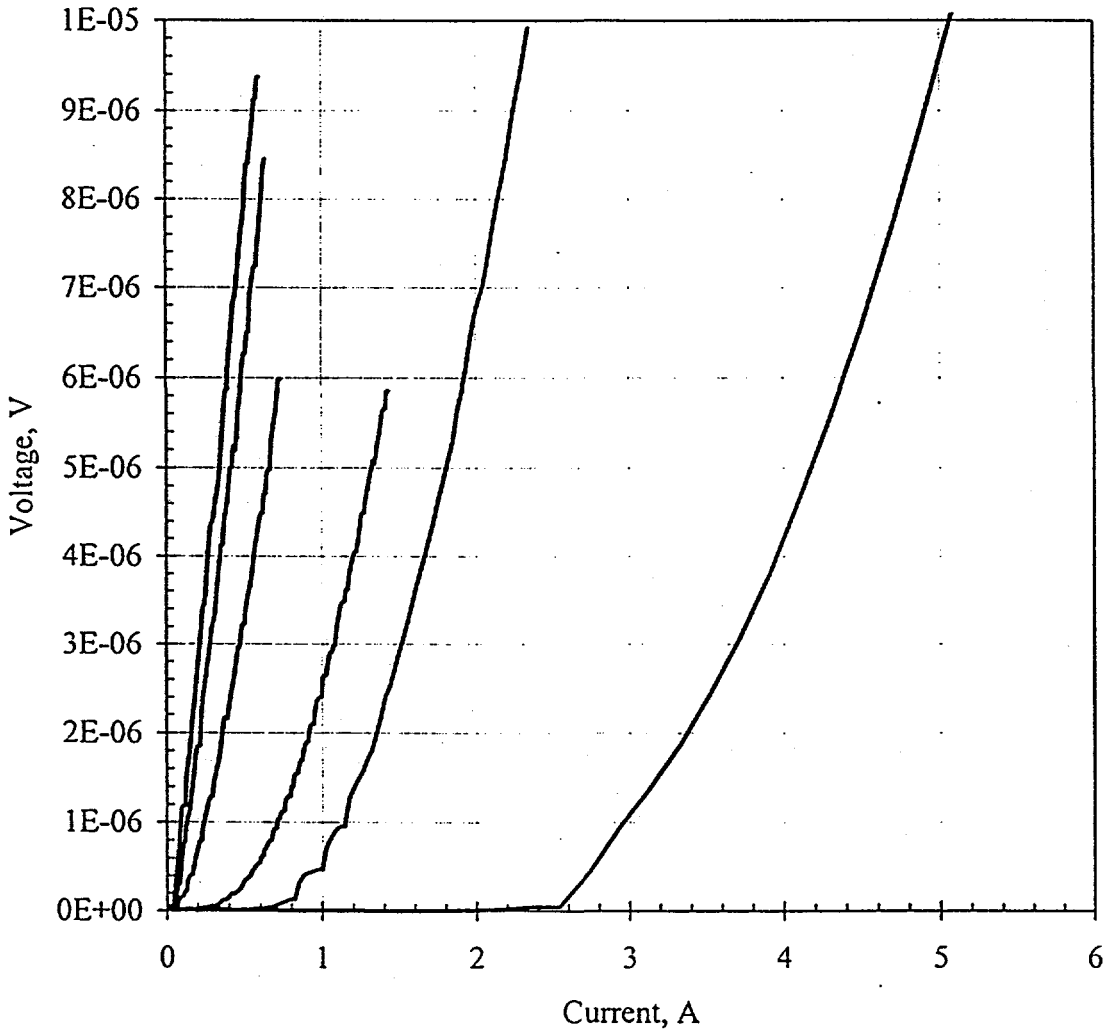

Fig. 7a. The VCC as a function of magnetic field (B|| tape plate) at 77K for L1 conductor. Magnetic field: 0, 0.5, 1.0, 2.0, 3.0, and 4.0T respectively.

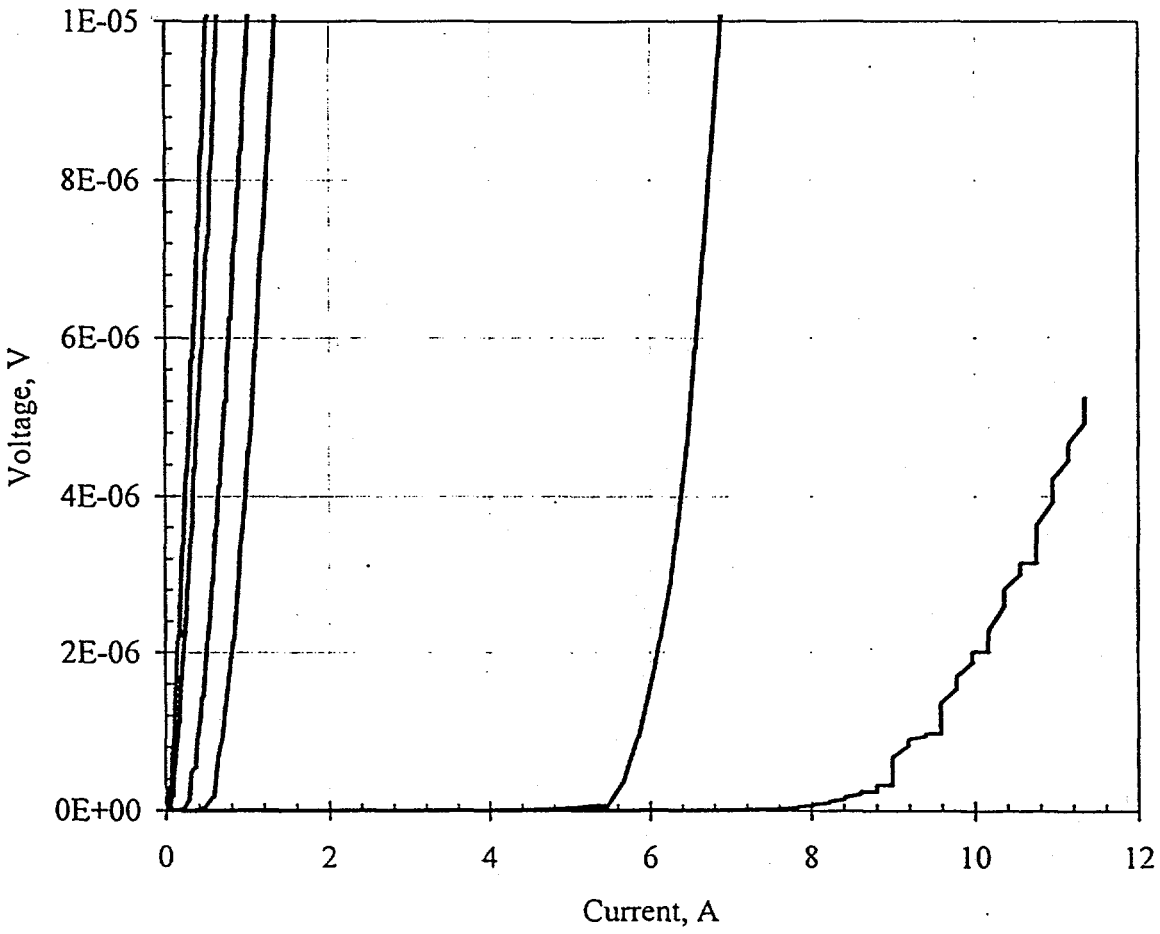

Fig. 7b. The VCC as a function of magnetic field (B|| tape plate) at 77K for L2 conductor. Magnetic field: 0, residual field, 0.5, 1.0, 2.0, and 3.0T respectively.

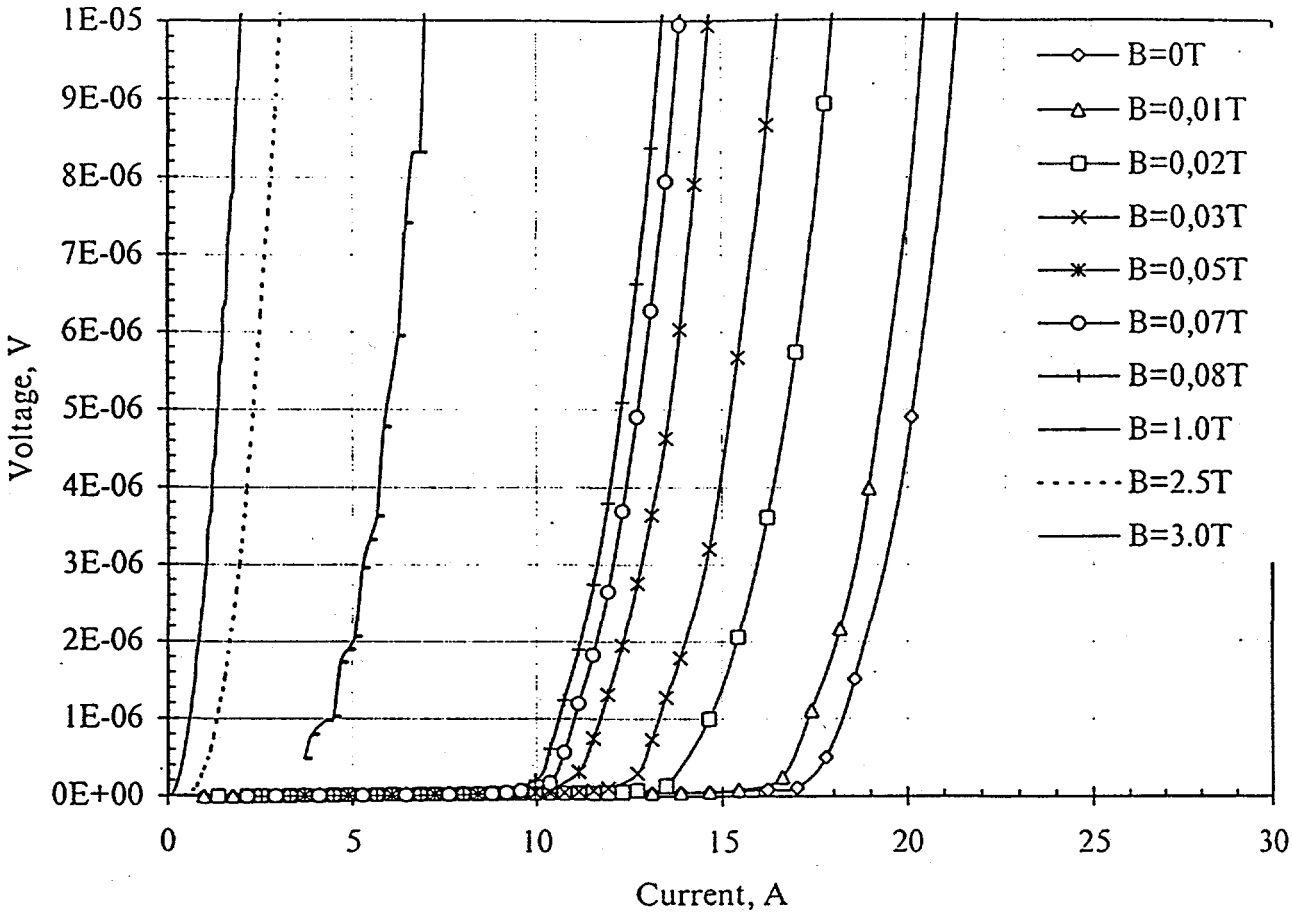

Fig. 7d. The VCC as a function of magnetic field (B || tape plate) at T=77K for 19-filament conductor (L5) BiPb-2223 /Ag.

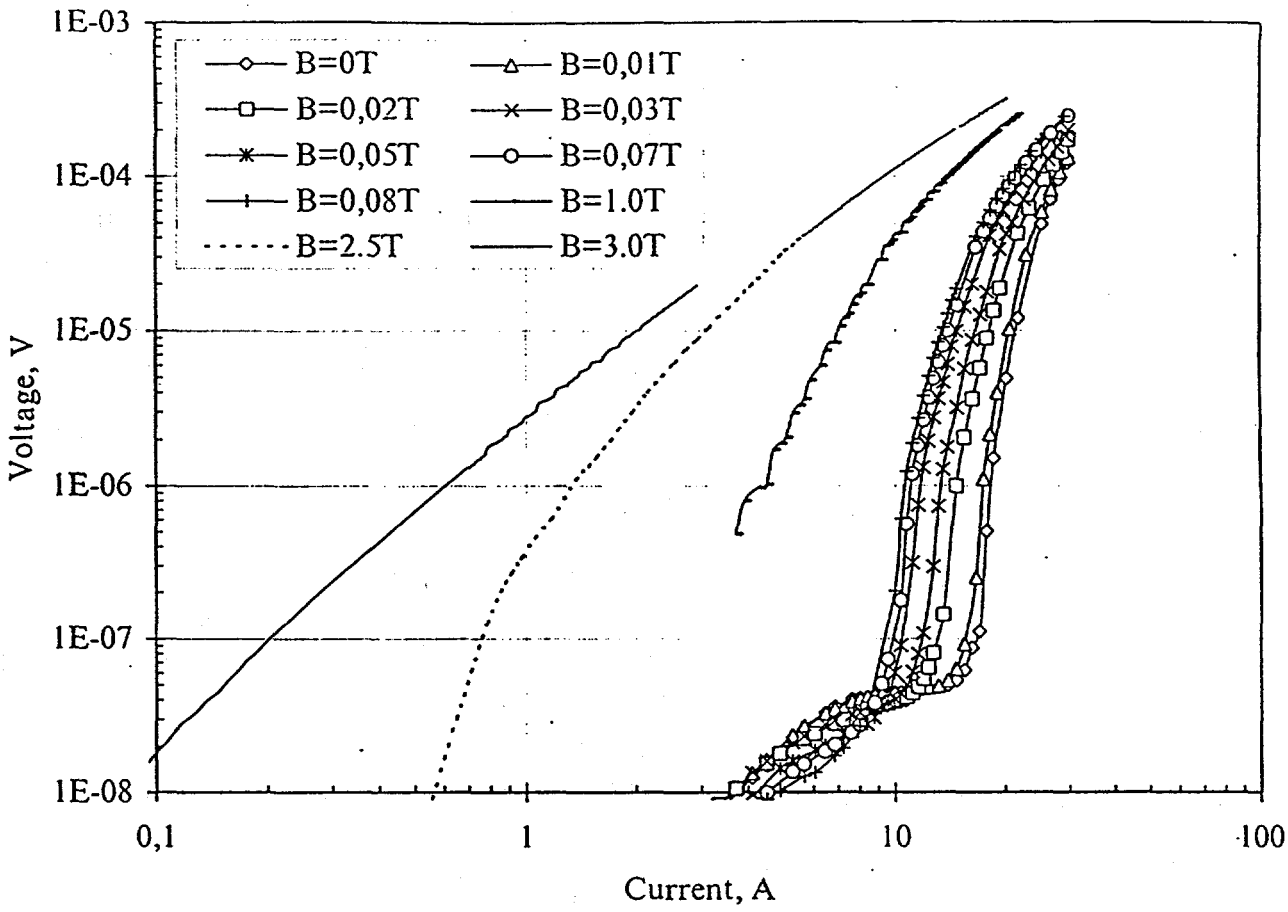

Fig. 7e. The VCC as a function of magnetic field (B || tape plate) at T=77K for 19-filament conductor (L5) BiPb-2223 /Ag.

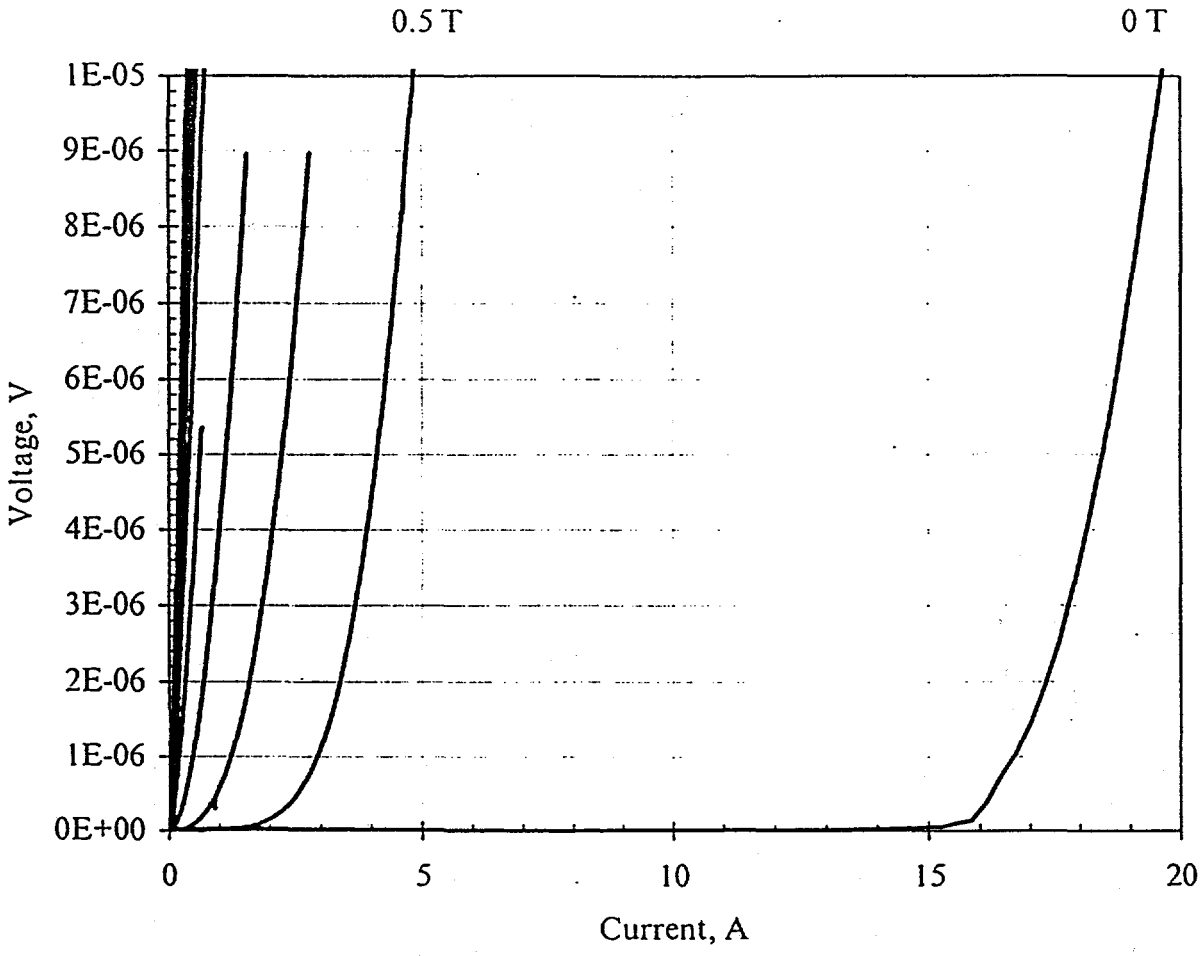

Fig. 7f. The VCC as a function of magnetic field (B || tape plate) at T=77K for 19-filament conductor (L6) BiPb-2223 /(Ag + Ni,Y_2O_3). Magnetic field: 0, 0.5, 1.0, 1.5, 2.0, 2.5, 3.0, 3.5, and 4.0T respectively.

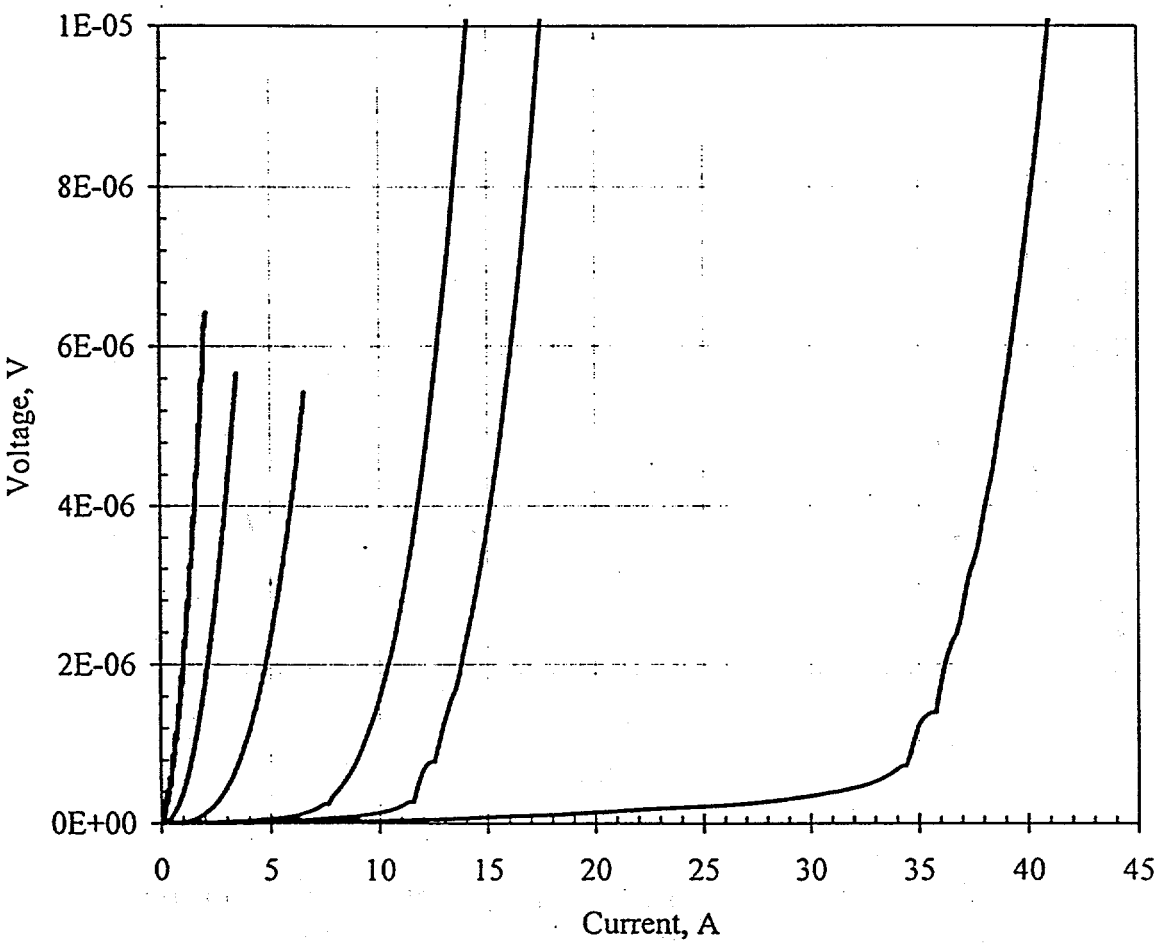

Fig. 7g. The VCC as a function of magnetic field (B|| tape plate) at 77K for 61-filament conductor. Magnetic field: 0, 0.5, 1.0, 2.0, 3.0, and 4.0T respectively.

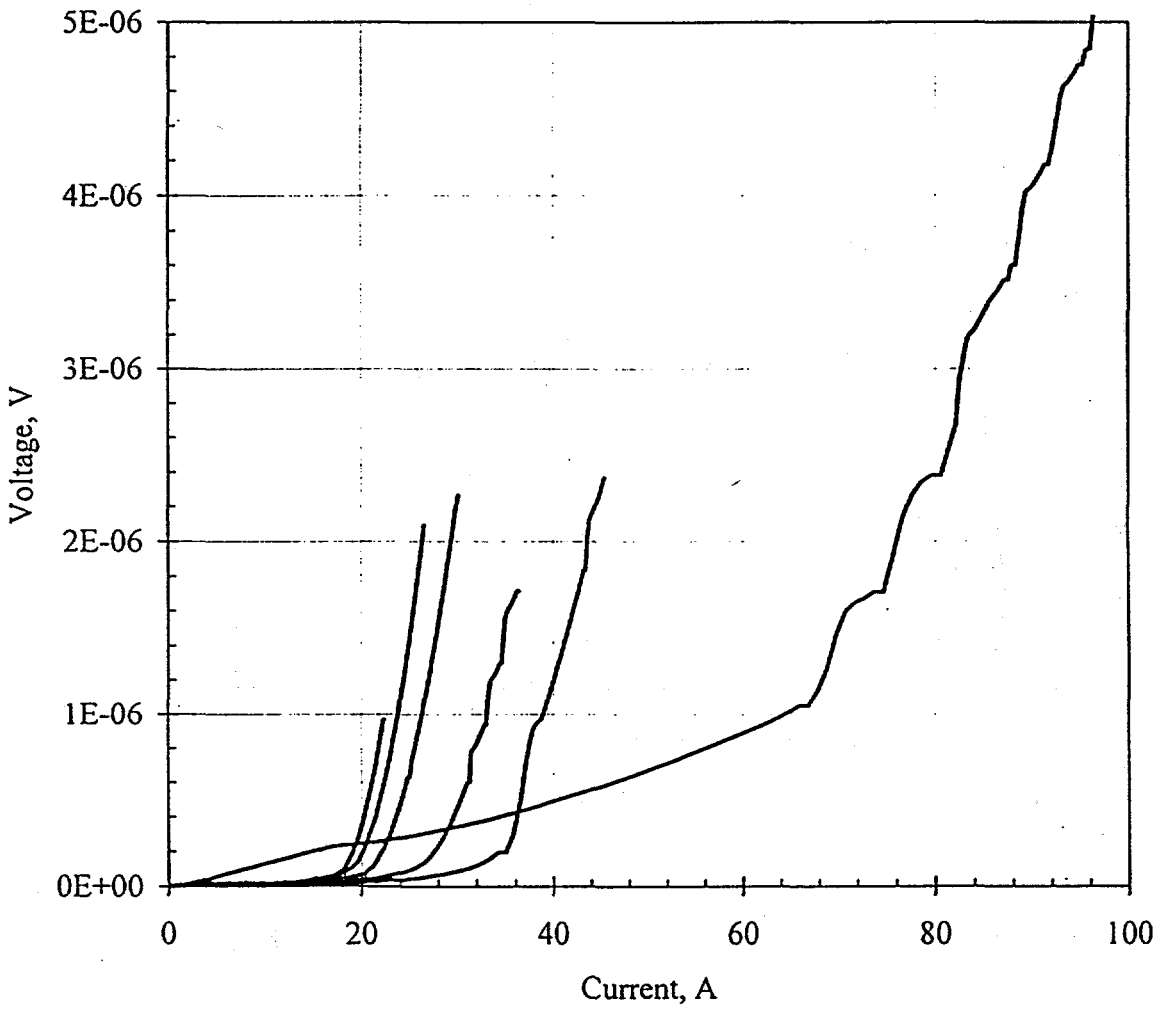

Fig. 8a. The VCC as a function of magnetic field (B|| tape plate) at 4.2K for L1 conductor. Magnetic field: 0, 0.5, 1.0, 2.0, 3.0, and 4.0T respectively.

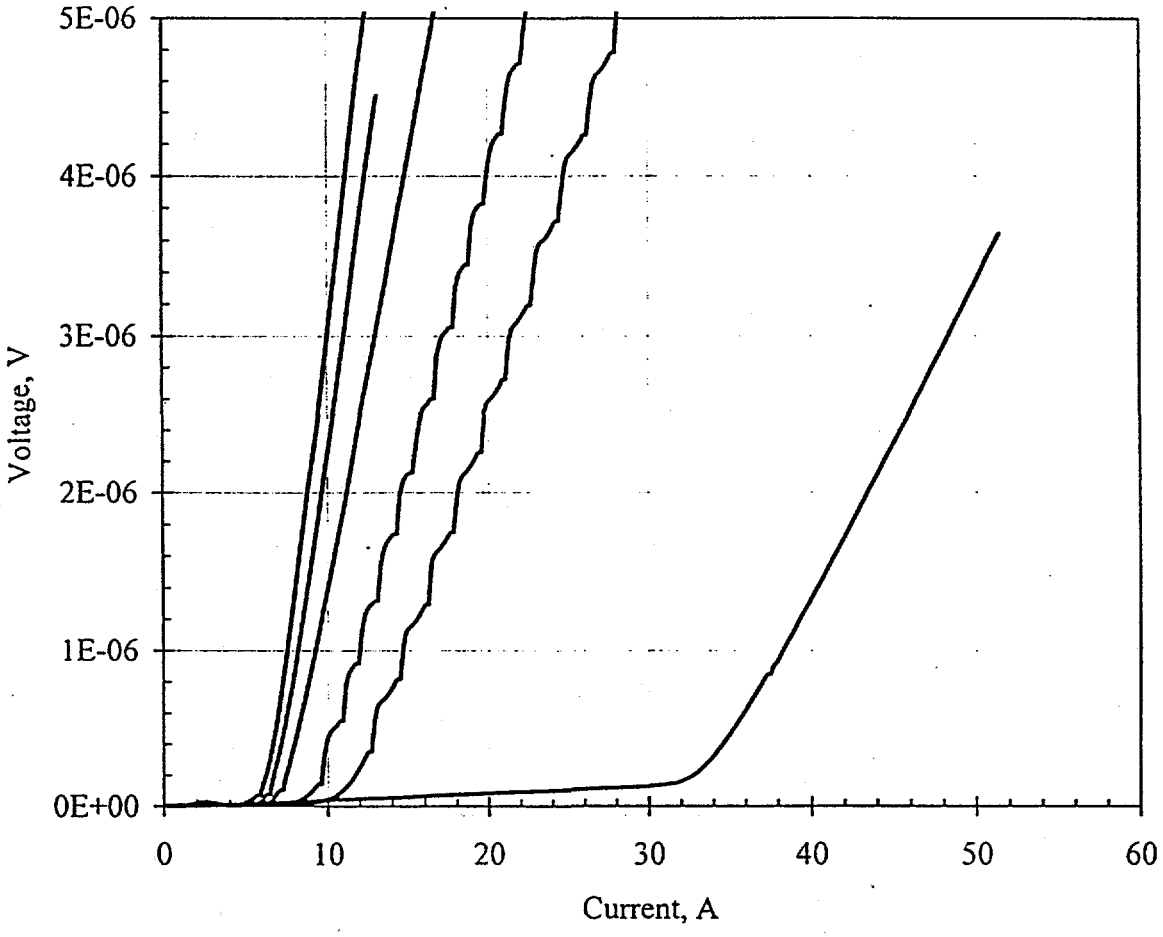

Fig. 8b. The VCC as a function of magnetic field (B|| tape plate) at 4.2K for L2 conductor. Magnetic field: 0, 0.5, 1.0, 2.0, 3.0, and 4.0T respectively.

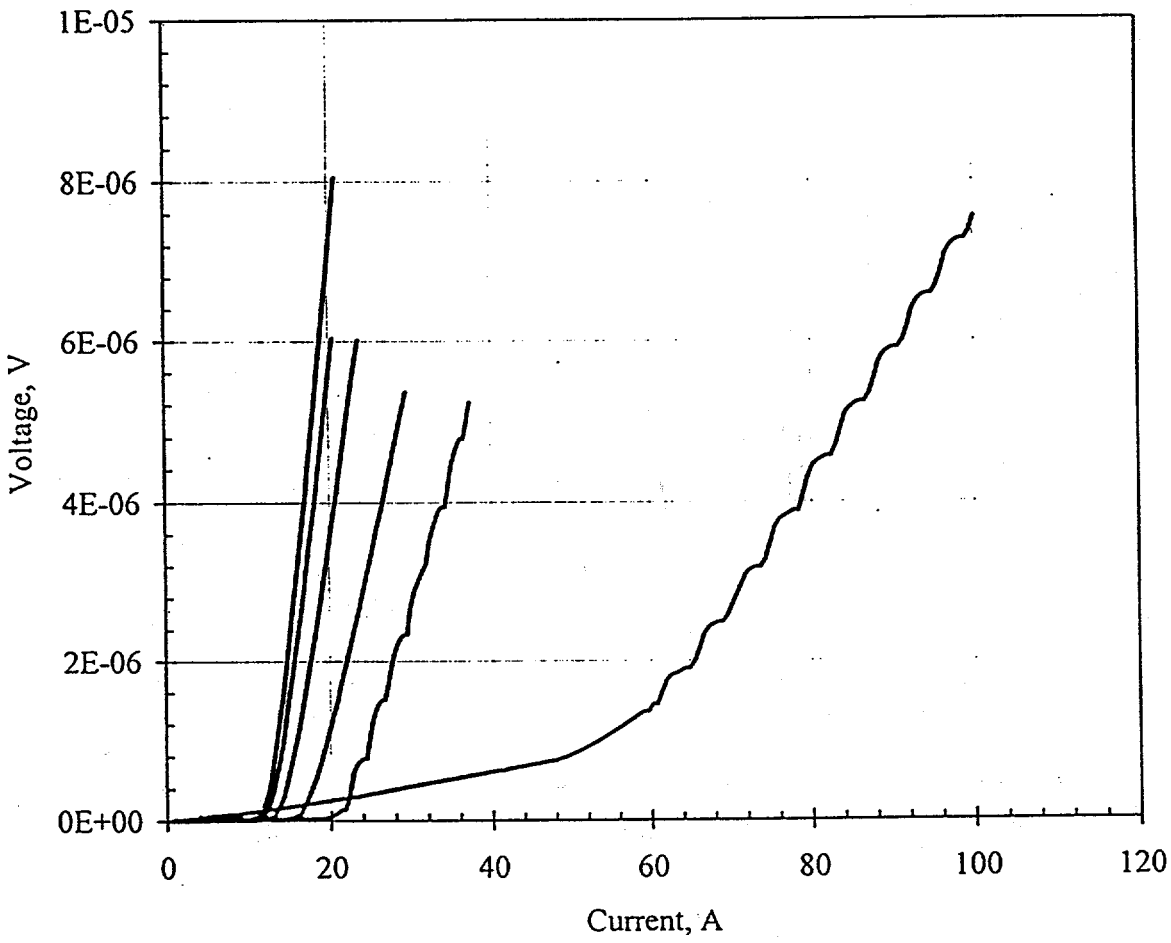

Fig. 8c. The VCC as a function of magnetic field (B|| tape plate) at 4.2K for L3 conductor. Magnetic field: 0, 0.5, 1.0, 2.0, 3.0, and 4.0T respectively.

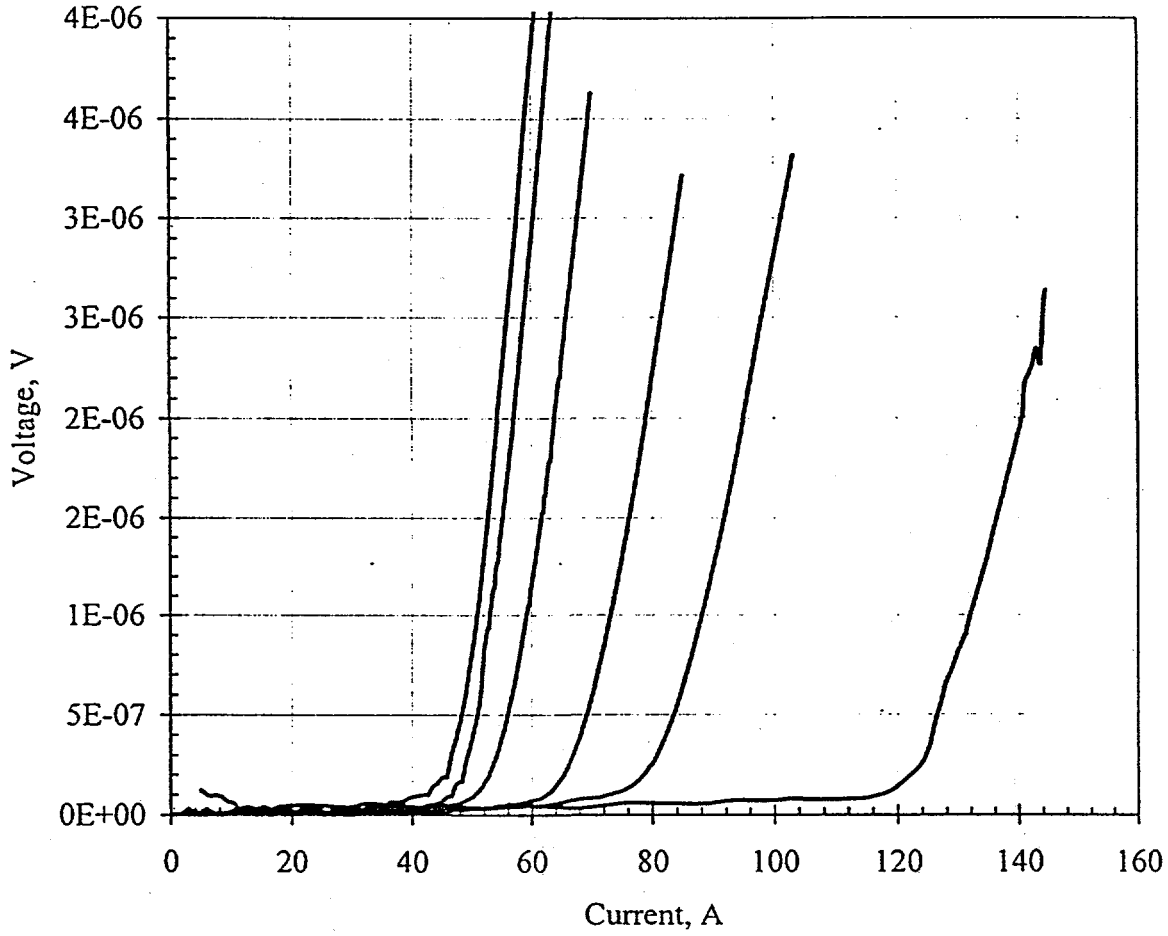

Fig. 8d. The VCC as a function of magnetic field (B|| tape plate) at 4.2K for L5 conductor. Magnetic field: 0, 0.5, 1.0, 2.0, 3.0, and 4.0T respectively.

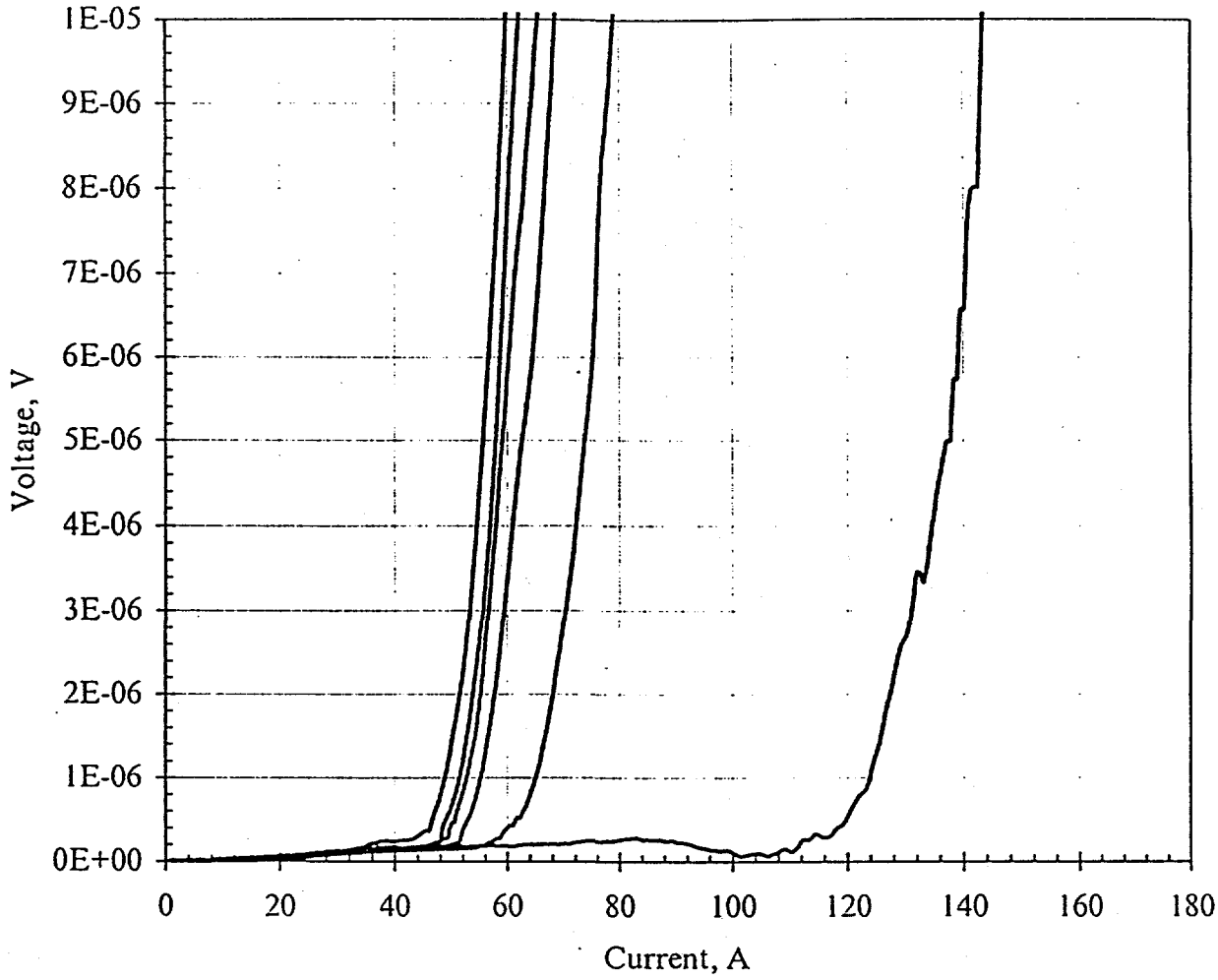

Fig. 8e. The VCC as a function of magnetic field (B || tape plate) at T=4.2K for 19-filament conductor (L6) BiPb-2223 /(Ag + Ni,Y_2O_3). Magnetic field: 0, 1.0, 2.0, 2.5, 3.0, and 4.0T respectively.

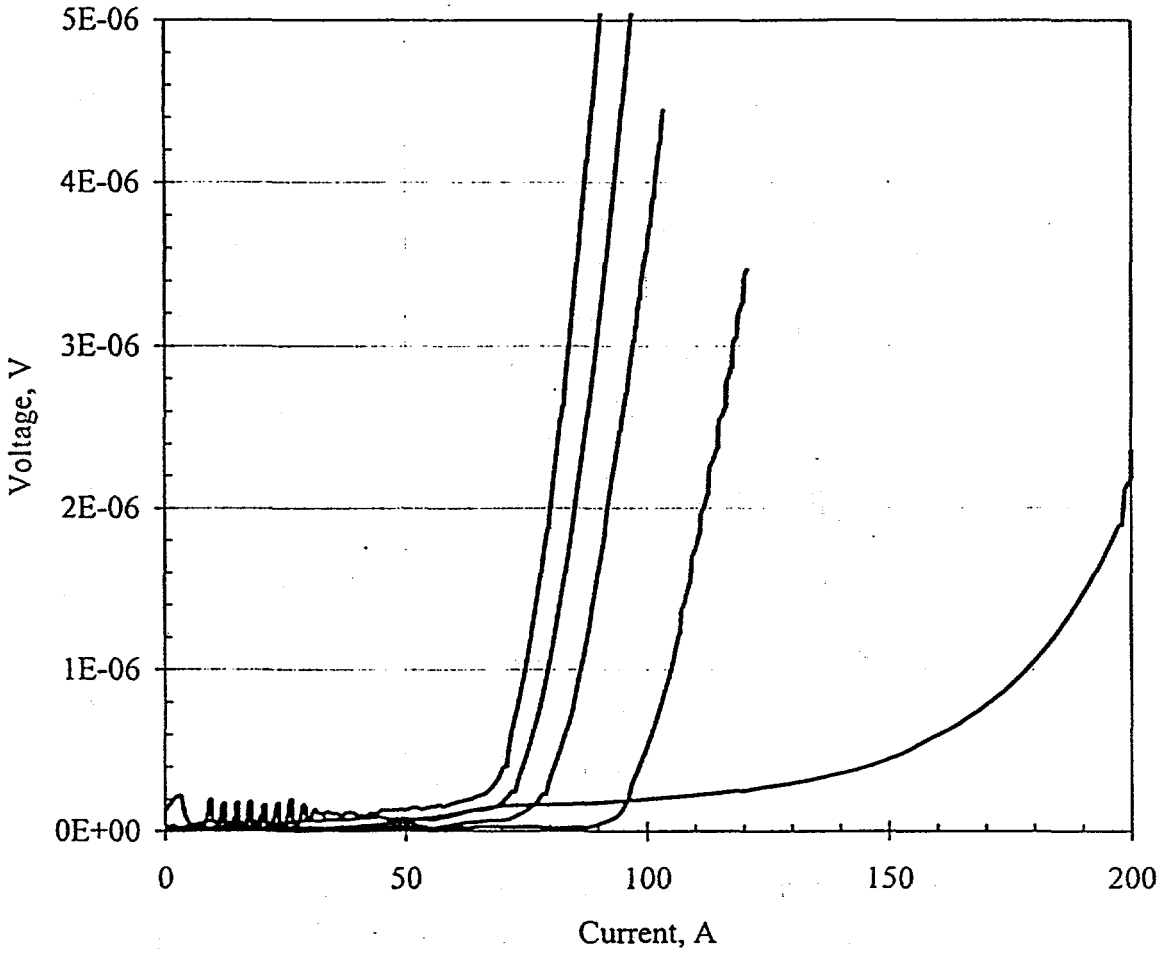

Fig. 8g. The VCC as a function of magnetic field (B|| tape plate) at 4.2K for 61-fil. conductor. Magnetic field: 0, 1.0, 2.0, 3.0, and 4.0T respectively.

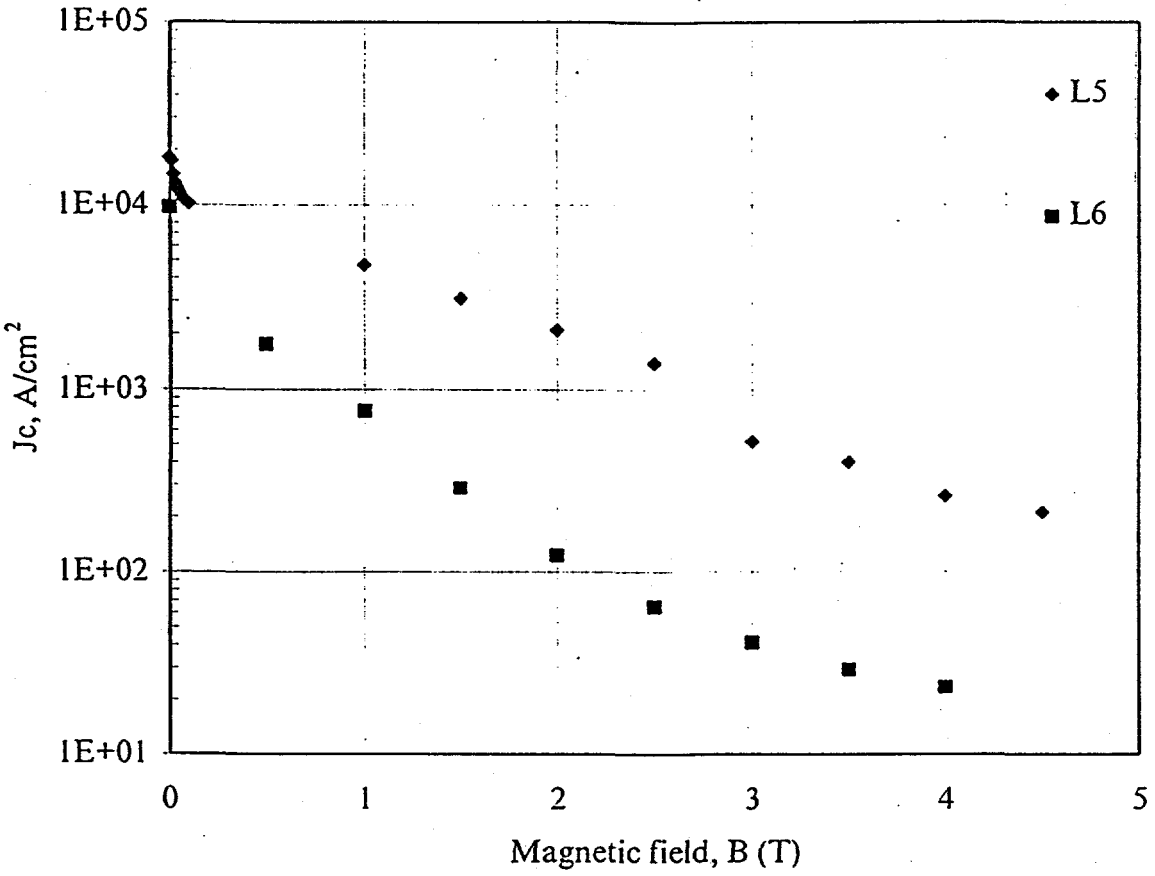

Fig. 9a The critical current density as a function of magnetic field (B || tape plate) at T=77K for Bi-2223 tapes

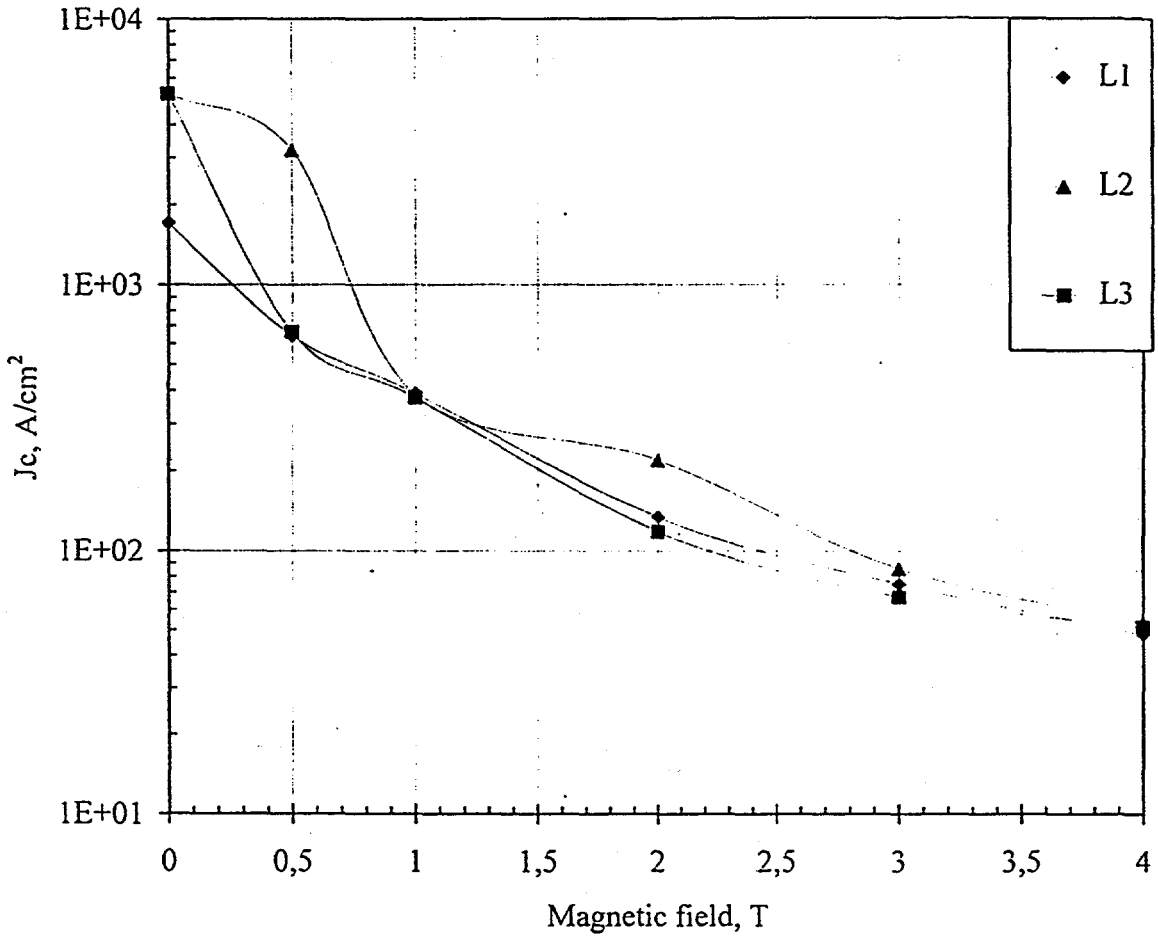

Fig. 9b The critical current density as a function of magnetic field (B || tape plate) at T=77K for Bi-2223 tapes

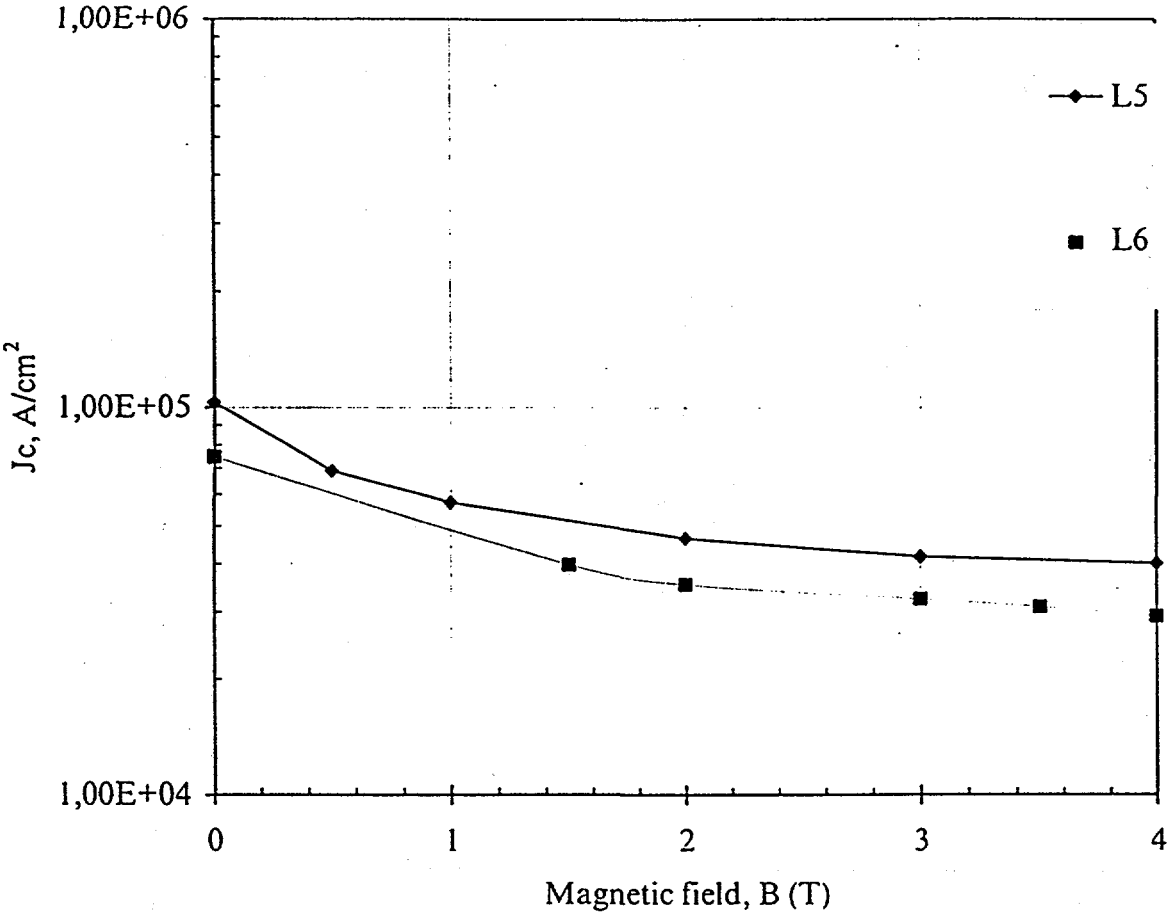

Fig. 10a The critical current density as a function magnetic field (B || tape plate) at T=4.2K for Bi-2223 tapes

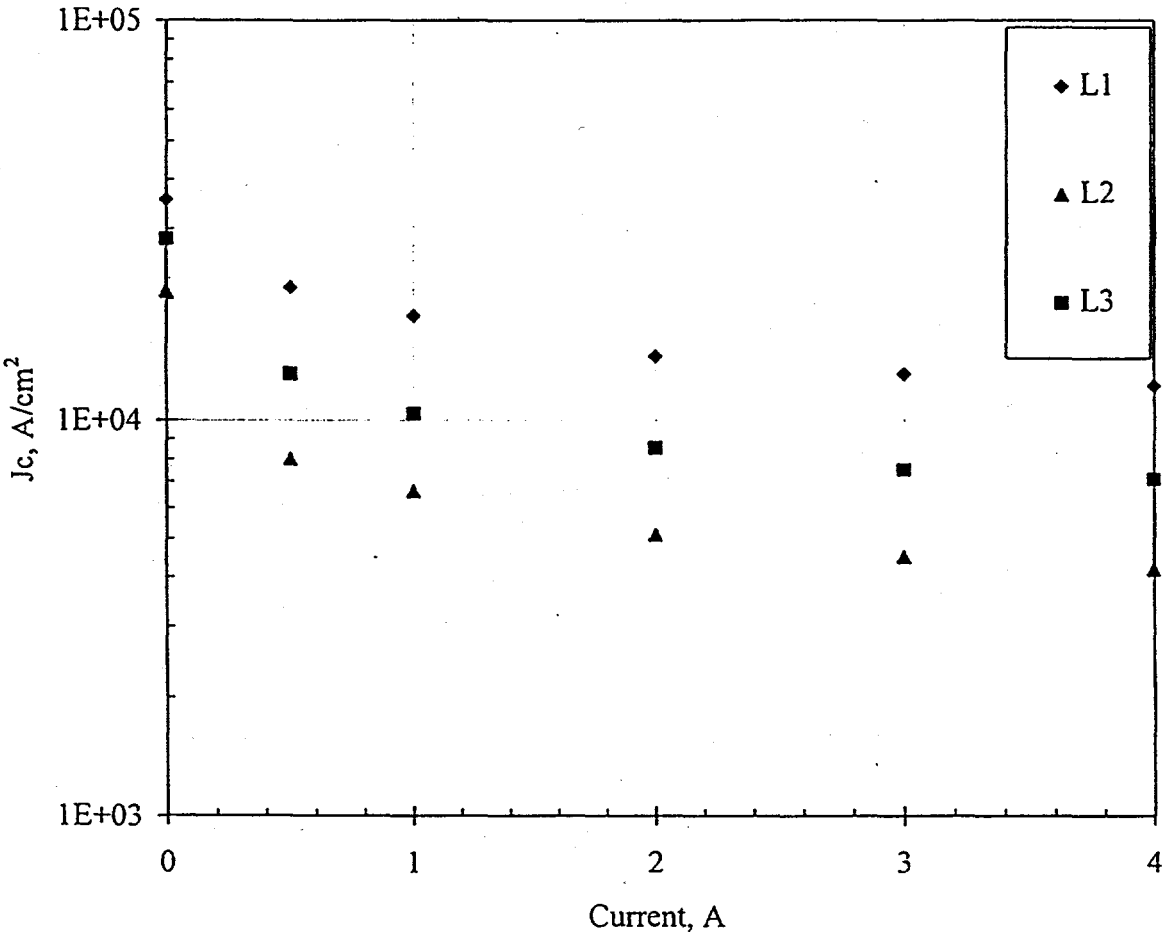

Fig. 10b The critical current density as a function magnetic field (B || tape plate) at T=4.2K for Bi-2223 tapes

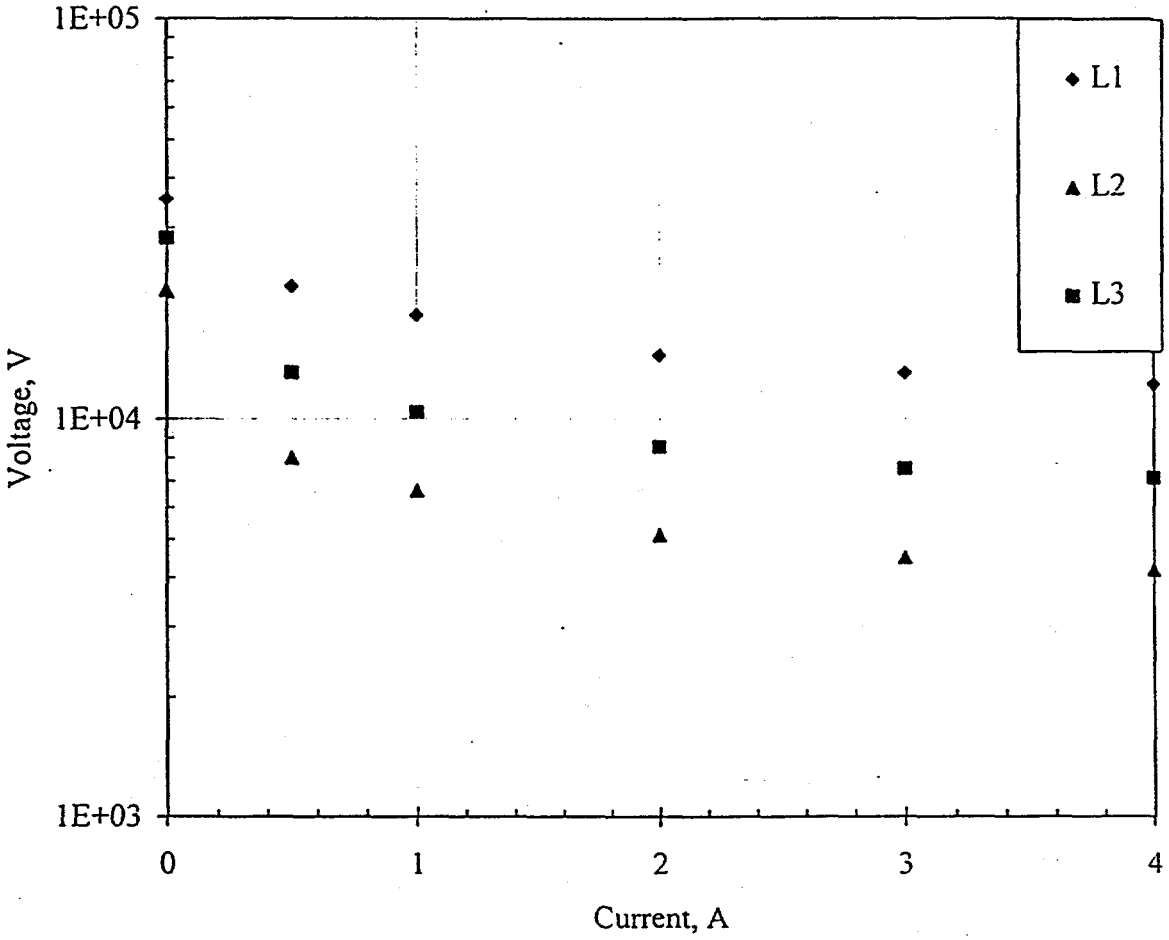

Fig. 10b The critical current density as a function magnetic field (B || tape plate) at T=4.2K for Bi-2223 tapes

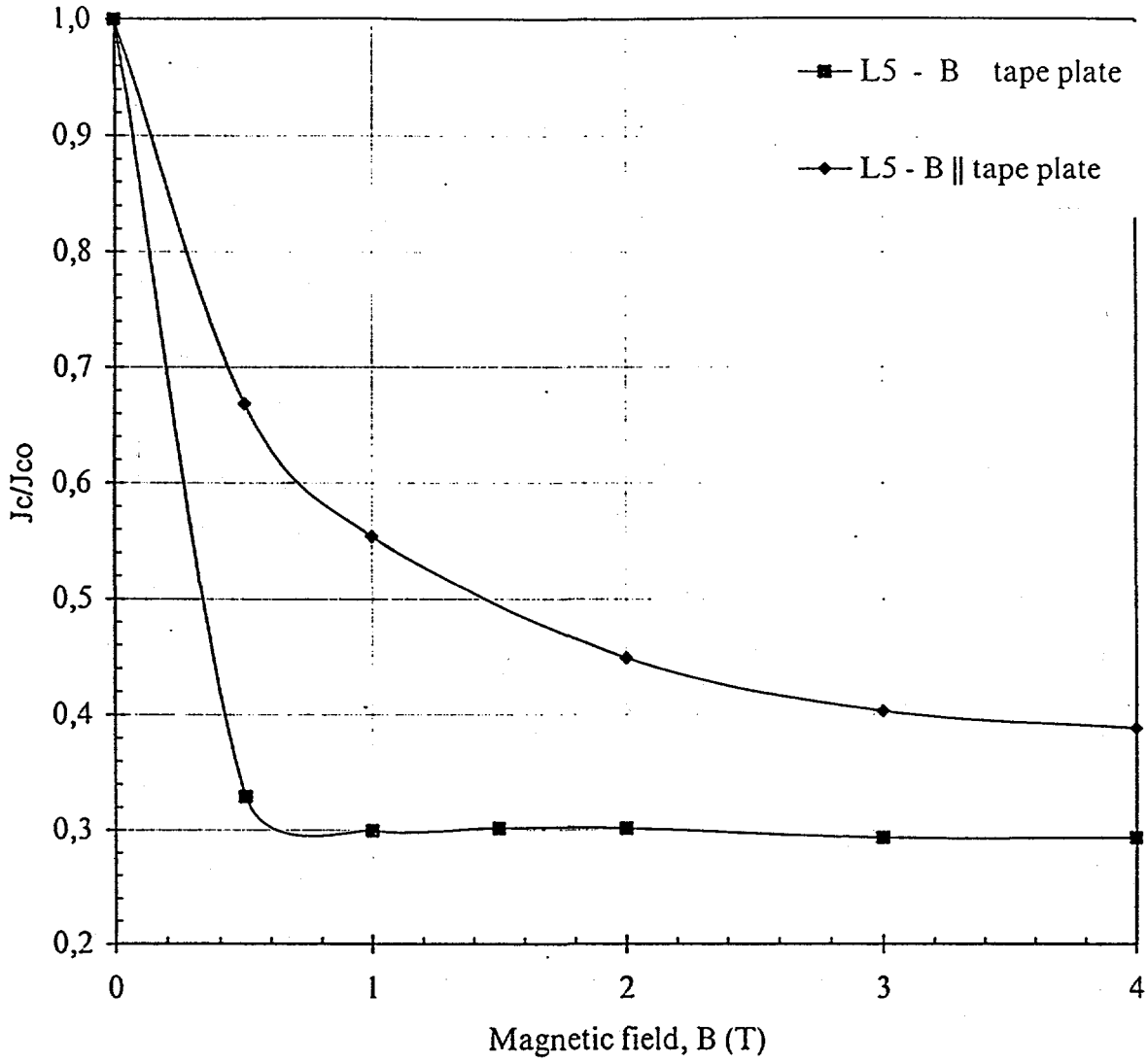

Fig. 11. The normalized critical carrent density as a function of magnetic field at T=4.2K for Bi-2223 tapes

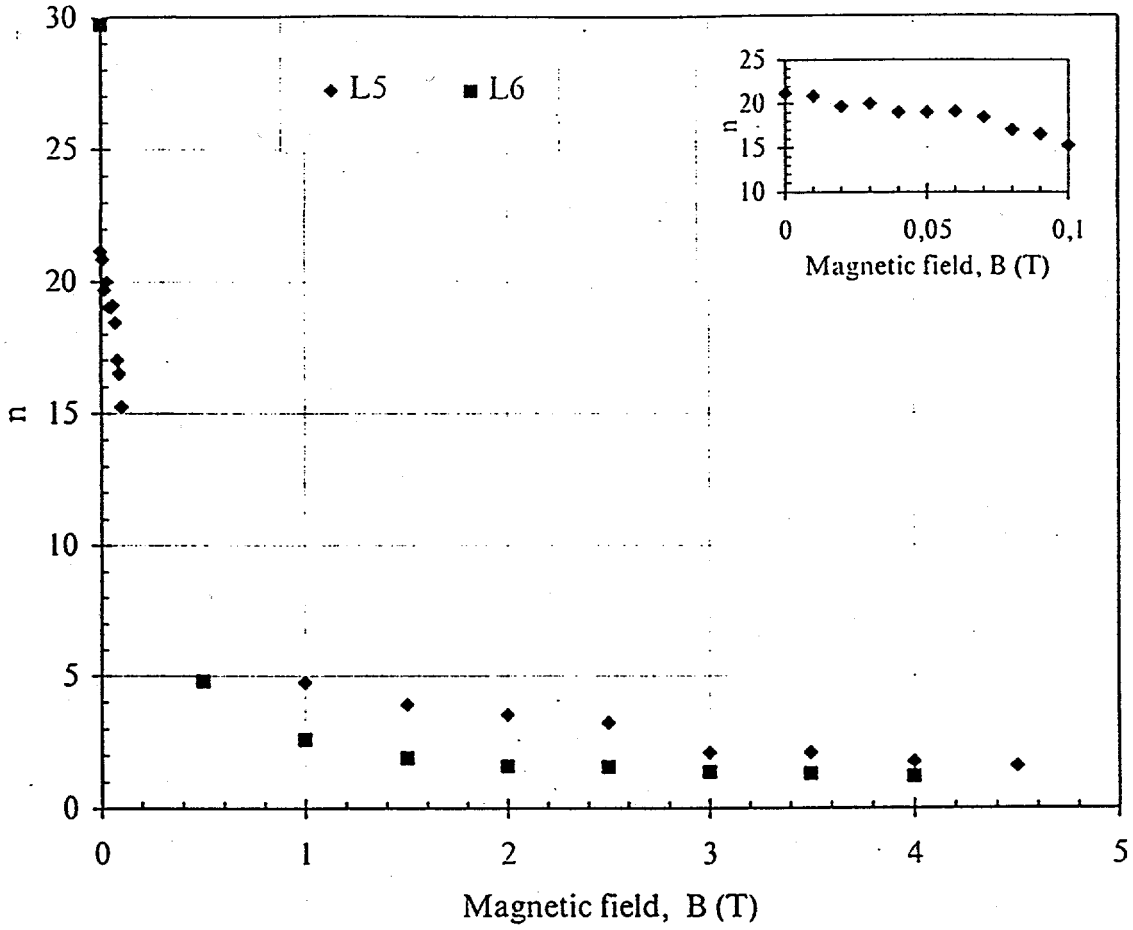

Fig. 12. The index "n" as a function of mgnetic field (B || tape plate) for Bi-2223 tapes at T=77K

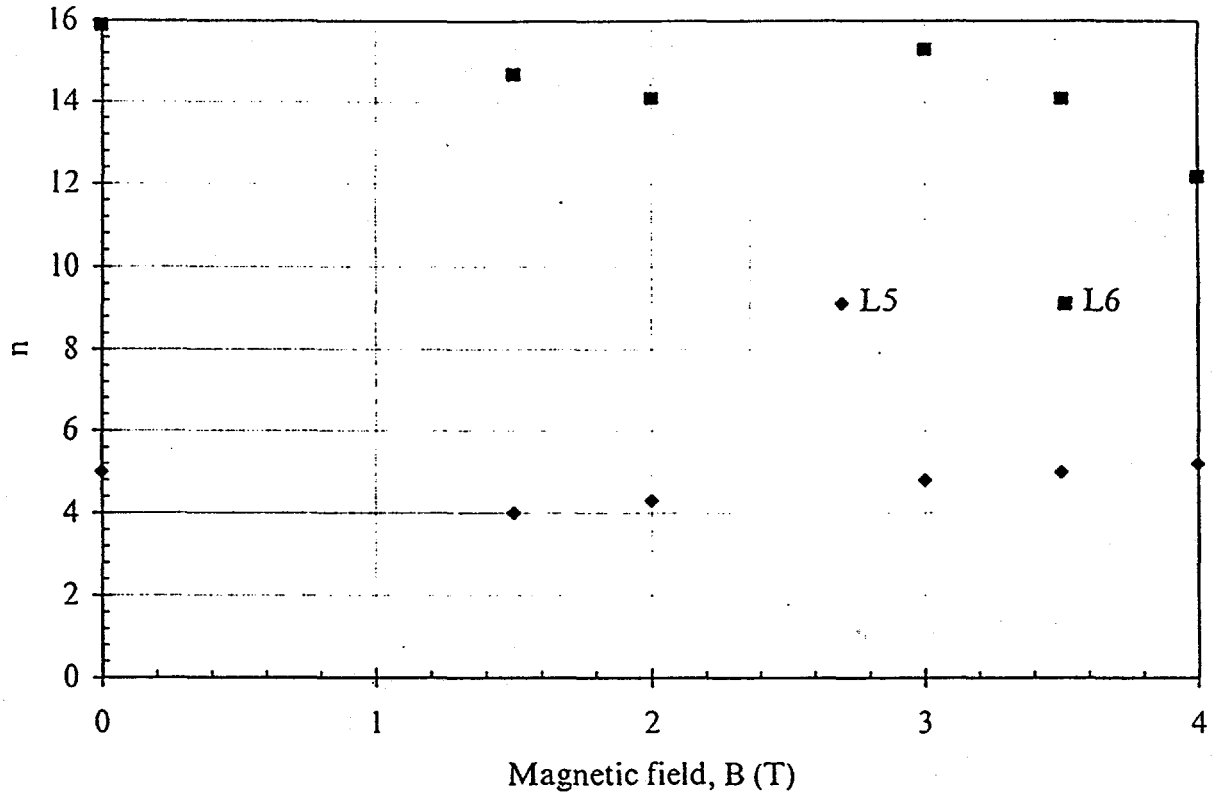

Fig. 13. The index "n" as a function of magnetic field (B || tape plate) for Bi-2223 tapes at T=4.2K

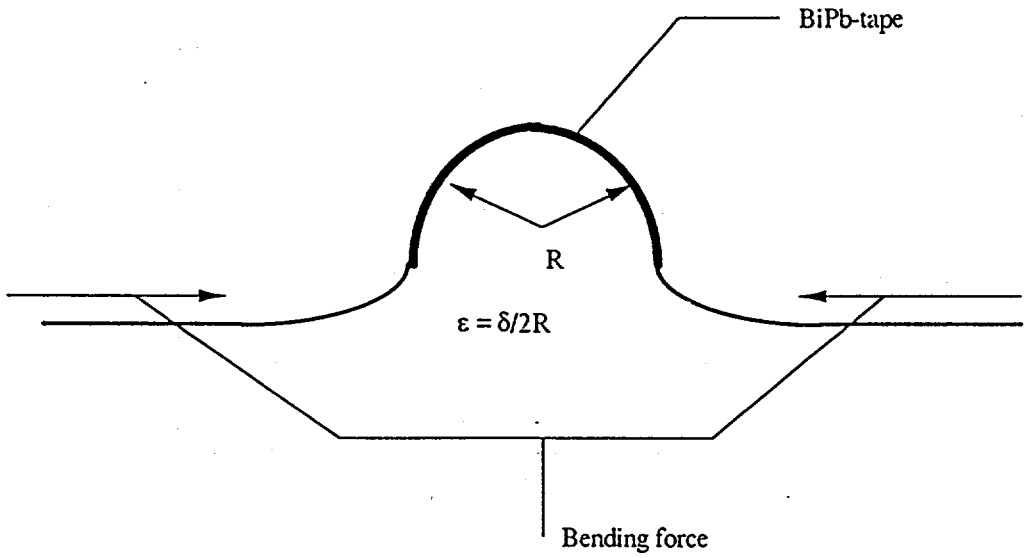

Fig. 14 Bending scheme for Bi-2223 tape

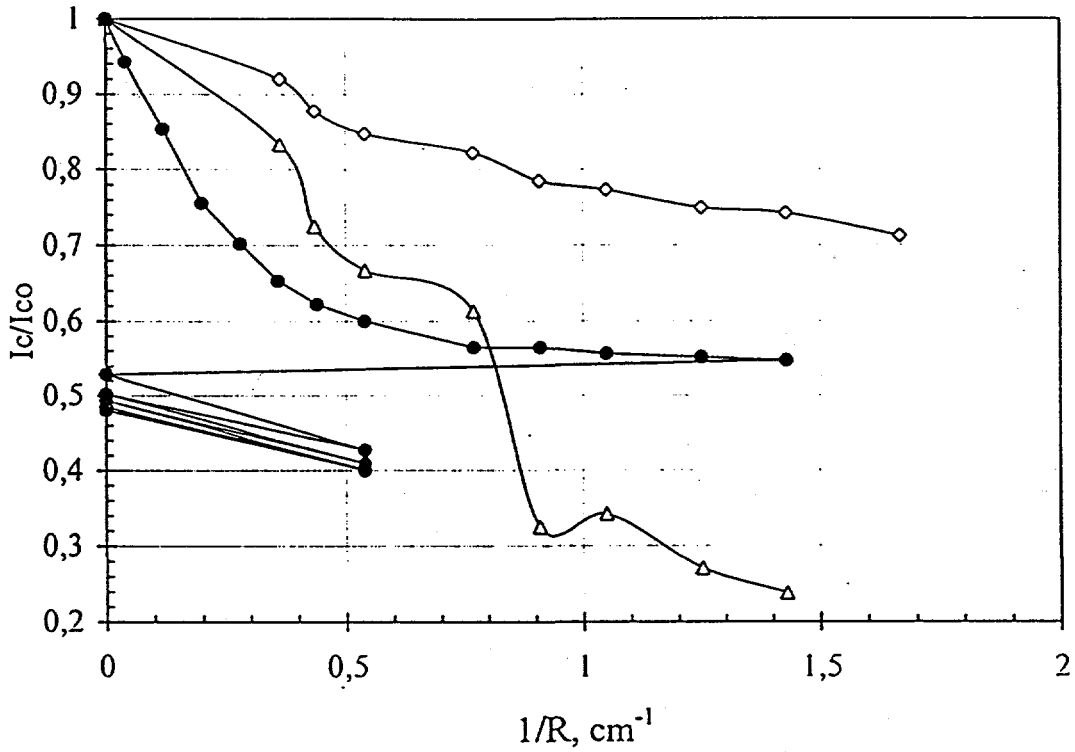

Fig. 16. The normalized critical current Ic/Io (77K, 0T) as a function of bending radius.

△ L1; ◇ L3; ● L5

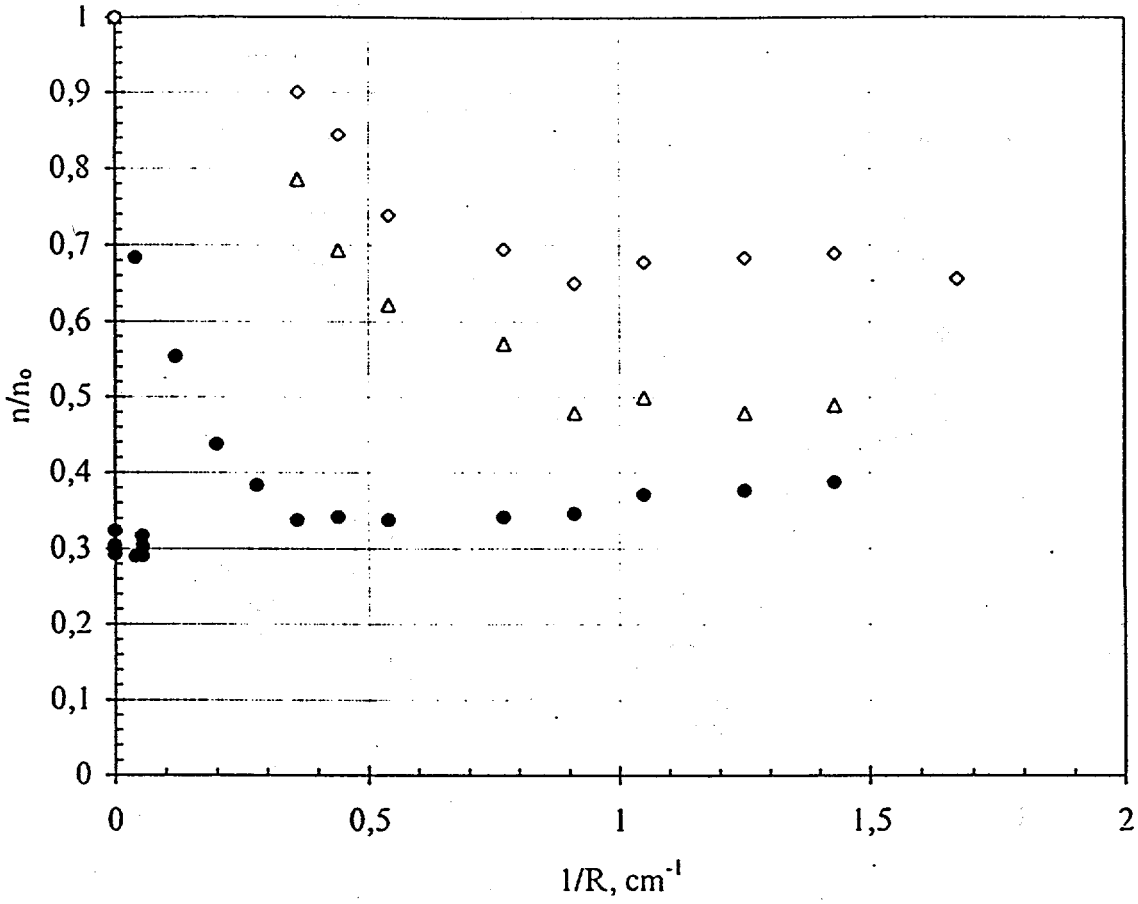

Fig. 17. Normalized "n" - parameter n/n0 as a function of bending radius.

△ L1; ◇ L3; ● L5

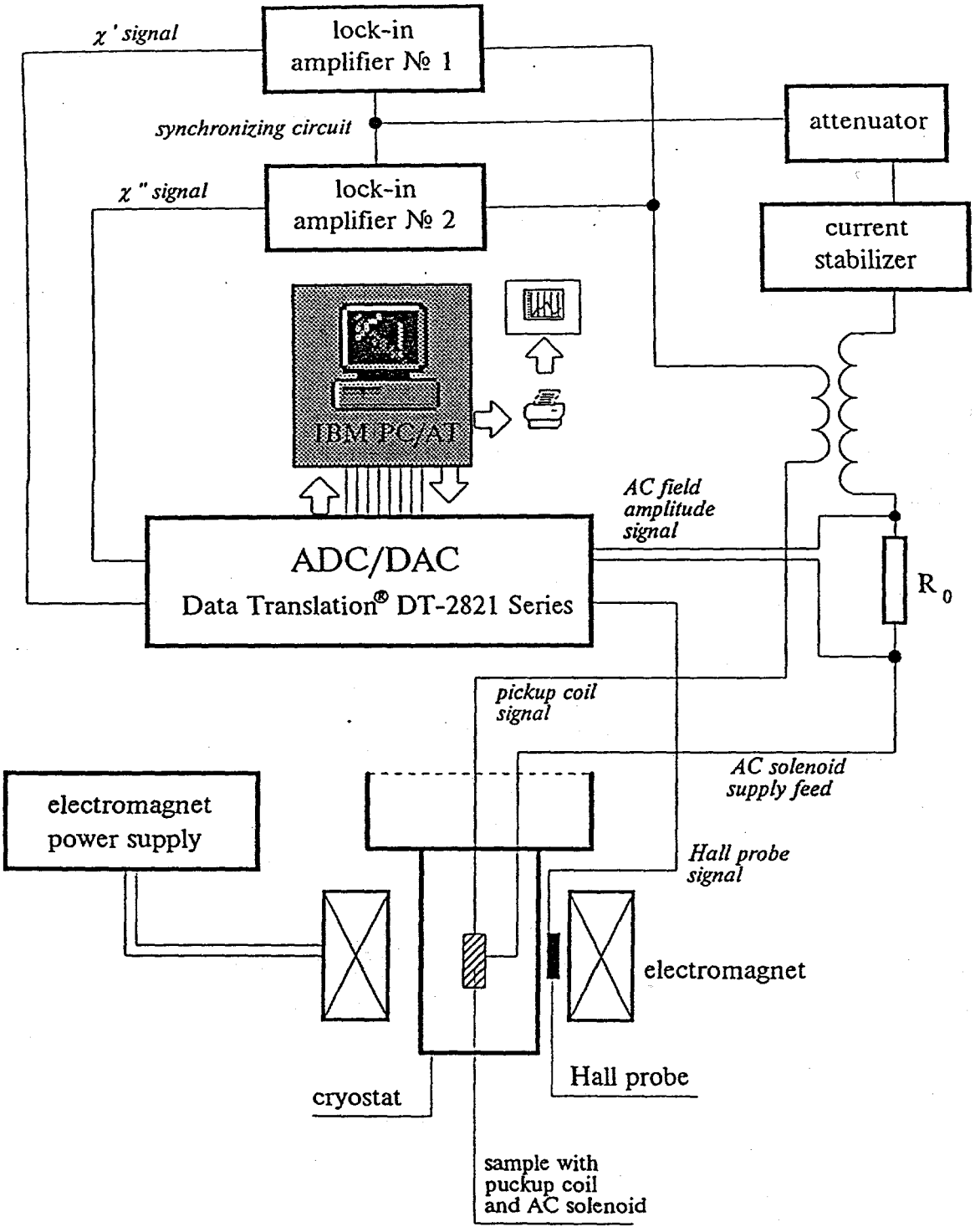

Fig. 18 The sketch of the experimental setup for measurements of the AC magnetic susceptibility.

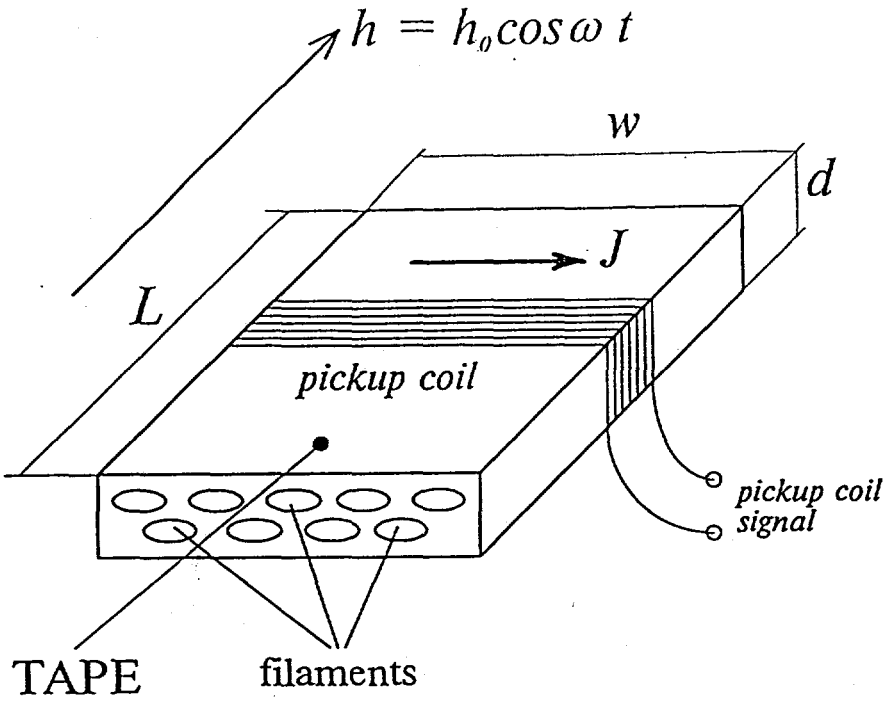

a)

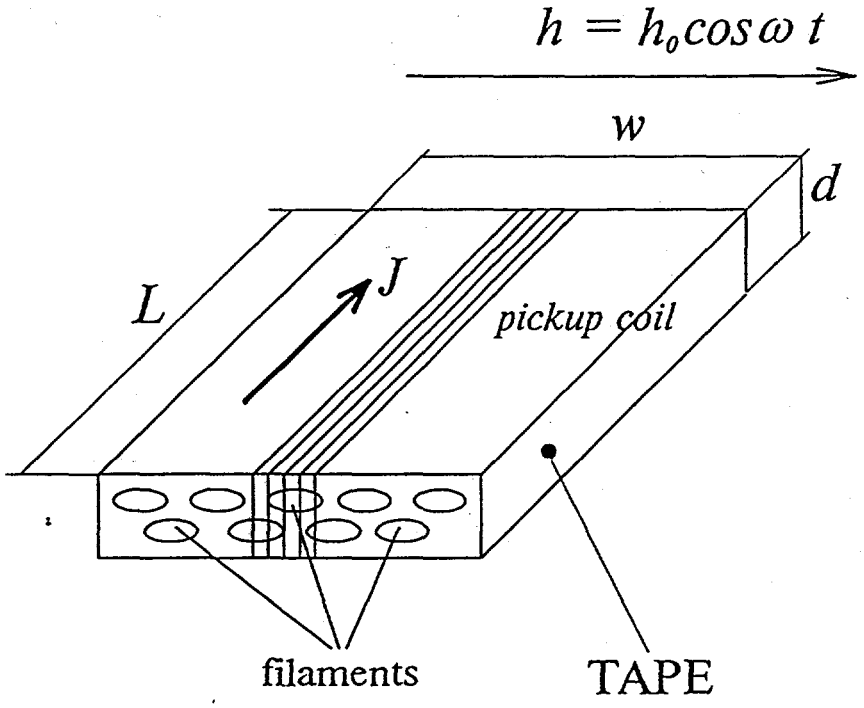

b)

Fig. 19. The geometry of AC measurements for testing the critical current density across (a) and along (b) the filaments.

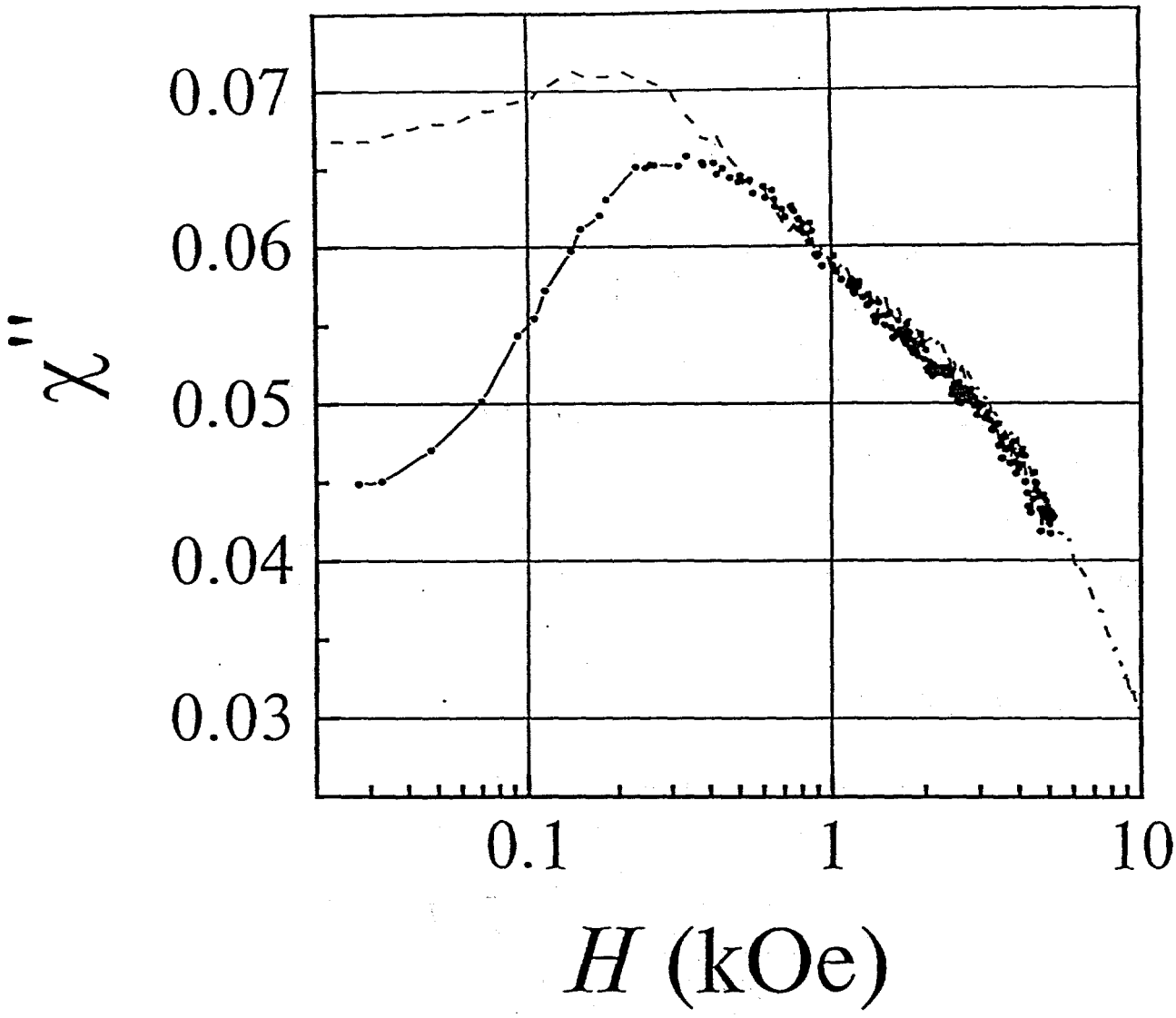

Fig. 20a. The dependencies of the AC magnetic susceptibility vs. magnetic field for two parts of the sample L1.

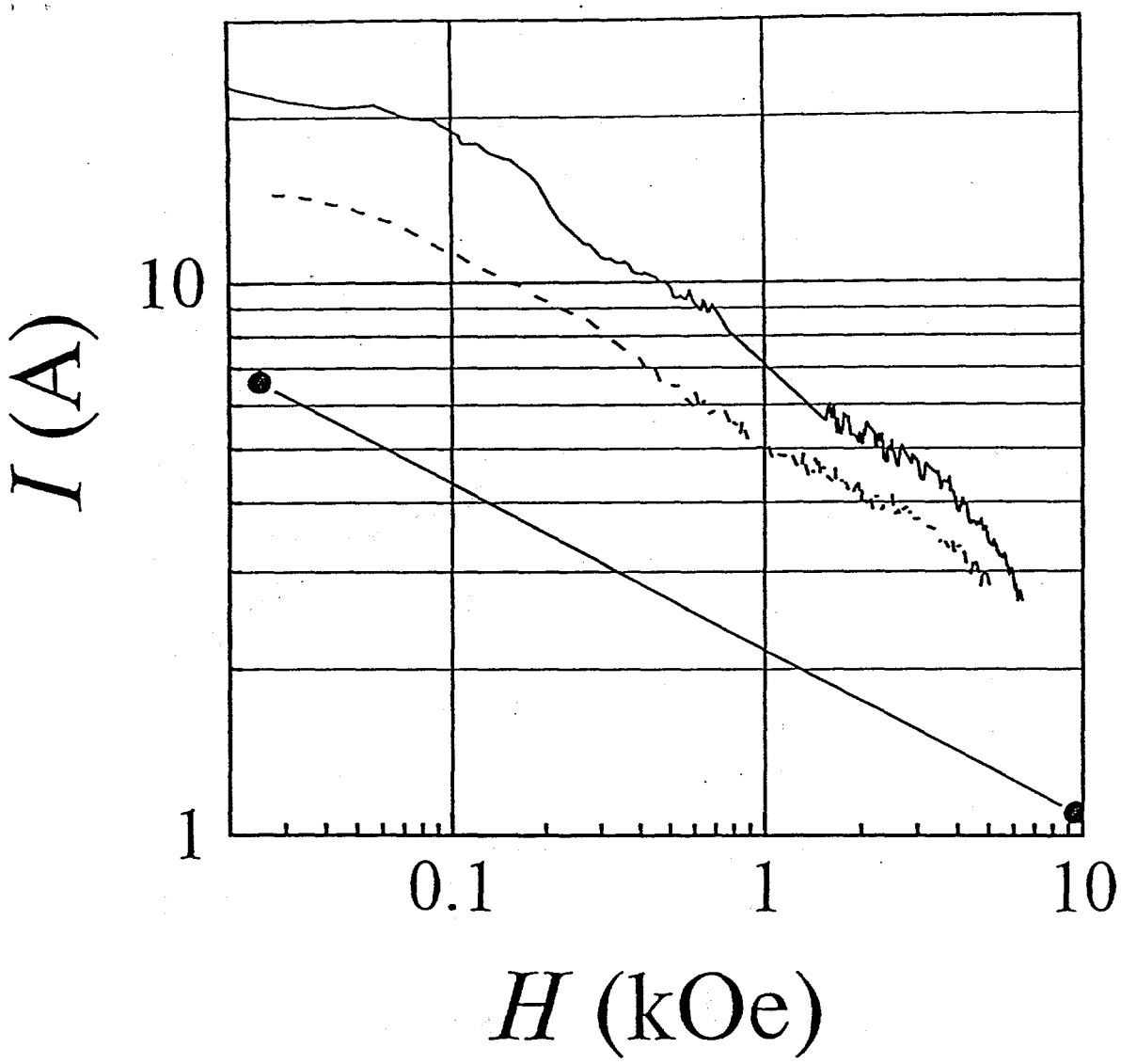

Fig. 20b. The critical current calculated from the data of Fig.20a for the sample No.10 (part of the L1 tape). The current flows across (solid line) and along (dashed line) the tape. The close symbols correspond to the four-probe data.

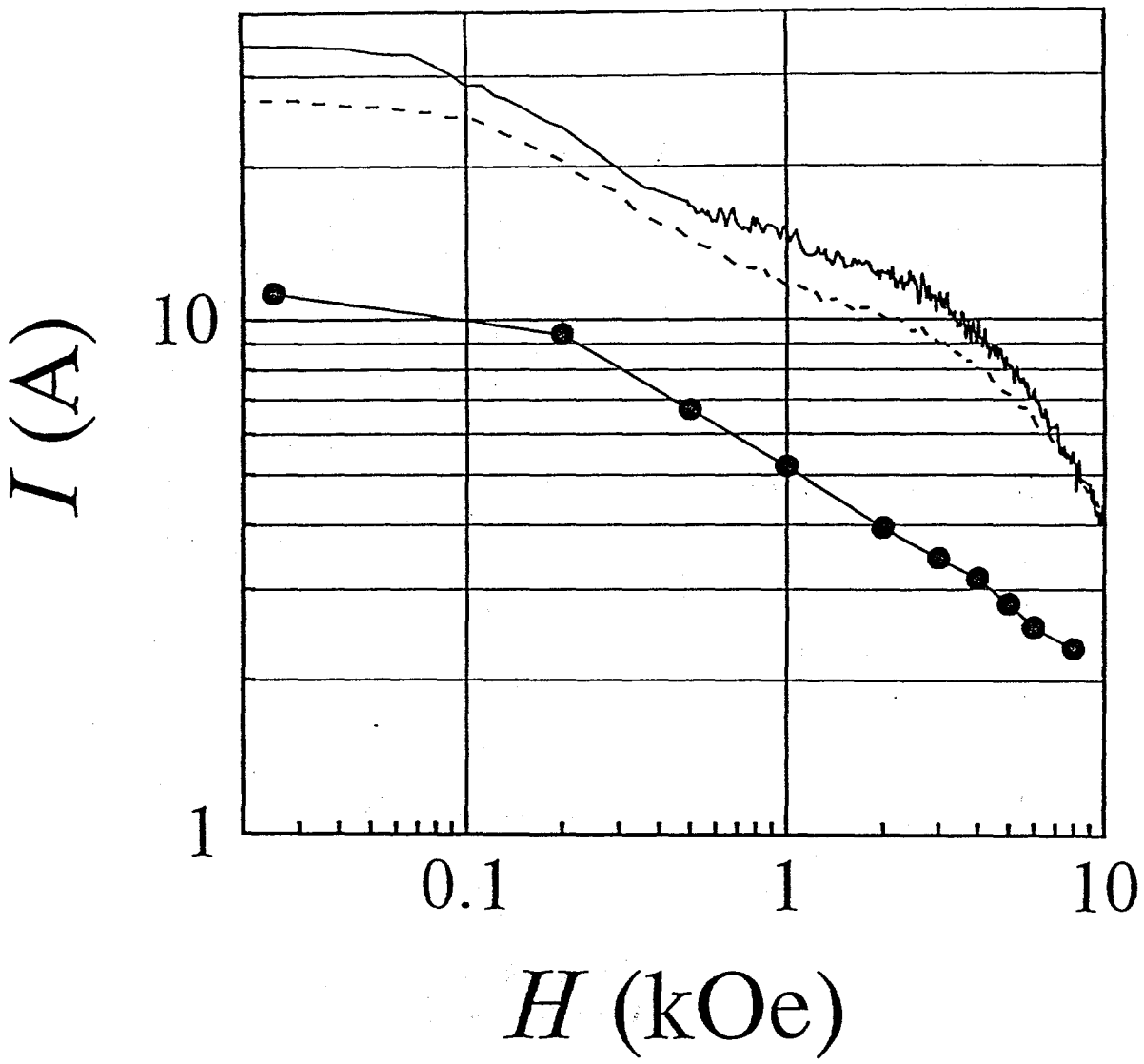

Fig. 20c. The critical current calculated from the data of Fig.20a for the sample No.12 (part of the L1 tape). The current flows across (solid line) and along (dashed line) the tape. The close symbols correspond to the four-probe data.

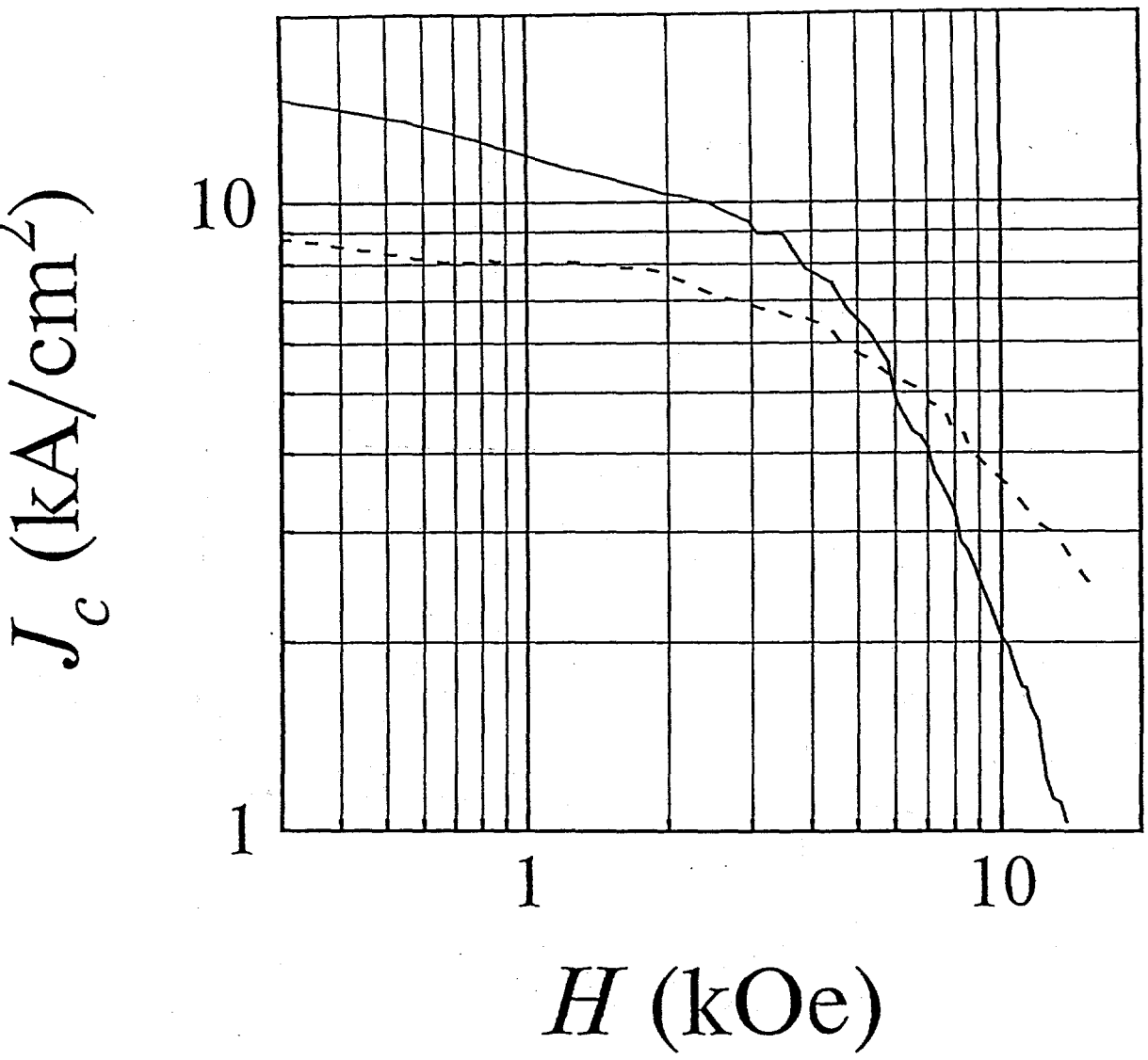

Fig. 20d. The magnetic field dependensies of the critical current density for the sample L6. The testing current flows across (solid line) and along (dashed line) the filaments. The magnetic field was aligned in the tape plane.

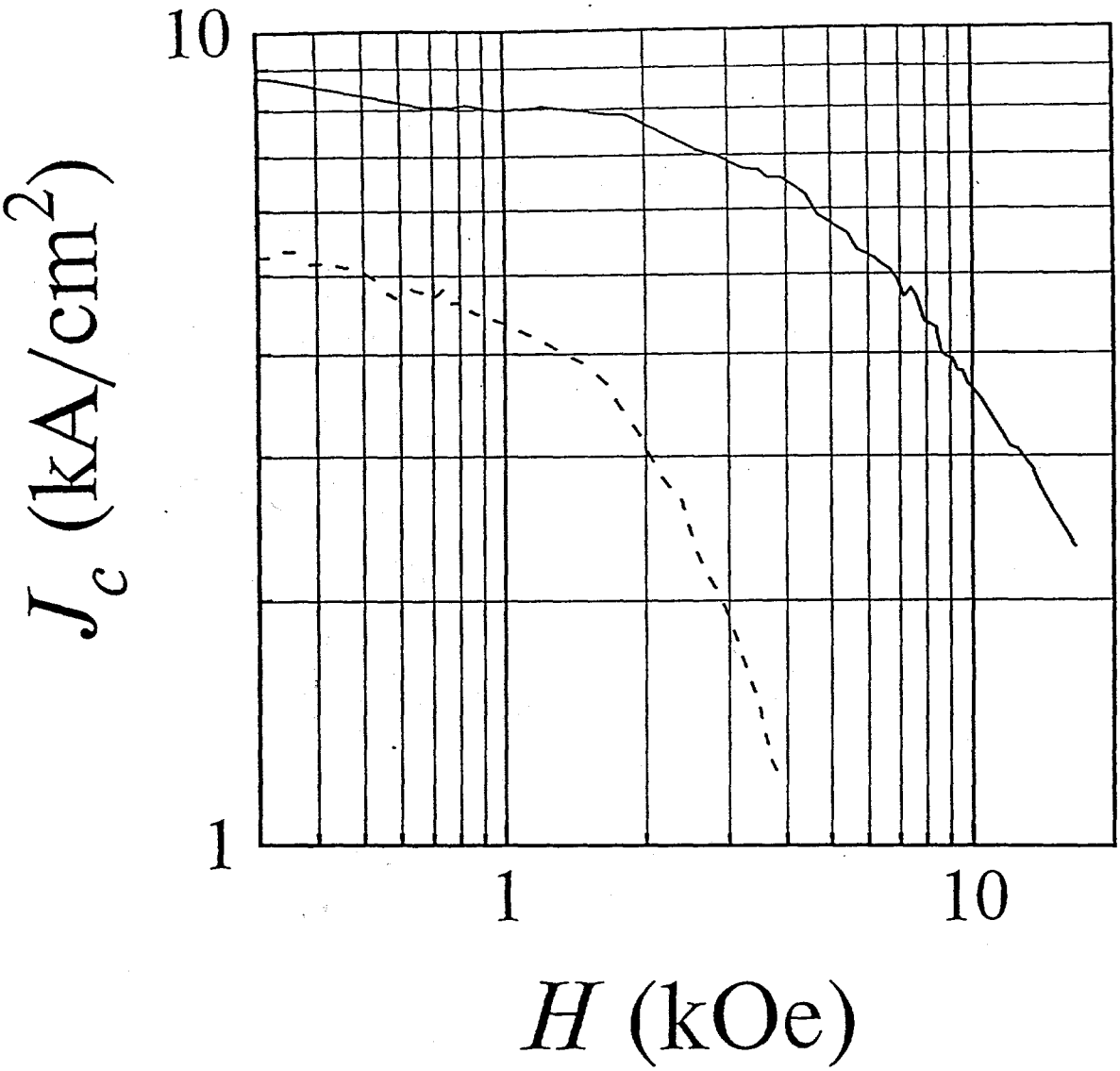

Fig. 20e. The magnetic field dependensies of the critical current density for the sample L6. The magnetic field was directed along the tape plane (solid curve) and perpendicular to it (dashed curve). The testing current flows along the filaments.

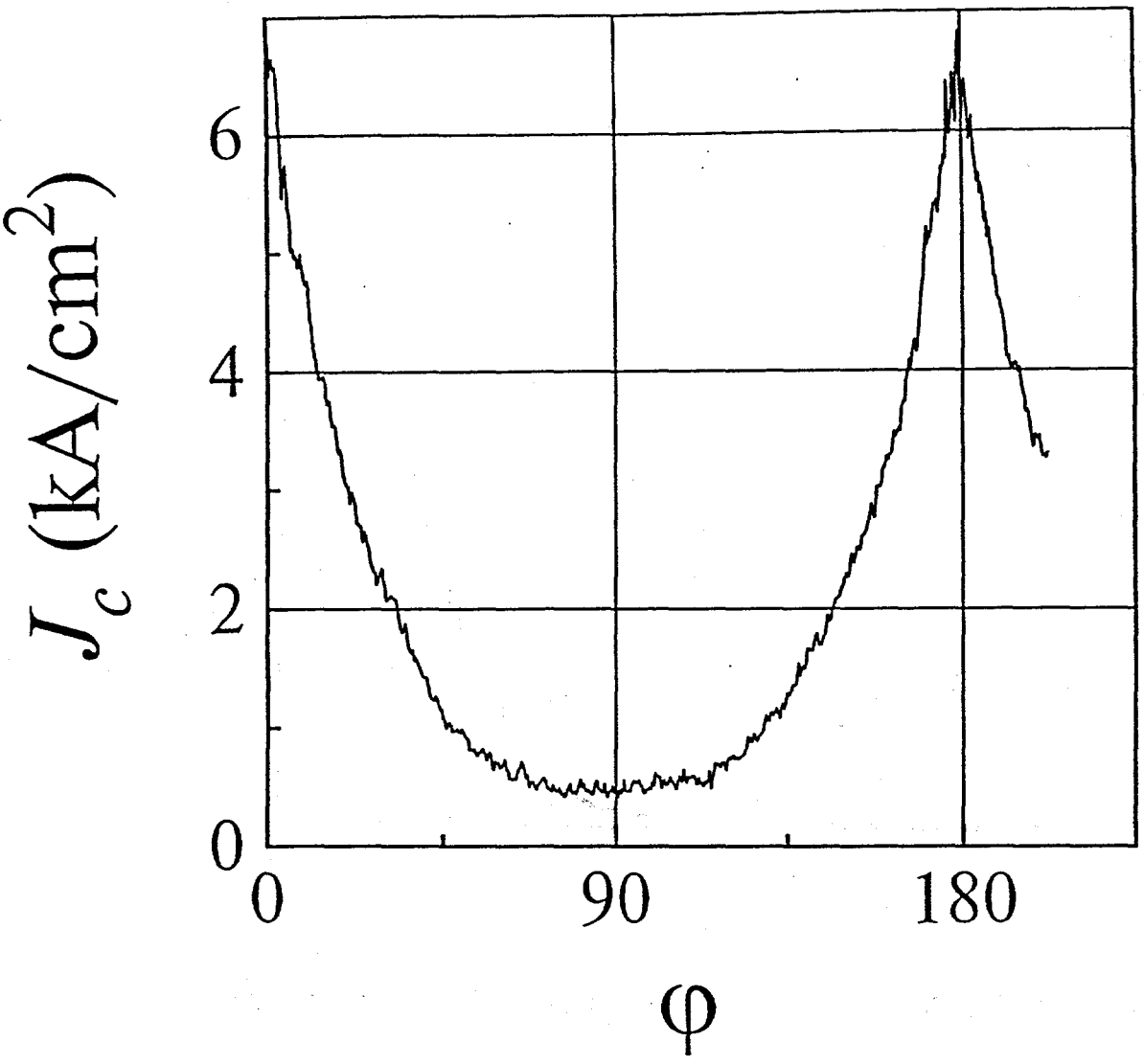

Fig. 20f. The dependence of the critical current density on the angle between the tape plane and the magnetic field direction.

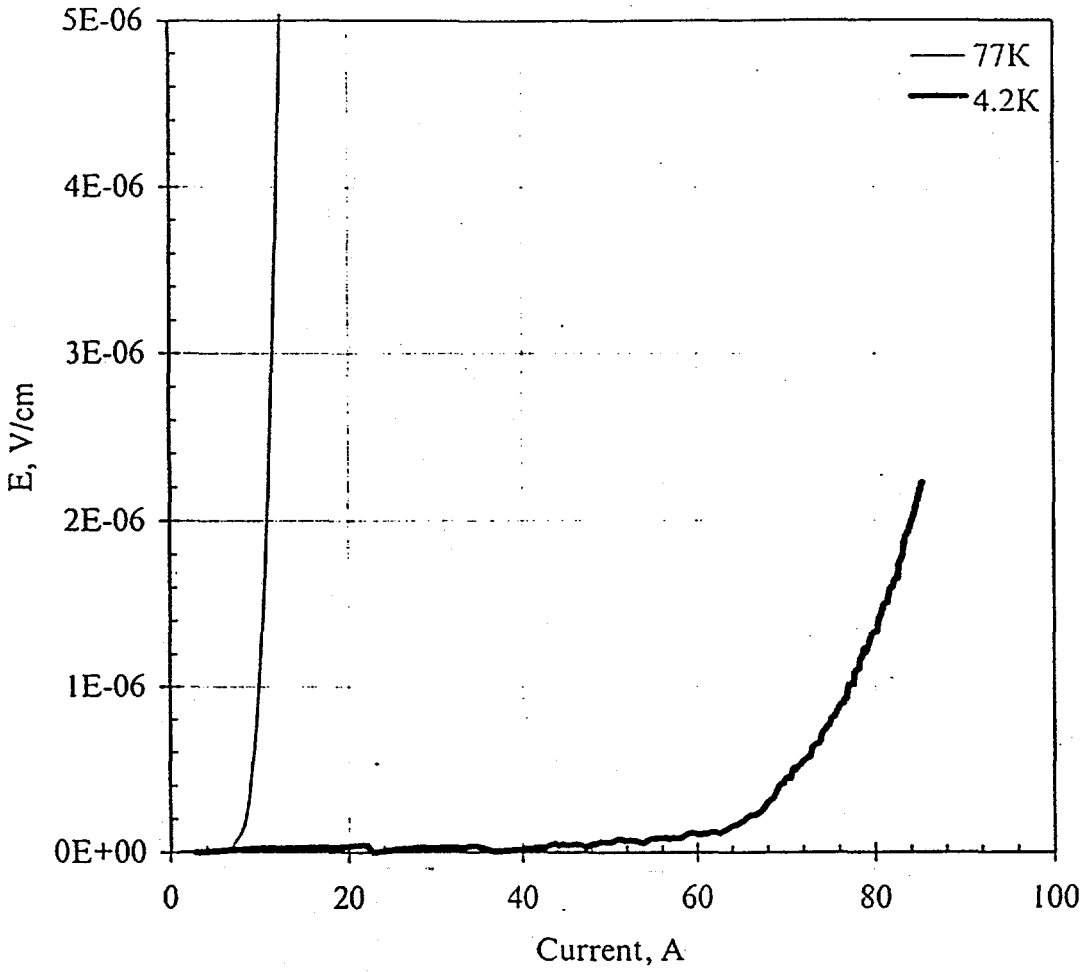

Fig. 21. The VCC of pancake coil (L5) at T=77K and T=4.2K in self field

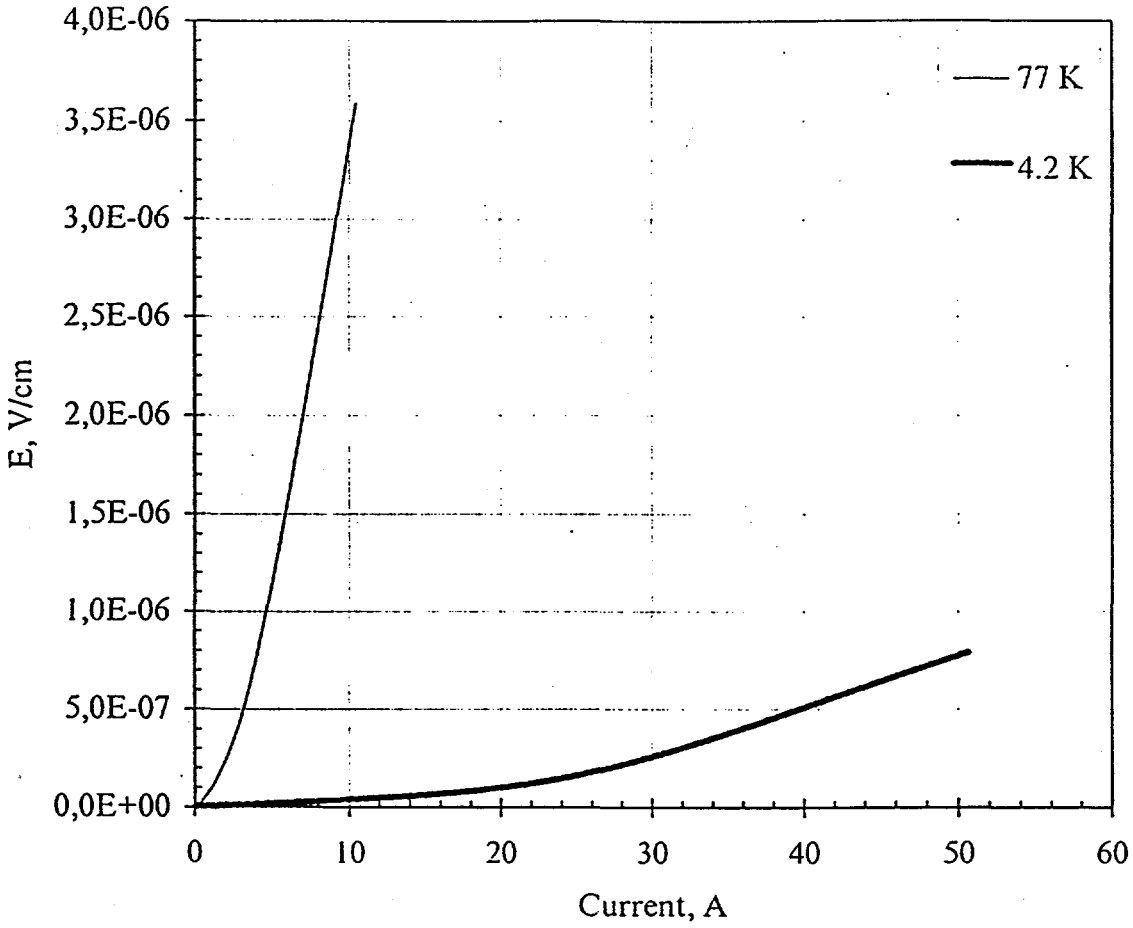

Fig. 22. The VCC of 5-stacked pancake coils (L1) at T=77K and T=4.2K in self field

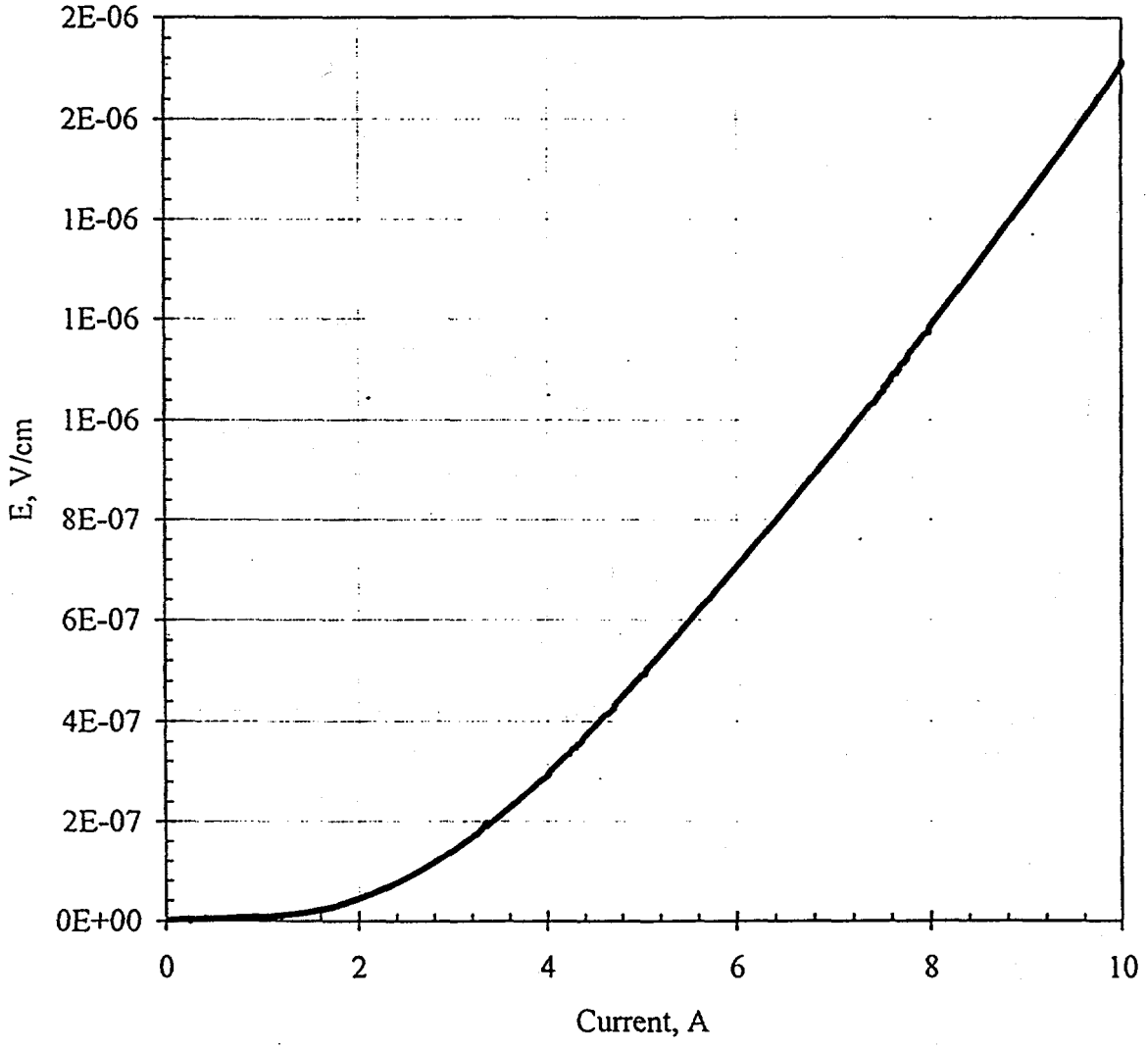

Fig. 23. The VCC of pancake coil ("racetrack") L6 conductor at T=77K in self field.

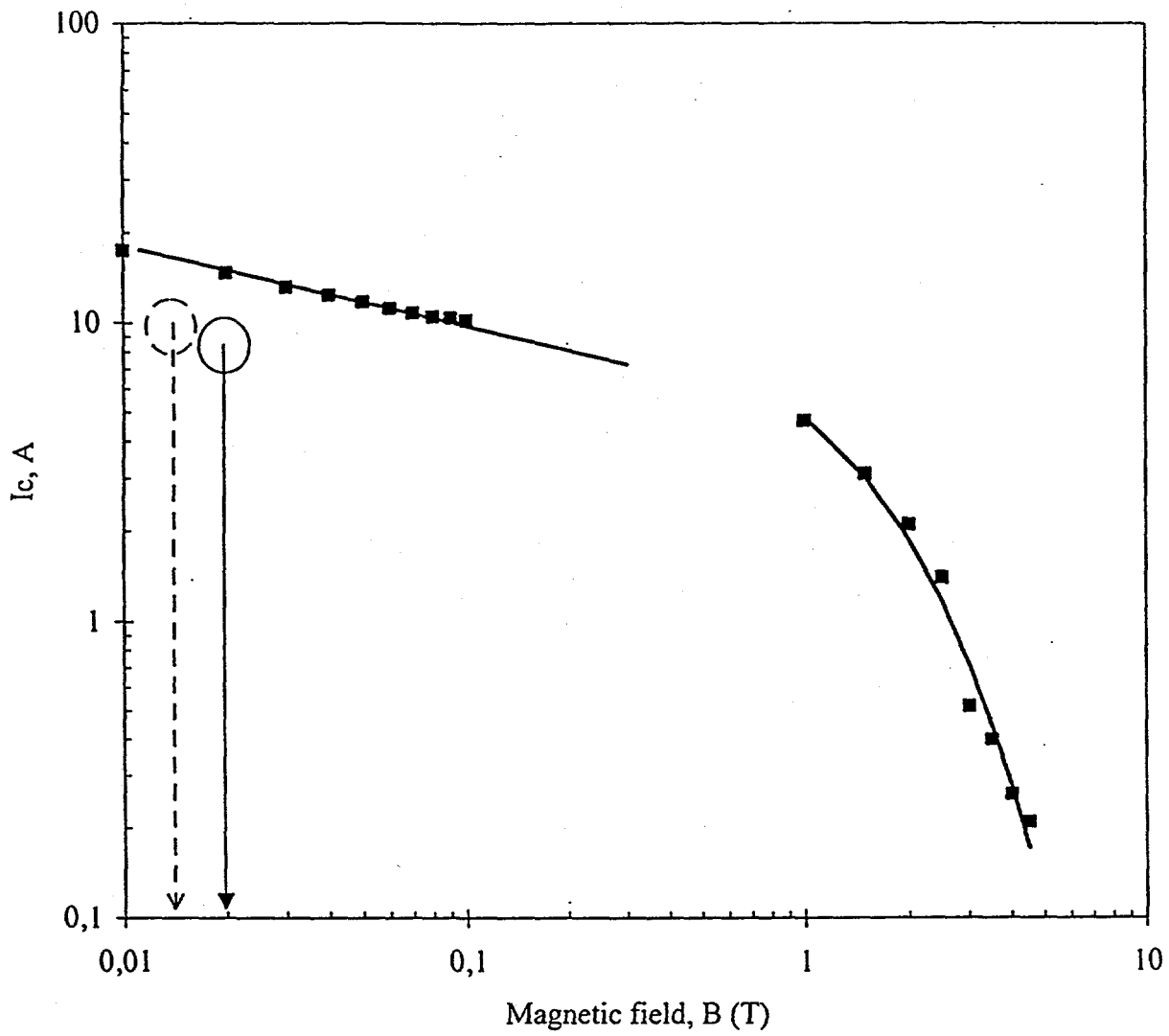

Fig. 24. The critical current as a function of magnetic field (B || tape plate) at T=77K for short sample "L5".

○ - experimental Ic of pancake coils;
— – – - the values of magnetic field calculated for two pancake coils are indicated by dashed and mono arrows.

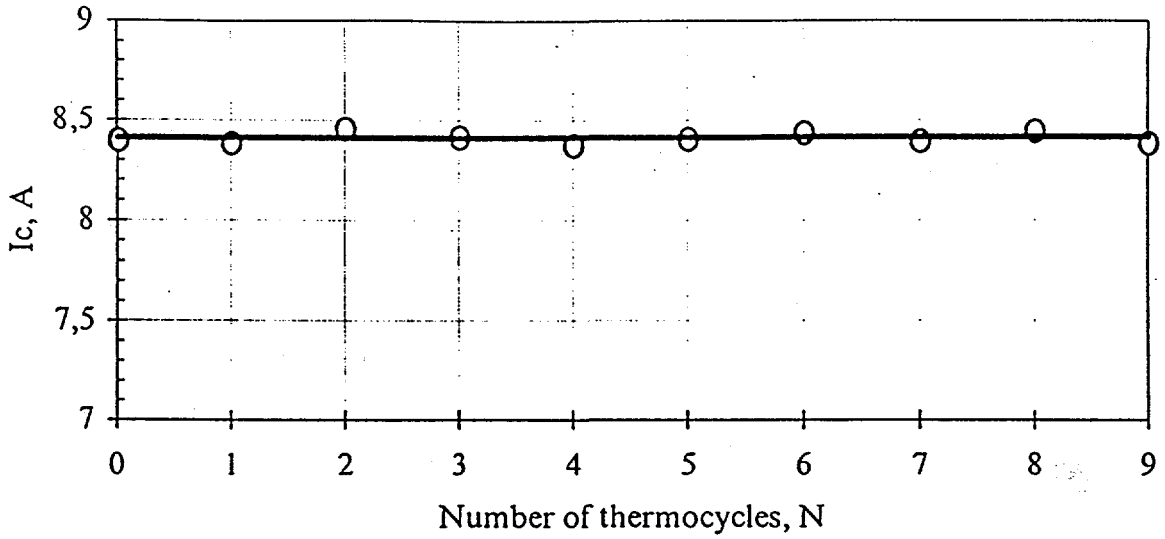

Fig. 25 Critical current as a function of thermocycling (77K↔293K) for the pancake coil (L5)

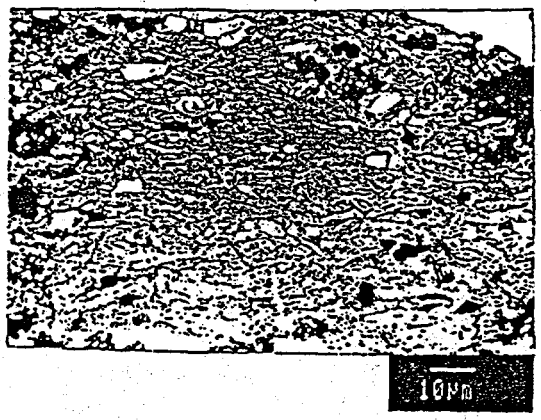

monofilamentary Bi-2223/Ag tape

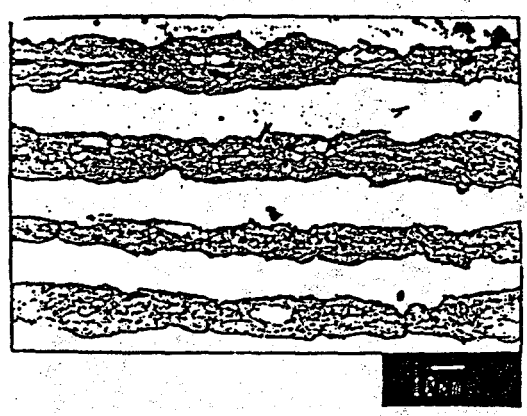

19-filamentary Bi-2223/Ag tape

Figure 26. Cores structure of different Bi-2223/Ag tapes

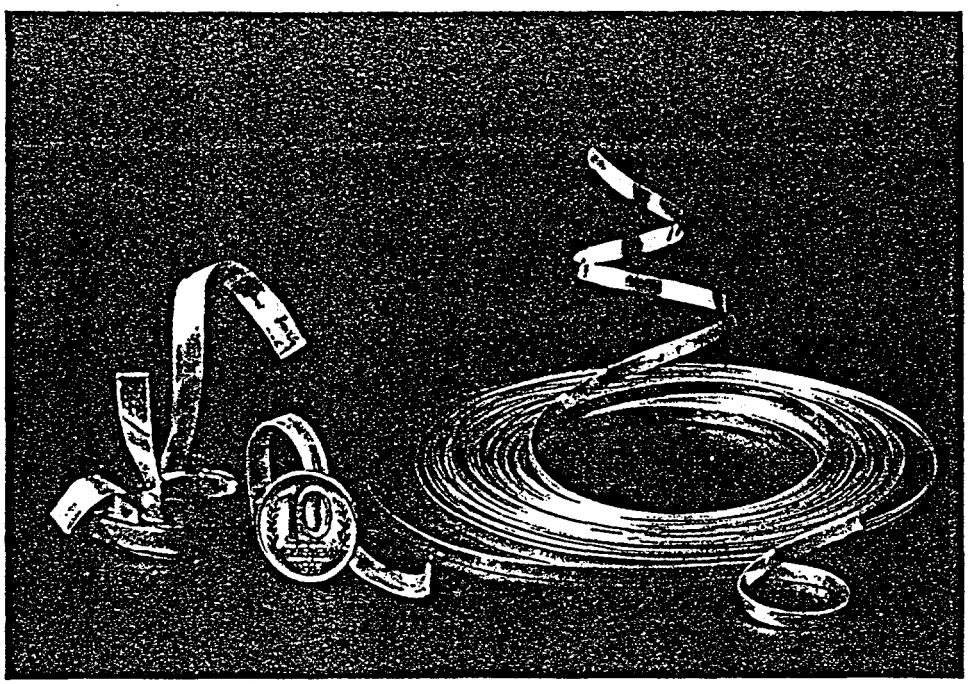

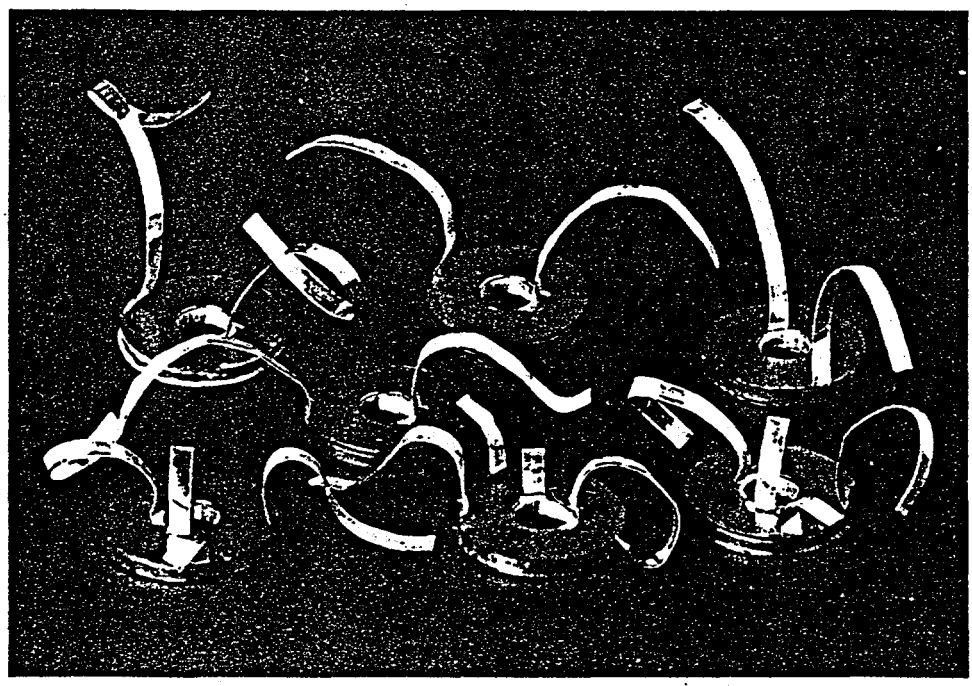

Figure 27. Conductors and coils.